공학박사 학위논문

Gaussian Mixture-based Equivalent Linearization Method for Nonstationary Responses of Nonlinear Structures

구조시스템의 추계학적 비선형 응답 평가를 위한
GM-ELM 개발

2020년 2월

서울대학교 대학원

건설환경공학부

이 상 리

Abstract

Gaussian Mixture-based Equivalent Linearization Method for Nonstationary Responses of Nonlinear Structures

Yi, Sang-ri

Department of Civil & Environmental Engineering

The Graduate School

Seoul National University

Reliability assessment of a structural system subjected to stochastic excitations, e.g. earthquake, wind and wave, plays an important role in design and maintenance decisions. However, the random nature of excitations and the complex behavior of nonlinear structures may make the evaluation a challenging task. In this regard, stochastic dynamic analysis has often been considered as a useful tool and substantial progress has been made in the past decades. Nevertheless, the analysis of general multi-degree-of-freedom nonlinear systems subjected to general nonstationary excitations remains as a challenging task with significant difficulties. To tackle the challenges, Gaussian Mixture-based Equivalent Linearization Method (GM-ELM) was recently developed. Unlike conventional linearization methods, GM-ELM identifies a set of *multiple* linear oscillators as an equivalent linear system (ELS), which collectively reproduce the nonlinear responses. Specifically, the decomposition is made by approximating a general response PDF of a nonlinear system in terms of the Gaussian mixture (GM) model. The main motivation of this

decomposition is that the response of the linear system under a Gaussian excitation is guaranteed to be a Gaussian distribution. Using the multiple linear oscillators, accurate estimates of nonlinear response statistics can be obtained for the whole response range up to the extreme criteria. The response statistics include instantaneous failure probability, mean crossing rates and first-passage probabilities for different threshold levels, and mean peak responses. In this dissertation, GM-ELM is further developed to promote its application in more realistic problems, especially focusing on the earthquake engineering applications, as well as to increase its accuracy and efficiency.

First, in order to account for the energy dissipation of the nonlinear hysteretic behaviors, *bivariate GM-ELM* is developed. Instead of using univariate response PDF for GM-based linearization, it is proposed to use the joint PDF of the response and its derivative when identifying ELS. The additional information on the response time derivative allows us to optimize equivalent damping values, as well as the equivalent stiffness values. This extension removes the previous heuristic assumptions on equivalent damping and therefore improves the accuracy in a class of random vibration problems. Moreover, bivariate GM-ELM is still consistent with the basis of GM-ELM since the derivative of stationary Gaussian random process is also a Gaussian process, i.e. the joint PDF of response and the derivative response of the linear system is inherently a bivariate Gaussian distribution. The modified response combination equations are derived accordingly.

Next, to facilitate the applications of GM-ELM to practical earthquake engineering problems, several remaining challenges were diagnosed and addressed. First, to incorporate nonstationary responses, *temporal-average GM-ELM* is

proposed. It is shown that by introducing a GM model that fits the temporal-average of response PDF, and by identifying the corresponding ELS, the average response statistics of nonlinear system can be obtained. Secondly, an extended version of GM-ELM analysis is proposed to identify the ELS that is invariant to the scaling of ground motions. It is termed the *intensity-augmented GM-ELM* since this property is gained by pre-implementing the intensity dependency to the response space by augmenting another variable which is related to the seismic intensity. It is shown that the ELS identified by this intensity-augmented response PDF does not depend on the ground motion intensity levels, therefore, it is termed *universal ELS*. This kind of consistency in ELS improves the efficiency of seismic fragility analysis. The temporal-average and intensity-augmented GM-ELM can be incorporated either separately or simultaneously. Lastly, to further increase the efficiency of GM-ELM-based fragility analysis, an approximation technique called a *simple scaling* approach is proposed. It is shown that once the response PDF given a certain ground motion intensity is identified, e.g. by sampling, the intensity-augmented PDF could be easily approximated via a series of elementary calculations.

On the other hand, accurate assessment of the first-passage probability is another challenging topic in which the exact solution is unavailable in general linear system responses. In order to evaluate the probability of the first passage failure, the original version of GM-ELM analysis adopted well-known Poisson assumptions, which may give overly conservative estimation in highly narrowband responses. To overcome this inaccuracy, an alternative equation is first proposed to gain more consistent accuracy over various spectral shapes and bandwidths. The new formulation is derived by modeling the crossing events as a *Poisson branching*

process (PBP) while the branching probability is derived by identifying the joint distribution of neighboring extrema values. Finally, the proposed PBP-based first-passage probability equation is further modified to facilitate its implementations to GM-ELM. To this aim, a modification factor that can account for the bandwidth of the nonlinear response and the arbitrarily PDF shape of its envelope process is proposed for GM-ELM. The proposed approach allows us to accurately estimate the first-passage probability of the responses of nonlinear systems.

The proposed methods are demonstrated by numerical examples of earthquake engineering applications. The encouraging results obtained for various nonlinear multi-degree-of-freedom systems under nonstationary excitations confirm the merits and potentials of GM-ELM in solving challenging engineering problems that involve nonlinear stochastic dynamic analysis.

Keyword: GM-ELM, Gaussian mixture, Random vibration analysis, Equivalent linearization method, Fragility analysis, First-passage probability

***Student Number*:** 2015-21302

Table of Contents

List of Figures

List of Tables

Chapter 1. Introduction

1.1 Nonlinear random vibration analysis

Infrastructures are inherently subjected to various vibrational loads such as earthquake, wave, and wind load, and reliability assessment on corresponding vibratory responses is important in design and maintenance decisions. However, the random nature of the vibrations may make the evaluation a challenging task.

One of the compelling approaches to estimate the vibratory behavior of the structure is based on stochastic dynamic analysis. By mathematically modeling the stochastic excitations in terms of its frequency contents, e.g. as a power spectral density (PSD) function, the propagation of randomness to the structural responses can be quantified by means of stochastic parameters using the random vibration analyses.

When a linear system is of interest, various response statistics can be obtained by well-established closed-form formulations (Lutes and Sarkani 2004). However, these formulations are not directly applicable to nonlinear systems for which the superposition principle does not hold. To overcome the challenges in such nonlinear analysis, researchers developed various stochastic dynamic analysis methods, which can be categorized as classical, simulation-based, and equivalent linearization methods (Broccardo 2017; Lutes and Sarkani 2004).

1.2 Equivalent linearization methods

To overcome the challenges in nonlinear stochastic dynamic analysis, various random vibration analysis techniques have been proposed in recent decades, among which the equivalent linearization method (ELM) has gained wide popularity (Caughey 1963; Atalik and Utku 1976; Wen 1980; Crandall 2001). ELM is computationally efficient and applicable to general, multi-degree of freedom (MDOF) nonlinear systems. Moreover, in applications of earthquake engineering, ELM enables us to use of code-specified elastic design spectra in analyzing nonlinear structures. This property makes ELM especially attractive in engineering practice when compared to other approaches, e.g. Fokker-Planck equation, stochastic averaging, moment closure, and perturbation.

Conventional ELM approaches determine the equivalent linear system via minimizing the mean-square error between the responses of the nonlinear and linear systems (Atalik and Utku 1976; Wen 1980; Crandall 2001). This approach could be accurate in estimating the mean-square responses, but it may not capture the non-Gaussianity of the nonlinear responses. As a consequence, ELM-based estimates on response probability distributions (especially in the tail region) and mean peak responses could be inaccurate.

Structural reliability methods (Ditlevsen and Madsen 1999; Der Kiureghian 2005), which were initially developed for time-invariant problems, have been utilized for stochastic dynamic analysis as well. A sequence of studies along this idea has been carried out during the last two decades (Li and Der Kiureghian 1996; Der Kiureghian 1996; Zhang and Der Kiureghian 1997; Der Kiureghian 2000; Franchin 2004; Koo *et al.* 2005; Barbato and Conte 2006). A well-acknowledged achievement

in this line of research is the development of a non-parametric ELM, named tail-equivalent linearization method (TELM) (Fujimura and Der Kiureghian 2007). In TELM, an equivalent linear system is numerically obtained in terms of a discretized impulse-response function or frequency-response function, using knowledge of the 'design point' determined by the first-order reliability method (FORM) (Ditlevsen and Madsen 1999; Der Kiureghian 2005). In comparison to the conventional ELM, TELM has superior accuracy in estimating the response probability distributions, especially in the tail region.

However, the high accuracy of TELM is achieved at the cost of more computational demand, since TELM requires performing FORM analysis for a sequence of response threshold values. Recent studies (see, e.g. Fujimura and Der Kiureghian 2007; Wang *et al*. 2016) on efficient algorithms to find a sequence of design points could alleviate the computational cost of TELM, yet TELM may still require a large number of sensitivity analysis. Moreover, in contrast to ELM, the equivalent linear system in TELM is dependent on the response threshold, i.e., the equivalent linear system varies as one specifies different response thresholds in FORM analysis. As a result, it is impossible to use TELM in conjunction with the response spectrum method in a way the conventional ELM could be used.

Motivated by the benefits and limitations of conventional ELM and TELM, and using the concept of mixture distribution models, a new equivalent linearization method, namely the Gaussian mixture based equivalent linearization method (GM-ELM) was recently developed (Wang and Song 2017). The method employs a univariate Gaussian mixture (GM) (McLachlan and Peel 2000) distribution model to approximate the non-Gaussian probabilistic distribution of a nonlinear system

response under stationary and ergodic assumptions. Properties of the GM distribution model enable the GM-ELM to decompose the non-Gaussian response of a nonlinear system into multiple Gaussian responses of linear single-degree-of-freedom (SDOF) oscillators. Using a probabilistic combination technique, a mixture of equivalent linear system identified by GM-ELM can provide an accurate estimation of the nonlinear response distribution.

As with conventional ELMs, GM-ELM is also a parametric method in which the parameters of the linear SDOF oscillators are identified using the parameters of the GM model. In contrast to ELM, GM-ELM can capture the non-Gaussianity of the nonlinear responses, and it has superior accuracy in estimating response statistics such as the mean up-crossing rate, the maximum response distribution and the mean peak response. On the other hand, as with TELM, the GM-ELM is developed using the concept of an equivalence in probability distribution rather than an equivalence in statistical moments. In comparison with TELM, instead of obtaining each linear system for each response threshold, GM-ELM identifies a set of linear oscillators for the whole range of the response. Moreover, GM-ELM does not require reliability analysis such as FORM that may have convergence issues and thus requires smooth constitutive laws in structural models. It has been also shown that the widely used response spectrum analysis method (Franchin 2004) can be integrated with GM-ELM.

1.3 Objectives and outline

The objective of this research is to further develop GM-ELM from the original work of Wang and Song (2017) in terms of accuracy, efficiency, and applicability,

especially targeting the practical earthquake engineering problems. For example, one of the valuable contributions of TELM, which connected the performance-based earthquake engineering (PBEE) framework and random vibration theories by proposing formalized fragility analysis procedures (Fujimura and Der Kiureghian 2007; Broccardo 2014), motivated the direction of this research. This dissertation aims to achieve four goals: (1) increasing the equivalency of linear system to the original nonlinear system, (2) extending the method to nonstationary excitations and responses, (3) making fragility analysis more efficient, and finally, (4) increasing the accuracy of first-passage probability estimates of linear and nonlinear system responses.

Chapter 2 is a review of GM-ELM which summarizes the earlier work by Wang and Song (2017). After a brief introduction to the linear random vibration analysis, the fundamental ideas on how the new equivalent-linear-system concept is retrieved from a Gaussian mixture (GM) probability density function (PDF) model of the structural response is provided. The motivations, principles and mathematical backgrounds are presented followed by the step-by-step procedure of GM-ELM. The probabilistic response combination equations to estimate nonlinear responses such as instantaneous failure probability, mean up-crossing rate, first-passage probability, and mean peak responses are discussed,

Chapter 3 introduces a new concept of bivariate GM-ELM. This chapter investigates how the estimation accuracy could be significantly improved in certain problems by increasing the dimension of response PDF through augmenting its time derivatives. The modified procedure to optimize ELS is provided and corresponding probabilistic combination equations are derived.

Chapter 4 extends GM-ELM specifically to promote applications to seismic fragility analysis in terms of versatility and efficiency. Temporal-average GM-ELM is first proposed to incorporate nonstationary excitations and responses, and intensity-augmented GM-ELM is also proposed for more efficient fragility analysis. Intensity-augmented GM-ELM identifies a universal ELS that does not depend on the scaling of the ground motion model. To further improve the efficiency of GM-ELM-based fragility analysis, an approximation method called a simple scaling approach is proposed.

Chapter 5 proposes formulations and techniques to improve the estimate of the first-passage probability in the nonlinear system by GM-ELM. A new equation for the first-passage probability is first derived under stationary Gaussian assumption. The proposed approach accounts for the temporal correlations within the sequence of the threshold-crossing events by adopting a Poisson branching process model (PBP). Then the proposed PBP-based equation is implemented into the GM-ELM analysis. To this aim, a modification factor is introduced to reflect bandwidth characteristics and envelope properties of the nonlinear responses.

Chapter 6 provides a summary of the developments and discusses the major findings. This dissertation is concluded by discussions on current limitations, requirements and potential future studies of GM-ELM.

Chapter 2. Introduction to Gaussian Mixture based Equivalent Linearization Method (GM-ELM)

2.1 Introduction

This section revisits the Gaussian Mixture based Equivalent Linearization method (GM-ELM) which was recently developed by Wang and Song (2017). GM-ELM is a nonlinear stochastic dynamic analysis approach that proposed a unique perspective on the probabilistic linearization. The main concept of GM-ELM is to identify a set of linear oscillators that collectively describes the shape of the response PDF of the nonlinear system. As its name implies, the Gaussian Mixture (GM) distribution model fitting of the response PDF of the nonlinear system is involved for this decomposition. This linearization allows us to estimate nonlinear response statistics, such as instantaneous failure probability, mean crossing rate, first-passage probability and mean peak responses, by only linear random vibration analysis and pre-derived closed-form combination equations. This chapter starts with a brief review of the random vibration theories and then the concepts, formulations, and procedures of GM-ELM are summarized.

2.2 Linear random vibration analysis at a glance

2.2.1 Objective and problem setting in random vibration analysis

Random vibration analysis deals with the response of a dynamic system under the stochastic excitations. The excitation is modeled as a random process, and by

quantifying the uncertainty propagating through the system, the dynamic behavior of the system is also described as a random process (Figure 2.1). The further interest of the random vibration analysis lies on the inference of the structural failure statistics.

Although the unknown system property could be another important uncertainty source, the randomness considered in this dissertation will be limited to those from the input excitation. Therefore, the system properties are assumed to be known and deterministic. Throughout this study, zero-mean excitation is considered, i.e. $f_g(t) = f_g^*(t) - \mu_{f^*}(t)$, in which $f_g^*(t)$ is any differentiable stochastic process and $\mu_{f^*}(t)$ is its mean, with the known spectral contents.

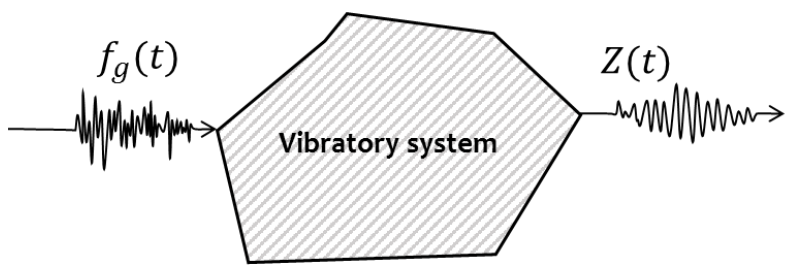

Figure 2.1 Problem setting in random vibration analysis

2.2.2 Propagation of uncertainty through a linear system

The excitation of the system is often represented in terms of power spectral density function (PSD) which is the frequency-domain counterpart of the auto-correlation function (Lutes and Sarkani 2004). PSD is an effective representation of the random process since it describes the contributions of each frequency content as well as the bandwidth characteristics, e.g. indication on the wide- or narrowband process.

Especially for a linear system subjected to a stationary excitation, in light of the superposition principles, the PSD of the response $Z(t)$ could be conveniently derived by

$$S_{ZZ}(\omega) = |H(\omega)|^2 S_{ff}(\omega) \tag{2.1a}$$

$$H(\omega) = \int_{-\infty}^{\infty} h(t) e^{-i\omega t} dt \tag{2.1b}$$

where $S_{ff}(\omega)$ denotes the PSD of the excitation. The functions $H(\omega)$ and $h(t)$ are respectively the frequency response function (FRF) and the impulse response function (IRF), both of which depend on the system properties and the response of interest. For example, if one is interested in the displacement response of a linear oscillator with mass, damping, and stiffness of m_o, c_o, and k_o, respectively, subjected to an acceleration input, the following FRF could be derived:

$$H(\omega) = \frac{m_o}{k_o + i\omega c_o - m\omega_o^2} \tag{2.2}$$

For a nonstationary input, the excitation is often presented in terms of evolutionary PSD, i.e., in the mathematical form of $S_{ff}(\omega, t) = |A(\omega, t)|^2 S_{\mathrm{o}}(\omega)$ in which $S_{\mathrm{o}}(\omega)$ is the PSD of a base stationary process and $A(\omega, t)$ is the frequency-time modulating function. In such cases, the following nonstationary response PSD can be derived:

$$S_{ZZ}(\omega, t) = |m(\omega, t)|^2 S_o(\omega) \tag{2.3a}$$

$$m(\omega, t) = \int_{-\infty}^{\infty} A(\omega, \tau) h(t - \tau) e^{-i\omega(t-\tau)} d\tau \tag{2.3b}$$

These relationships essentially describe the second-order properties of the process, and therefore it is not restricted to specific types of distributions. However, it is

noteworthy that, when the excitation is modeled as a Gaussian process, as generally adopted in the earthquake analysis, the PSD or the evolutionary PSD fully defines the characteristics of the process. Furthermore, since the linear transformation of a Gaussian random variable is also a Gaussian, the response of a linear system subjected to a Gaussian excitation is also a Gaussian process. Therefore, the stochastic properties of the linear responses can be fully identified. However, in nonlinear systems, the superposition principles do not hold and Gaussianity of the response is not guaranteed. In those cases, the properties discussed in this subsection do not hold.

2.2.3 Failure analysis of a linear system subjected to a Gaussian excitation

The failure of the system performance is often defined as an occurrence of the excessive response, such as *instantaneous failure* or the *first-passage failure* event, or the accumulation of the fatigue (Lutes and Sarkani 2004). Among these failure modes, this dissertation will focus on the former criteria. Under the Gaussian process assumption, the instantaneous failure probability given the threshold of a at a certain time-point is represented as

$$P(Z(t) > a) = 1 - F_{Z(t)} = 1 - \Phi\left(\frac{a - \mu_Z(t)}{\sigma_Z(t)}\right) \tag{2.4}$$

where $F_{Z(t)}$ denotes the cumulative distribution function (CDF) of $Z(t)$, $\Phi(\cdot)$ is standard normal CDF, and $\mu_z(t)$ and $\sigma_z(t)$ are respectively the mean and the standard deviation of the response.

On the other hand, the first-passage failure probability, which refers to the occurrence of at least one failure during a certain time interval $t \in [0, T_d]$, is often

more challenging to estimate. This is because the estimation involves the distribution of the peaks as well as their correlations. The general exact solution is unavailable for this problem, therefore, approximation approaches need to be introduced. It is common practice to assume that the crossing events follow a Poisson point process model, i.e. the interarrival times of the crossing events follow the exponential distribution and are independent of each other. This setting is often referred to as the *Poisson assumption*. The first-passage probability under the Poisson assumption is calculated by

$$Pr[\max Z(t) > a]_{t\in T_d} = 1 - A \exp\left[-\int_0^{T_d} \nu^+(a;t)dt\right] \tag{2.5}$$

where the parameter $\nu^+(a;t)$ is called mean up-crossing rate of the response, and A accounts for the condition that the initial value of the process is located below the threshold, i.e. $A = P(Z(0) < a)$. For the stationary case, Eq. (2.5) could be further simplified as

$$Pr[\max Z(t) > a]_{t\in T_d} = 1 - A \exp[-\nu^+(a)T_d] \tag{2.6}$$

It is known that the mean up-crossing rate given threshold of a can be derived from the joint PDF of response and its time derivative as (Lutes and Sarkani 2004).

$$\nu^+(a;t) = \int_0^{\infty} v f_{Z(t)\dot{Z}(t)}(a,v)dv \tag{2.7}$$

When the system response of interest is zero-mean and covariant stationary Gaussian, Eq. (2.7) can be simplified as

$$\nu^+(a) = \frac{1}{2\pi}\sqrt{\frac{\lambda_2}{\lambda_0}}\exp\left(-\frac{a^2}{2\lambda_0}\right) \tag{2.8}$$

$$\lambda_j = 2\int_0^\infty \omega^j S_{ZZ}(\omega)\, d\omega, \qquad j = 0,1,2 \tag{2.9}$$

where λ_j is the j-th order spectral moment. It is remarked that for the linear system responses, $S_{ZZ}(\omega)$ in Eq. (2.9) could be conveniently substituted with Eq. (2.9) to get closed-form approximation of its first-passage probability.

This Poisson assumption is known to be asymptotically exact for the higher threshold values for Gaussian process. However, this assumption may significantly overestimate the failure probabilities when a highly narrowband process is involved. There are advanced approximations that reflect the spectral properties in terms of the bandwidth parameters, such as Vanmarcke (1975) and Lutes (2012), which are developed under stationary Gaussian conditions.

2.3 Gaussian Mixture based ELM

This section summarizes the fundamental ideas of how an equivalent linear system concept is retrieved from a Gaussian mixture (GM) probability density function (PDF) model and random vibration theories. GM-ELM establishes a set of linear oscillators as an equivalent linear system through a Gaussian mixture representation of the PDF of a generic nonlinear response of interest, and a physical interpretation of the GM model, as shown in Figure 2.2. Specifically, GM-ELM identifies a *group* of multiple single degree-of-freedom (SDOF) oscillators as an ELS, which collectively reproduce stochastic properties of nonlinear response using combination rules formulated based on linear random vibration theories. ELS achieves the equivalence by capturing the whole shape of the response PDF by the superposition of the response PDFs of the linear oscillators.

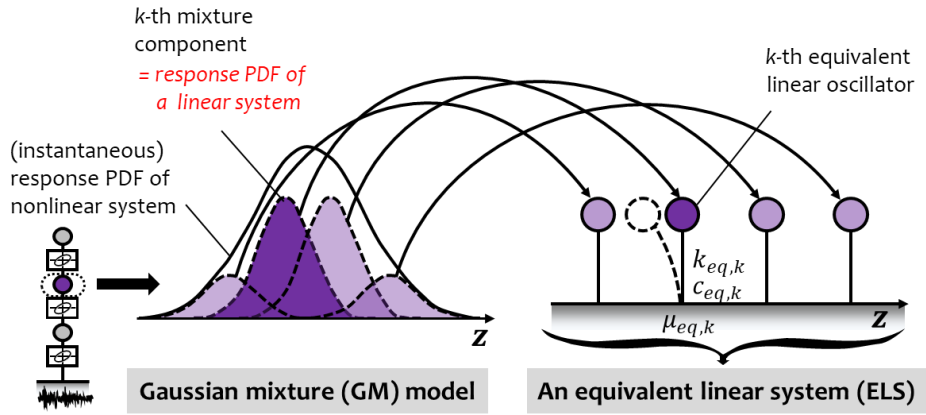

Figure 2.2 Gaussian mixture-based linearization and terminologies

The underlying assumption of GM-ELM analysis is that the input excitation is represented as a *stationary* Gaussian random process, for example, by considering strong and stationary period during an earthquake event, or using a memoryless linear or nonlinear transformation (Soong and Grigoriou 1993) of a stationary Gaussian process. Although the response of a system under stationary input is not necessarily stationary even if the system is linear (Ditlevsen and Madsen 1999), in the developments and applications of GM-ELM so far, it has been assumed that the nonlinear response of the excitation is almost stationary such that the response at any time point in the duration can be represented by the non-Gaussian PDF of a single random variable representing the target response. The non-Gaussian PDF is fitted by a GM model to describe the response by multiple Gaussian PDFs. Because the dynamic response of a linear structure excited by a Gaussian input process also follows a Gaussian distribution, the densities in the fitted GM model lead to multiple linear SDOF oscillators that collectively describe the nonlinear response. Despite its simplicity, GM model is able to represent general probability densities showing complex shapes and even multiple modes (McLachlan and Peel 2000).

Consider a general MDOF structural system subjected to a zero-mean, stationary Gaussian ground motion excitation, and let the PDF of a generic nonlinear response $Z(t)$, for example, inter-story drift at certain parts of the system, be denoted as $f(z;t)$. Assuming $Z(t)$ achieves stationarity, the PDF $f(z;t)$ is written as $f(z)$ in the following discussions. Given an estimate of $f(z)$ (see Section 2.4 for how to obtain the PDF), a GM surrogate PDF model $f_{GM}(z;\boldsymbol{\nu})$, in which vector $\boldsymbol{\nu}$ represents parameters of the GM distribution model, is employed, i.e.

$$f(z) \simeq f_{GM}(z;\boldsymbol{\nu}) = \sum_{k=1}^{K} \alpha_k f_{\mathcal{N}}(z;\mu_{z,k},\sigma_{z,k}) \tag{2.10}$$

in which K denotes the number of Gaussian densities in the mixture, α_k, $k = 1,\dots,K$, are relative weights of the Gaussian densities satisfying the conditions $\sum_{k=1}^{K}\alpha_k = 1$ and $\alpha_k > 0$ for $\forall k$, and $f_{\mathcal{N}}(z;\mu_{z,k},\sigma_{z,k})$ denotes the univariate Gaussian PDF with mean $\mu_{z,k}$ and standard deviation $\sigma_{z,k}$. Thus, the distribution parameters of the GM model are summarized as $\boldsymbol{\nu} = \{\alpha_1,\dots,\alpha_K,\mu_{z,1},\dots,\mu_{z,K},\sigma_{z,1},\dots,\sigma_{z,K}\}$.

If the probability distribution of a nonlinear response is successfully represented by a GM model, the random nonlinear response $Z(t)$ can be described as

$$Z(t) \cong \sum_{k=1}^{K} I_k(t)\cdot Z_k(t) = \sum_{k=1}^{K} I_k(t)\cdot\left[\mu_{z,k} + D_k(t)\right] \tag{2.11}$$

where $I_k(t)$ is the *k*-th element of a *K*-dimensional random vector in which only one element takes 1 while the others take 0 according to the probabilities α_k, and $Z_k(t)$ follows Gaussian distribution with mean $\mu_{z,k}(t)$ and standard deviation $\sigma_{z,k}(t)$. In Eq. (2.11), $Z_k(t)$ is alternatively described as $\mu_{z,k} + D_k(t)$ in which $D_k(t)$ is a zero-mean Gaussian process with standard deviation $\sigma_{z,k}$.

Eq. (2.11) depicts the concept of the *probabilistic decomposition* of a non-Gaussian response into multiple Gaussian responses, which is analogous to the modal analysis approach. In the modal analysis approach, the response of a linear MDOF system is represented by multiple linear oscillators. In GM-ELM, the non-Gaussian response of a nonlinear system is represented by multiple linear oscillators whose relative importance (in a probabilistic sense), 'location' (with respect to the origin of the *z*-axis, see Figure 2.3), and root-mean-square oscillation around the specified location are represented respectively by α_k, $\mu_{z,k}$ and $\sigma_{z,k}$. As a result, linear-system concept can be retrieved from a GM structural response PDF model.

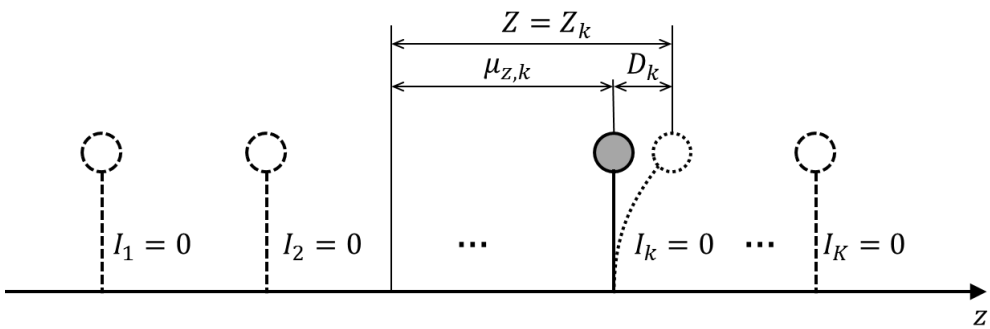

Figure 2.3 A physical interpretation of densities in the Gaussian mixture model (after Wang and Song (2017))

2.4 Procedure of GM-ELM

The followings are details of the main steps of GM-ELM analysis. The procedure is summarized in Figure 2.4 and Table 2.1.

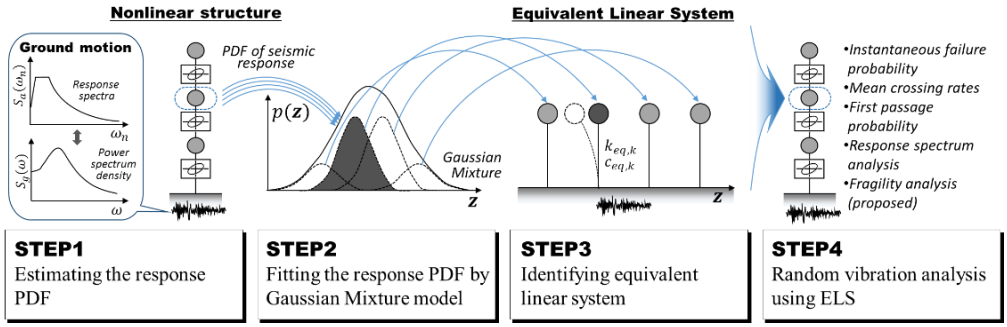

Figure 2.4 Main steps of GM-ELM analysis

[Step1] Estimating the response PDF

In GM-ELM, to determine the parameters $\boldsymbol{v}$ of the GM model in Eq. (2.10), one needs to first obtain the PDF $f(z)$ for the response of interest. Only for some specialized, and usually simple nonlinear systems, one may obtain analytical response PDFs using Fokker-Planck equations. For general applications, the PDF can be approximated by use of FORM-based approach (Wang *et al*. 2016), expansion method (Chakraborty and Chowdhury 2014; Schöbi *et al.* 2015), response surface method (Alibrandi 2014; Alibrandi and Der Kiureghian 2012; Faravelli 1989), or numerical integration method using dimensional reduction (Rahman and Xu 2004). Approximation methods to solve Fokker-Planck approximations can also be used (Spencer and Bergman 1993; Chen *et al.* 2017). Another general approach is to generate samples of the response process $Z(t)$ to represent the response PDF $f(z)$. In this approach, by assuming ergodicity as well as stationarity, responses sampled at the equally discretized time points can be utilized for efficient estimation of $f(z)$. As a result, only several rounds of nonlinear time history analysis can provide sufficient amount of the samples. It is important to note that the methodology of GM-ELM is independent of how the PDF $f(z)$ is constructed.

[Step2] Fitting the response PDF by GM model

Next, the estimated PDF $f(z)$ is fitted by GM model as in Eq. (2.10). If the response PDF is estimated by the direct samplings discussed in Step 1, the Expectation-Maximization (EM) approach can be utilized to obtain parameters with the maximum likelihood (Bishop 2006). Otherwise, if the shape of PDF is estimated at discrete grid points, the modified EM-algorithm used in Kawabata (2008) could be employed. When the PDF is constructed in the functional form, both the EM and modified EM algorithm can be used, by either directly generating samples from the PDF, or by discretizing the PDF into the finite grid-point values, respectively.

[Step3] Identifying equivalent linear system

The Gaussian densities in the fitted GM model are now used to identify the physical parameters of the equivalent linear oscillators, one of which is randomly activated at every time point, and spontaneously "switches" from one to another. In this regard, α_k represents the occurrence rate of the *k*-th equivalent oscillator during the response duration, μ_k is interpreted as shifted origins of the base location of the oscillator, and σ_k is the response variance of the *k*-th linear oscillator. In order to identify parameters of the ELS given the knowledge of response variances, the following relationship is considered (Lutes and Sarkani 2004):

$$\sigma_{z,k}^2 = 2\int_0^\infty |H_k(\omega)|^2 S_g(\omega) d\omega \tag{2.12}$$

where $S_g(\omega)$ is the auto-PSD of the ground motion excitation, and $H_k(\omega)$ is the FRF of the k-th linear system, i.e.

$$H_k(\omega) = \frac{s_{eq,k}}{k_{eq,k} + i\omega c_{eq,k} - m_{eq,k}\omega^2} \tag{2.13}$$

in which $m_{eq,k}$, $c_{eq,k}$, and $k_{eq,k}$ are respectively the mass, damping, and stiffness of the *k*-th oscillator, the parameter $s_{eq,k}$ can be determined appropriately based on the response quantity of interest. For example, when the deformation of the structure under seismic excitation is of interest, $s_{eq,k} = m_{eq,k}$ is used. It is impossible to identify all three parameters of the FRF in Eq. (2.13) by only using Eq. (2.12), although they need to be identified to fully define an equivalent system. To remedy this issue, Wang and Song (2017) proposed to identify only the parameter $k_{eq,k}$ by substituting Eq. (2.13) into Eq. (2.12), while pre-specifying $m_{eq,k}$ and $c_{eq,k}$ respectively as the mass and initial damping of the nonlinear system.

For applications to a response of MDOF system, m_{eq}, c_{eq} and s_{eq} can be presumed as

$$\begin{aligned} m_{eq} &= \boldsymbol{\psi}^T \boldsymbol{M} \boldsymbol{\psi} \\ c_{eq} &= \boldsymbol{\psi}^T \boldsymbol{C}_0 \boldsymbol{\psi} \\ s_{eq} &= (\boldsymbol{q}^T \boldsymbol{\psi}) \cdot (\boldsymbol{\psi}^T \boldsymbol{\mathcal{F}}) \end{aligned} \tag{2.14}$$

where $\boldsymbol{M}$ and $\boldsymbol{C}_0$ are the mass and initial damping matrix of the nonlinear system, $\boldsymbol{\mathcal{F}}$ is the spatial distribution of the input ground motion, $\boldsymbol{q}$ is a deterministic vector which depends on the response quantity of interest, and $\boldsymbol{\psi}$ is a 'representative' response shape vector. The shape vector $\boldsymbol{\psi}$ can be selected as the modal vector (for a linear system with the initial structural properties of the nonlinear system) which contributes the most to the response quantity of interest. If the initial structural properties would lead to an unsuitable linear system (e.g. a system with zero stiffness), one could use the equivalent linear system obtained from conventional

ELM to set $\boldsymbol{\psi}$, m_{eq}, c_{eq} and s_{eq} values. With three parameters determined from Eq. (2.14), Eq. (2.13) is substituted into Eq. (2.12) to determine the stiffness $k_{eq,k}$.

From the complete knowledge of FRF of equivalent linear oscillator, response statistics such as the mean up-crossing rate and first-passage probability can be conveniently computed. The next section explains Step 4 of the GM-ELM analysis using the ELS identified by Steps 1-3.

Table 2.1 Procedure of GM-ELM

Step	Procedure
1	Obtain the response PDF, $f(z)$, of a nonlinear response of interest
2	Identify the Gaussian mixture PDF model $f_{GM}(z;\boldsymbol{v})$ that best fits the PDF as in Eq. (2.10)
3	Obtain the frequency response functions associated with each Gaussian density in GM model by Eq. (2.12) and Eq. (2.13)
4	Compute the crossing rate and first-passage probability, or/and compute the mean peak response using elastic response spectra. (Details discussed in Section 2.5)

2.5 Nonlinear stochastic dynamic analysis

2.5.1 GM-ELM for random vibration analysis

The identified ELS is used to evaluate stochastic nonlinear responses in terms of instantaneous failure probability, mean up-crossing rate, first passage probability, and mean peak response by performing linear random vibration analysis for each oscillator and combine the results. It is noted that the first passage probability is useful in computing the probability of failure during a finite time period, e.g. earthquake duration, therefore, is often used for seismic fragility analysis. A combination rule was derived to calculate the first-passage probability using the

mean up-crossing rates of the linear oscillators in ELS. Firstly, the instantaneous failure probability with respect to a threshold a can be computed as

$$\begin{aligned} Pr(Z > a) &= \sum_{k=1}^{K} Pr(I_k = 1) Pr(Z > a | I_k = 1) \\ &= \sum_{k=1}^{K} \alpha_k \left[1 - \Phi\left(\frac{a - \mu_{z,k}}{\sigma_{z,k}} \right) \right] \end{aligned} \tag{2.15}$$

For the mean up-crossing rate, consider the expression (Hagen and Tvedt 1991)

$$\nu^+(a) = \lim_{\delta t \to 0} \frac{Pr\{Z(t) < a \cap Z(t + \delta t) > a\}}{\delta t} \tag{2.16}$$

From an intuition that, for an infinitesimal δt, it is unlikely that the linear oscillator 'switches' from one of the *K* equivalent linear oscillator to another, Eq. (2.16) can be rewritten as

$$\begin{aligned} \nu^+(a) &= \lim_{\delta t \to 0} \frac{\sum_{k=1}^{K} \alpha_k \, Pr\{Z_k(t) < a \cap Z_k(t + \delta t) > a\}}{\delta t} \\ &= \sum_{k=1}^{K} \alpha_k \nu_k^+(a) \end{aligned} \tag{2.17}$$

in which $Z_k(t) = D_k(t) + \mu_{z,k}$ denotes the response of the k-th linear oscillator, and $\nu_k^+(a)$ denotes the up-crossing rate of the k-th linear oscillator. The mean up-crossing rate $\nu_k^+(a)$ is computed by Rice formula (Rice 1944) in which zeroth and second order spectral moments are computed by using the frequency response function of the equivalent SDOF oscillator, that is

$$\nu_k^+(a) = \frac{1}{2\pi} \sqrt{\frac{\lambda_{2,k}}{\lambda_{0,k}}} \exp\left[-\frac{\left(a - \mu_{z,k}\right)^2}{2\lambda_{0,k}} \right] \tag{2.18}$$

where the j-th order spectral moment of the response $\lambda_{j,k}$ is computed by

$$\lambda_{j,k} = 2\int_0^\infty \omega^j |H_k(\omega)|^2 S_g(\omega)\, d\omega \qquad j = 0,1,2 \tag{2.19}$$

Assuming that the passage events follow a Poisson random process, the single- and double-sided first-passage probability can be represented in terms of mean up-crossing rates, i.e.

$$Pr[\max Z(t) > a]_{t\in T_d} = 1 - A \exp\left[-\sum_{k=1}^{K} \alpha_k \nu_k^+(a)\, T_d\right] \tag{2.20}$$

where A is probability of starting from the safe zone, i.e. $\mathrm{P}(Z(0) < a)$. The parameter T_d denotes the duration of the excitation. When GM-ELM is applied to earthquake problems, the strong (stationary) motion duration can be used as T_d for an approximation. If the response is assumed as symmetric, the double-sided first passage probability can be estimated as

$$Pr[\max|Z(t)| > a]_{t\in T_d} = 1 - A \exp\left[-2\sum_{k=1}^{K} \alpha_k \nu_k^+(a)\, T_d\right] \tag{2.21}$$

2.5.2 GM-ELM for response spectrum analysis

It is noted that by using GM-ELM, the mean peak response of a *nonlinear* system can be conveniently derived from a set of *linear elastic* response spectra. Although one could compute the mean peak response by a numerical integration of the first-passage probability distribution, when only the mean peak response is of interest, response spectrum analysis has been widely used as a powerful and practical tool for the seismic analysis and design. It is noted that this is a unique characteristic of GM-ELM, which is not attainable in TELM.

The procedure of GM-ELM response spectrum analysis can be understood through an analogy to modal combination methods, such as complete quadratic combination (CQC) (Der Kiureghian 1981) or square root of the sum of the squares (SRSS). While traditional modal combination rules synthesize contributions of each mode to the behavior of *linear MDOF* system, the proposed GM-ELM response spectrum method approximates the mean peak response of nonlinear SDOF or MDOF system response by the mean peak responses of equivalent linear SDOFs, which can be obtained conveniently from the ordinates of elastic response spectra. But unlike conventional modal analysis, GM-ELM decomposes the nonlinear system based on stochastic characteristics, therefore different combination rules specialized for GM-ELM are used.

Specifically, the mean peak absolute response of *k*-th linear oscillator could be expressed as

$$E[\max|Z_k(t)|]_{t\in T_d} \simeq D_{k,max} + |\mu_k| = \Gamma S_a(\omega_k, \zeta_k) + |\mu_k| \tag{2.22}$$

where ω_k and ξ_k respectively denote the natural frequency and damping ratio of the k-th equivalent linear oscillator, $S_d(\omega_k, \xi_k)$ is the ordinate of the linear displacement response spectrum at ω_k and ξ_k, and $\Gamma = |s_{eq}|/m_{eq}$ is a scaling factor of $S_d(\omega_k, \xi_k)$. The combination rule is written as a weighted average of the response of each oscillator, i.e.

$$E[\max|Z(t)|]_{t\in T_d} \simeq \sum_{k=1}^{K} \bar{\alpha}_k E[\max|Z(t)|]_{t\in T_d} \tag{2.23}$$

where $\sum_{k=1}^{K} \bar{\alpha}_k = 1$. It is noted that when $\bar{\alpha}_k = \alpha_k$, Eq. (2.23) will provide the lower bound of the mean peak responses (Wang and Song 2017). To relax the lower bound, a heuristic weighting factor is introduced as

$$\bar{\alpha}_k = \frac{l_k \alpha_k}{\sum_{j=1}^{K} l_j \alpha_j} \tag{2.24}$$

in which l_k is a binary function that gives 1 if $E[\max|Z_k(t)|]_{t\in T_d}$ satisfies

$$E[\max|Z_k(t)|]_{t\in T_d} \in \left[0.95\sum_{k=1}^{K}\alpha_k E[\max|Z_k(t)|]_{t\in T_d}\ , \max\left\{E[\max|Z_k(t)|]_{t\in T_d}\right\}\right] \tag{2.25}$$

and gives 0 otherwise. The combination rule in Eq. (2.23) is heuristic in its nature, despite the fact that the equation is found to be fairly accurate in many cases.

2.6 Conclusions

This chapter reviews the main features of GM-ELM to facilitate the readers' understanding. GM-ELM is a new equivalent linearization method developed by Wang and Song (2017) for random vibration analysis of the nonlinear system response. By decomposing arbitrary non-Gaussian response of the nonlinear system into the multiple Gaussian responses of the linear SDOF oscillators, the equivalent linear system (ELS) is obtained. Once the ELS is acquired, the probabilistic combination techniques enable us to approximate the nonlinear failure statistics by means of only linear random vibration analysis. Along with the instantaneous failure probability, nonlinear responses of the mean crossing rate, first-passage probability, and mean peak response can be estimated by GM-ELM analysis. Due to its distinctive definition, GM-ELM possesses several advantages over other ELM approaches. Since it captures the non-Gaussianity of the nonlinear responses, estimated response statistics are relatively accurate even with the extremely high thresholds compared to conventional ELM. Also, GM-ELM does not require reliability analysis such as FORM that may have convergence issues as in TELM.

Further, GM-ELM does not have any restrictions on the choice the nonlinear model. In the subsequent chapters, retaining these useful properties of GM-ELM, the method is modified and generalized to further strengthen its applications.

Chapter 3. Bivariate GM-ELM

3.1 Introduction

The previous chapter introduced the concept of GM-ELM, why it works and how it could be applied to random vibration analysis. However, it was shown that the system parameters of equivalent linear oscillators in GM-ELM are determined by the parameters of the fitted Gaussian densities in the mixture, while the fitted GM does not provide sufficient information on the structural properties, i.e. only equivalent stiffness values were optimized. To handle this problem, a strategy to pre-specify several system parameters was introduced and discussed in Section 2.4, which provides reasonable estimates for typical nonlinear structural models. However, it is later found that the provided heuristic presets may result in significant errors depending on the characteristic of the nonlinear system and ground motions. To address this issue, this chapter further develops GM-ELM by using a bivariate GM model fitted to the response and the time rate of the response (Yi *et al.* 2018).

3.2 Needs for the development of bivariate GM-ELM

The GM-ELM hinges on the idea of decomposing a nonlinear system based on the property of Gaussian probability density function, but the process is inevitably subjective. As discussed in Section 2.4, a majority of parameters in FRF is pre-defined arbitrarily, and thus the equivalent linear system is represented solely by $k_{eq,k}$ in Eq. (2.13).

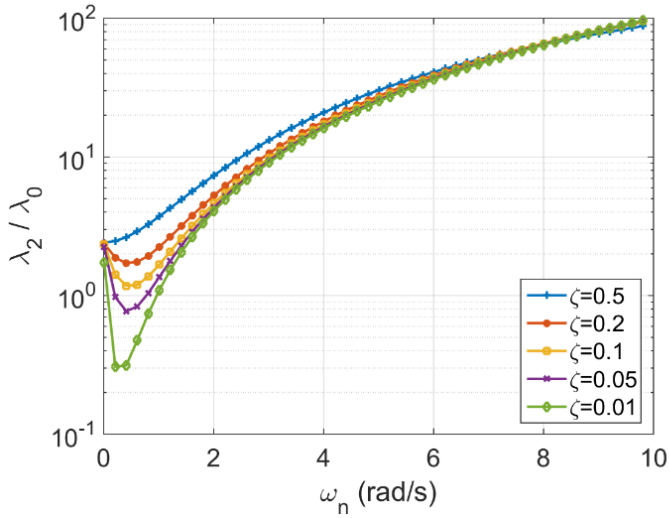

Figure 3.1 The ratios of the second to zeroth spectral moments of linear SDOF systems subjected to ground motion described by modified Kanai-Tajimi model

For some typical nonlinear structures and ground motions whose resulting structural behaviors are not sensitive to the range of damping, the practical assumption can be valid. However, for systems with stiffer equivalent linear components, the response can be sensitive to the arbitrary choice of $c_{eq,k}$. For example, Figure 3.1 shows the ratio of the second to zeroth spectral moments (Lutes and Sarkani 2004), i.e. ratio of the variance of the velocity to that of the displacement, for an SDOF oscillator (with the natural frequency ω_n and the damping ratio ζ) excited by ground motions modeled by a modified Kanai-Tajimi filter whose auto-PSD is

$$S_f(\omega) = S_0 \frac{\omega_f^4 + 4\zeta_f^2\omega_f^2\omega^2}{\left(\omega_f^2 - \omega^2\right)^2 + 4\zeta_f^2\omega_f^2\omega^2} \cdot \frac{\omega^4}{(\omega_s^2 - \omega^2)^2 + 4\zeta_s^2\omega_s^2\omega^2} \qquad (3.1)$$

where $S_0 = 0.01\ \mathrm{m^2/s^3}$ is a scale factor, and $\omega_f = 15\ \mathrm{rad/s}$, $\zeta_f = 0.6$, $\omega_s = 1.5\ \mathrm{rad/s}$ and $\zeta_s = 0.6$ are the filter model parameters. It is shown that, as the

natural frequency decreases, the ratio gets more sensitive to the damping ratio. However, it is difficult to pre-specify $m_{eq,k}$ and $c_{eq,k}$ because it is challenging to predict how nonlinearity will affect the converged mixture model. The discrepancy caused by an improper choice of those parameters is large especially when calculating mean crossing rates for low thresholds, as will be shown in the numerical examples of this chapter.

The limitation can be understood in another point of view as follows. For a complete definition of a general linear SDOF system subjected to a ground acceleration excitation, one needs to specify two parameters, namely natural frequency $\omega_{eq,k}$ and damping ratio $\zeta_{eq,k}$. However, by identifying one parameter $k_{eq,k}$ while assuming other parameters, i.e. c_{eq} and m_{eq} arbitrarily, one of the two variables ($\omega_{eq,k}$ and $\zeta_{eq,k}$) should be automatically determined by the other through the relationship of $\zeta_{eq,k} = c_{eq}/(2m_{eq}\omega_{eq,k})$. To get rid of this restriction and bias in estimates, it is desirable to introduce one more system parameter and identify the parameters independently.

Therefore, it is proposed to incorporate additional information to GM-ELM by using the joint PDF of the response $Z(t)$ and its time derivative $\dot{Z}(t)$ modeled by a bivariate Gaussian mixture, instead of univariate mixture for $Z(t)$ only. In the proposed method, each bivariate Gaussian density in the mixture represents an equivalent SDOF linear system with shifted response and shifted time rate of response. The proposed bivariate GM-ELM has the following advantages: **a)** The bivariate GM-ELM can incorporate the coupling effects between the response and its time derivative into the estimation; **b)** The bivariate GM-ELM is consistent with the theoretical backgrounds of probabilistic decomposition, since the derivative of

stationary Gaussian random process for the response of equivalent linear oscillators is also a Gaussian process; **c)** In order to account for the dissipated energy from nonlinear hysteretic behaviors via ELS, it is insufficient to define only equivalent stiffness, which does not reveal the energy dissipation mechanism, and it is desirable to decide equivalent damping as well; **d)** additional conditions regarding time derivative of the response increases the flexibility of the method to involve equivalent damping and abolishes heuristic constraints; **e)** The bivariate GM-ELM does not require additional computational effort for nonlinear dynamic analysis compared to the univariate version because the time derivative response can be easily acquired as the by-product of dynamic analysis or by post-processing; and **f)** the proposed development also provides mathematical reasoning beyond the intuitive explanation for response statistics, such as mean up-crossing rate and first-passage probability equations, as will be illustrated in Section 3.4.

3.3 Development of bivariate GM-ELM

3.3.1 Parameters of bivariate Gaussian mixture model

In the proposed bivariate GM-ELM, instead of univariate GM model in Eq. (2.10), bivariate GM model $f_{GM}(\boldsymbol{z};\boldsymbol{\nu})$ is introduced in the space of generic nonlinear response $Z(t)$ and its time derivative $\dot{Z}(t)$, denoted by $\boldsymbol{z}=\{z,\dot{z}\}$ as follows:

$$f(\boldsymbol{z}) \simeq f_{GM}(\boldsymbol{z};\boldsymbol{\nu}) = \sum_{k=1}^{K} \alpha_k f_{\mathcal{N}_2}(\boldsymbol{z};\boldsymbol{\mu}_k,\boldsymbol{\Sigma}_k) \tag{3.2}$$

in which K is the number of the bivariate Gaussian densities used in the mixture model, α_k is the relative weight, and $f_{\mathcal{N}_2}(\boldsymbol{z};\boldsymbol{\mu}_k,\boldsymbol{\Sigma}_k)$ denotes the bivariate

Gaussian PDF, each representing equivalent linear oscillators with mean $\boldsymbol{\mu}_k = \{\mu_{z,k}, \mu_{\dot{z},k}\}$ and (2×2) covariance matrix of $Z(t)$ and $\dot{Z}(t)$, denoted by $\boldsymbol{\Sigma}_k$. The parameter set is thus summarized as $\boldsymbol{\nu} = \{\alpha_1, \dots, \alpha_K, \boldsymbol{\mu}_1, \dots, \boldsymbol{\mu}_K, \boldsymbol{\Sigma}_1, \dots, \boldsymbol{\Sigma}_K\}$.

Given the joint probability density of a nonlinear response and its time derivative is successfully represented by a bivariate GM model with K densities, the random nonlinear response $Z(t)$ and derivative response $\dot{Z}(t)$ can be described as

$$\boldsymbol{Z}(t) \cong \sum_{k=1}^{K} I_k(t) \cdot \boldsymbol{Z}_k(t) = \sum_{k=1}^{K} I_k(t) \cdot [\boldsymbol{\mu}_k(t) + \boldsymbol{D}_k(t)] \tag{3.3}$$

where at a specified time point t, $I_k(t)$ is the *k*-th element of a *K*-dimensional random vector in which only one element takes 1 while the others take 0 according to the probabilities $\alpha_k(t)$, with $\sum_{k=1}^{K} \alpha_k(t) = 1$, while $\boldsymbol{Z}_k(t) = \{Z_k(t), \dot{Z}_k(t)\}$ follows the bivariate Gaussian distribution with mean $\boldsymbol{\mu}_k$, and covariance $\boldsymbol{\Sigma}_k$. In Eq. (3.3), $\boldsymbol{Z}_k(t)$ is alternatively described in terms of $\boldsymbol{D}_k(t)$ which is a zero-mean bivariate Gaussian process with covariance $\boldsymbol{\Sigma}_k$. Assuming that the response is stationary, the time term t in the processes and distribution parameters will be omitted for simplicity in the following discussions. A probabilistic decomposition in Eq. (3.3) is illustrated in Figure 3.2.

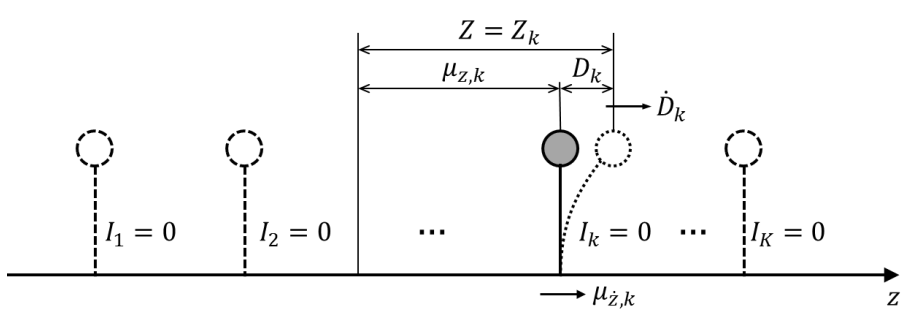

Figure 3.2 A physical interpretation of mixture components for bivariate GM-ELM

Next, given a set of samples $\boldsymbol{z}_i$ drawn from the nonlinear response PDF $f(\boldsymbol{z})$, the parameters $\boldsymbol{\nu}$ of the GM model $f_{GM}(\boldsymbol{z};\boldsymbol{\nu})$ that 'best' fit the observed data can be obtained by the maximum likelihood estimation (McLachlan and Peel 2000), i.e.

$$\boldsymbol{\nu}^* \cong \underset{\boldsymbol{\nu}}{\operatorname{argmax}} \frac{1}{N}\sum_{i=1}^{N} \ln f_{GM}(\boldsymbol{z}_i;\boldsymbol{\nu}) \tag{3.4}$$

in which $\arg\max$ denotes the argument of the maxima. An iterative updating rule in the so-called expectation-maximization (EM) algorithm can be used to solve Eq. (3.4), i.e. (see McLachlan and Peel (2000) for more details)

$$\mu_k = \frac{\sum_{i=1}^{N} \Upsilon_{i,k}\boldsymbol{z}_i}{\sum_{i=1}^{N} \Upsilon_{i,k}} \tag{3.5a}$$

$$\boldsymbol{\Sigma}_k = \frac{\sum_{i=1}^{N} \Upsilon_{i,k}(\boldsymbol{z}_i - \boldsymbol{\mu}_k)(\boldsymbol{z}_i - \boldsymbol{\mu}_k)^{\mathrm{T}}}{\sum_{i=1}^{N} \Upsilon_{i,k}} \tag{3.5b}$$

$$\alpha_k = \frac{\sum_{i=1}^{N} \Upsilon_{i,k}}{N} \tag{3.5c}$$

in which the coefficient $\Upsilon_{i,k}$ is expressed as

$$\Upsilon_{i,k} = \frac{\alpha_k f_{\mathcal{N}_2}(\boldsymbol{z}_i;\boldsymbol{\mu}_k,\boldsymbol{\Sigma}_k)}{\sum_{j=1}^{K} \alpha_j f_{\mathcal{N}_2}(\boldsymbol{z}_i;\boldsymbol{\mu}_j,\boldsymbol{\Sigma}_j)} \tag{3.6}$$

Note that the covariance matrix should be enforced to be diagonal ($\Sigma_{\boldsymbol{k}(i,j)} = 0,$ if $i \neq j$) in every iteration step to satisfy the uncorrelated relationship between the stationary response and its time derivative (Lutes and Sarkani 2004). The algorithm is summarized as follows:

1) *Initializing bivariate GM model*: Set value K (e.g. $K \geq 36$), which denotes the number of bivariate Gaussian distributions in the mixture. Set other initial parameters of the mixture $f_{GM}(\boldsymbol{z};\boldsymbol{\nu})$ as well. For example, one can set all α_k

to $1/K$, μ_k to a random number drawn from a uniform distribution that covers the response domain of interest, and all $\mathbf{\Sigma}_k$ to a diagonal matrix representing variance of each dimensions.

2) *Updating*: Use Eqs. (3.5) and (3.6) in the order (3.6), (3.5) iteratively to update parameters of the GM. Enforce $\mathbf{\Sigma}_k$ to be diagonal at every iteration step as explained above. Stop the updating process if $\left|L^{(s)} - L^{(s-1)}\right|/L^{(s)} \leq Tol$ is satisfied, where $L^{(s)} = \sum_{i=1}^{N} \ln f_{GM}(\boldsymbol{z}_i; \boldsymbol{\nu}^{(s)})\,/N$ is an indicator of the likelihood for the s-th step, and $\boldsymbol{\nu}^{(s)}$ denotes the parameters of the GM for that step.

It is found from the numerical examples in the dissertation that, for $f_{GM}(\boldsymbol{z}; \boldsymbol{\nu})$, $K = 64$, and at least $K \geq 36$ is sufficient to provide an accurate approximation of $f(\boldsymbol{z})$ in most cases, and the accuracy is not overly sensitive to the selected value of K. However, for a highly nonlinear system having eccentric tail behavior, a larger value of K may be required for GM fitting. In such case, an optimal number of mixture K can be empirically determined, e.g. by adding mixture components until the increase in likelihood of the samples $L = \sum_{i=1}^{N} \ln f_{GM}(\boldsymbol{z}_i; \boldsymbol{\nu})\,/N$ becomes relatively small.

3.3.2 Structural parameters of equivalent linear system (ELS)

While the univariate GM-ELM uses only the information on the response variances as in Eq. (2.12), the bivariate GM-ELM can use not only Eq. (2.12) but also the relationship for the variance of time-derivate response to provide additional information for identifying equivalent linear system (Lutes and Sarkani 2004)., i.e.

$$\sigma_{z,k}^2 = \int_{-\infty}^{\infty} |H_k(\omega)|^2 S_g(\omega) d\omega, \qquad k = 1, \dots, K \tag{3.7a}$$

$$\sigma_{\dot{z},k}^2 = \int_{-\infty}^{\infty} \omega^2 |H_k(\omega)|^2 S_g(\omega) d\omega, \qquad k = 1, \dots, K \tag{3.7b}$$

where, $H_k(\omega)$ is the FRF of the equivalent linear oscillator in Eq. (2.13). Using the knowledge on $\sigma_{z,k}$ and $\sigma_{\dot{z},k}$ available in Eqs. (3.7a) and Eq. (3.7b), respectively, the linear system parameter $c_{eq,k}$ and $k_{eq,k}$ can be determined without introducing heuristic constraints. If the response of interest is the displacement of a general SDOF system or inter-story drift of a general MDOF system, it is reasonable to set the modal mass of specific floor as pre-defined value of equivalent mass $m_{eq,k}$ and the scale factor s_{eq}.

3.4 Nonlinear stochastic dynamic analysis

3.4.1 Random vibration analysis by bivariate GM-ELM

Various statistics of nonlinear responses can be computed by linear random vibration analysis of the equivalent systems obtained by bivariate GM-ELM, including instantaneous failure probability, mean up-crossing rate, and the first-passage probability.

Firstly, the instantaneous failure probability with respect to a threshold a can again be computed as

$$\begin{aligned} Pr(Z > a) &= \sum_{k=1}^{K} Pr(I_k = 1) Pr(Z > a | I_k = 1) \\ &= \sum_{k=1}^{K} \alpha_k \left[1 - \Phi\left(\frac{a - \mu_{z,k}}{\sigma_{z,k}} \right) \right] \end{aligned} \tag{3.8}$$

Bivariate GM-ELM allows us to compute instantaneous probabilities with regards to the time derivative $\dot{Z}(t)$ as well. This can be done by replacing the mean and standard deviation of the response $Z(t)$ in Eq. (3.8) by those of the time derivative $\dot{Z}(t)$.

With the development of the bivariate GM-ELM, the mean crossing rate can be computed alternatively to Eq. (2.17). In theories of linear random vibration analysis (Lutes and Sarkani 2004; Newland 2005), the mean up-crossing rate of a general response $Z(t)$ can be computed by the joint PDF of $Z(t)$ and $\dot{Z}(t)$, i.e.

$$\nu^+(a) = \lim_{\Delta t \to 0} \frac{1}{\Delta t} \int_0^\infty \int_{a-\dot{z}\Delta t}^a f(z,\dot{z}) dz\, d\dot{z} = \int_0^\infty \dot{z}\, f(a,\dot{z}) d\dot{z} \tag{3.9}$$

Substituting the fitted bivariate GM model $f_{GM}(\boldsymbol{z};\boldsymbol{\nu})$ of Eq. (3.2) into Eq. (3.9), we get

$$\nu^+(a) = \sum_{k=1}^K \alpha_k \int_0^\infty \dot{z} f_{\mathcal{N}_2}(a,\dot{z};\boldsymbol{\mu}_k,\boldsymbol{\Sigma}_k) d\dot{z} = \sum_{k=1}^K \tilde{\alpha}_k \nu_k^+(a) \tag{3.10}$$

which leads to the same expression as Eq. (2.17) except the contribution factor of each linear component which is now modified using the statistics derived from the bivariate PDF, i.e.

$$\tilde{\alpha}_k = \sqrt{2\pi}\left(\varphi\left(\delta_{\dot{z},k}\right) + \delta_{\dot{z},k} - \delta_{\dot{z},k}\Phi\left(-\delta_{\dot{z},k}\right)\right) \tag{3.11}$$

where $\varphi(\cdot)$ and $\Phi(\cdot)$ are the PDF and CDF of standard normal distribution, respectively, and $\delta_{\dot{z},k} = \mu_{\dot{z},k}/\sigma_{\dot{z},k}$.

Assuming that the up-crossings follow a Poisson process with mean occurrence rate $\nu^+(a)$, single- and double-sided first-passage probabilities can be estimated via

$$Pr[\max Z(t) > a]_{t\in T_d} = 1 - A\exp[-\nu^+(a)T_d] = 1 - A\exp\left[-\sum_{k=1}^{K}\tilde{\alpha}_k\nu_k^+(a)\,T_d\right] \quad (3.12a)$$

$$Pr[\max|Z(t)| > a]_{t\in T_d} = 1 - A\exp[-2\nu^+(a)T_d] = 1 - A\exp\left[-2\sum_{k=1}^{K}\tilde{\alpha}_k\nu_k^+(a)\,T_d\right] \quad (3.12b)$$

where A denotes the probability of initial response being in the safe-domain, and T_d is the duration of excitation. Considering the fact that the equivalent linear system is developed under the stationary assumption, the excitation duration can be defined as, for example, strong (stationary) motion duration of a given earthquake event.

The procedure of bivariate GM-ELM for stochastic dynamic analysis is summarized in Table 3.1. It basically follows that of univariate GM-ELM introduced in Figure 2.4 and Table 2.1.

Table 3.1 Procedure of bivariate GM-ELM

Step	Procedure
1	Obtain the joint PDF, $f(\boldsymbol{z})$, of a nonlinear response of interest.
2	Identify a bivariate Gaussian mixture PDF model $f_{GM}(\boldsymbol{z};\boldsymbol{\nu})$ that best fits the PDF $f(\boldsymbol{z})$ as in Eq. (3.2) (Section 3.3.1)
3	Obtain the frequency response functions associated with each Gaussian density in the bivariate GM model $f_{GM}(\boldsymbol{z};\boldsymbol{\nu})$ by Eq. (3.7)
4	Compute the crossing rate and first-passage probability (Section 3.4.1), or/and compute the mean peak response using elastic response spectra. (Details discussed in 3.4.2)

3.4.2 Response spectrum analysis by bivariate GM-ELM

As discussed in Section 2.5.2, using GM-ELM, the mean peak responses of the nonlinear system can be presented in terms of the mean peak responses of the linear oscillators. This useful feature allows GM-ELM to utilize the elastic response spectrum curves, widely used in practical earthquake engineering applications, to predict the seismic response of the nonlinear system. Table 3.2 summarizes the procedure of response spectrum analysis using GM-ELM. The procedure for the univariate GM-ELM can be directly applied to the bivariate case without further modifications.

Figure 3.3 shows an illustrative example of response spectrum analysis for which four equivalent linear SDOF oscillators are identified by bivariate GM-ELM. The markers in the figure stand for the mean peak responses of equivalent linear oscillators.

Table 3.2 Procedure of response spectrum analysis using bivariate GM-ELM

Step	Procedure
1	Select a set of ground motions for the site of interest and derive mean response spectra for a set of damping ratios or use existing elastic response spectra if available (See Figure 3.3)
2	Construct power spectral density (PSD) that is compatible with the response spectra using a method available in the literature, e.g. those in Fan and Ahmadi (1990) and Cacciola and Zentner (2012)
3	Conduct a few rounds of nonlinear dynamic analysis using recorded or artificial accelerograms and find an equivalent linear system using GM-ELM
4	Mean peak response are obtained from response spectrum values $S_{d,k} = S_d(\omega_k, \xi_k)$ and one of the combination rules in Eq.(2.23) and Eq.(3.14).

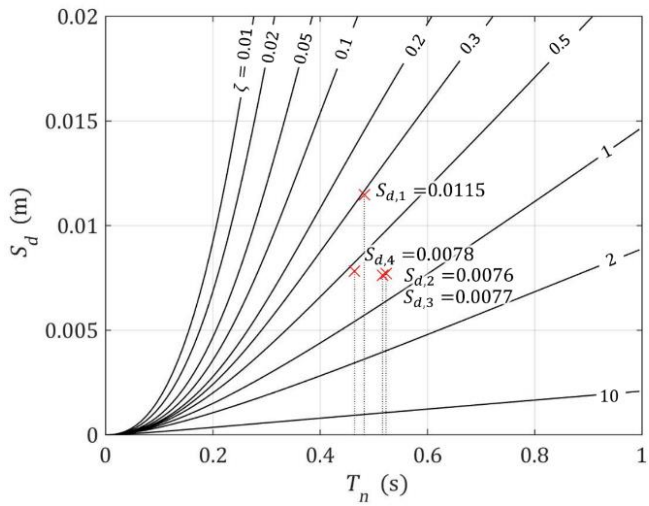

Figure 3.3 Illustrative example: elastic response spectra for a modified Kanai-Tajimi model excitation

As an alternative to the heuristic response spectrum formula introduced in Eq. (2.23), a less heuristic response spectrum formula is developed for GM-ELM via a modification of conventional approaches (see, e.g. Der Kiureghian 1981) for deriving seismic response spectrum formula. First, the mean peak response of interest, $E[\max|Z(t)|]_{t\in T_d}$, is expressed as

$$\begin{aligned} E[\max|Z(t)|]_{t\in T_d} &\cong p_z\sigma_z = \left[\sum_{k=1}^{K}\alpha_k p_z^2\left(\sigma_{z,k}^2+\mu_k^2\right)\right]^{1/2} \\ &= \left[\sum_{k=1}^{K}\alpha_k\left(\frac{p_z^2}{p_k^2}D_{k,max}^2+p_z^2\mu_{z,k}^2\right)\right]^{1/2} \\ &\cong \left[\sum_{k=1}^{K}\alpha_k\left(D_{k,max}^2+p_z^2\mu_{z,k}^2\right)\right]^{1/2} \end{aligned} \tag{3.13}$$

in which p_z and p_k are peak factors of the nonlinear system and the k-th oscillator, the last term presumes $p_z^2/p_k^2 \cong 1$, and $D_{k,\max}$ is the mean peak deformation for the k-th linear oscillator and $D_{k,\max}$ is directly related to the seismic response

spectrum. Here, based on the definition of peak factor, we replace p_z^2 with $D_{k,\max}^2/\sigma_{z,k}^2$, so that Eq. (3.13) is re-written as

$$E[\max|Z(t)|]_{t\in T_d} \cong \left[\sum_{k=1}^{K} \alpha_k \left(D_{k,max}^2 + \frac{D_{k,max}^2}{\sigma_{z,k}^2}\mu_{z,k}^2\right)\right]^{1/2} = \left[\sum_{k=1}^{K} \alpha_k \Gamma^2 \cdot {S_d}^2(\omega_k, \xi_k)\left(1 + \frac{\mu_k^2}{\sigma_{z,k}^2}\right)\right]^{1/2} \tag{3.14}$$

For a given problem, it is often not clear which response spectrum formula would provide the better result, thus the results by both Eq. (2.23) and Eq. (3.14) are provided in the numerical examples.

It is also noted that in some cases, the frequency and damping ratio of the equivalent linear oscillators may be identified outside the practical range, e.g. $0.01 \le \zeta \le 10$ and $0.01\text{s} \le T_n \le 10\text{s}$. Then, the response spectrum combination rules introduced above can ignore the corresponding oscillators. This is permissible because the combined spectral response is generally not much sensitive to a small fraction of the mixture components.

3.5 Numerical examples

3.5.1 SDOF hysteretic oscillator

Consider a hysteretic oscillator under seismic loading defined by the differential equation

$$m\ddot{X}(t) + c\dot{X}(t) + k_0[\alpha X(t) + (1-\alpha)Y(t)] = -m\ddot{U}_g(t) \tag{3.15}$$

where $X(t)$, $\dot{X}(t)$ and $\ddot{X}(t)$ denote the displacement, velocity and acceleration of the oscillator, respectively. The mass of $m = 3 \times 10^5$ kg, stiffness of $k_0 = 2 \times$

10^8 N/m, and damping of $c = 1.5 \times 10^5$ N · s/m is used. The initial natural period of this SDOF oscillator is $T = 0.24$ s. The parameter α, which controls the degree of hysteresis, is set to $\alpha = 0.1$. The term $Y(t)$ in Eq. (3.15) follows the Bouc-Wen hysteresis law (Wen 1980; Wen 1976)

$$\dot{Y}(t) = -\gamma\left|\dot{X}(t)\right||Y(t)|^{\bar{n}-1}Y(t) - \eta|Y(t)|^{\bar{n}}\dot{X}(t) + A\dot{X}(t) \tag{3.16}$$

where $\bar{n} = 3$, $A = 1$ and $\gamma = \eta = 1/(2u_y^{\bar{n}})$, in which $u_y = 0.003$ m is the yielding displacement of the oscillator. The ground acceleration $\ddot{U}_g(t)$ is modeled by a stochastic ground motion with the auto-PSD described by a modified Kanai-Tajimi model by Clough and Penzien (1975), i.e. Eq. (3.1) where $S_0 = 0.004$ m^2/s^3 is a scale factor, $\omega_f = 15$ rad/s and $\zeta_f = 0.6$ are the filter parameters representing, respectively, the natural frequency and damping ratio of the soil layer, and $\omega_s = 1.5$ rad/s and $\zeta_s = 0.6$ are parameters of a second filter that is introduced to assure finite variance of the ground displacement. The filtered ground motion is discretized in frequency domain as (Shinozuka and Deodatis 1991)

$$\ddot{U}_g(t) = \sum_{j=1}^{n/2} \sigma_j \left[u_j \cos(\omega_j t) + \hat{u}_j \sin(\omega_j t)\right] \tag{3.17}$$

in which u_j and $\hat{u}_j$ are independent standard normal random variables, the frequency point is given by $\omega_j = j\Delta\omega$ with a total $n/2 = 500$ frequency points, the cut-off frequency is set to $\omega_{cut} = 50\pi$ (therefore, $\Delta\omega = \pi/10$), and $\sigma_j = \sqrt{2S_f(\omega_j)\,\Delta\omega}$. The duration of the (strong stationary) excitation is assumed to be 27 seconds. Typical hysteretic loops for the SDOF system subjected to a ground motion consistent with the PSD model described above are shown in Figure 3.4.

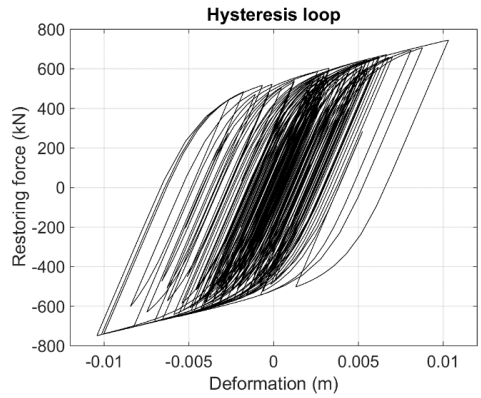

Figure 3.4 Typical hysteretic loops for the SDOF system

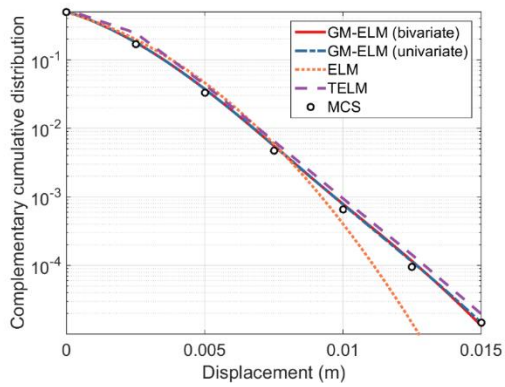

Figure 3.5 Complementary CDF estimations of the SDOF system by various methods

The results of uni- and bi-variate GM-ELM are obtained using 100 runs of dynamic analysis and 64 GM components. Since the GM-ELM depends on random samples of response values to identify the GM model, the final GM-ELM analysis results will fluctuate slightly. In this and the following example, typical results of GM-ELM are reported to illustrate the accuracy one could expect from the method.

First, the instantaneous complementary CDFs obtained by the bivariate GM-ELM, original univariate GM-ELM, the conventional ELM, TELM, and MCS (1.0×10^5 samples) are shown in Figure 3.5. In these results, both versions of GM-ELM produce accurate results while TELM overestimates the complementary CDFs.

As expected, the conventional ELM shows a large error especially at the tail region.

The mean up-crossing rates and first-passage probabilities obtained from bivariate GM-ELM, univariate ELM, TELM and MCS are illustrated in Figure 3.6. It is observed that, by using bivariate mixture, the accuracy of GM-ELM is significantly improved in both mean crossing rate and first-passage probability. This discrepancy could be explained by different strategies to choose equivalent damping used in the two GM-ELM methods. In the univariate GM-ELM, since the damping of equivalent linear oscillators are pre-fixed as the original damping, the linear oscillators could not reflect the extra energy dissipation that arises from the hysteresis mechanism. On the other hand, in bivariate GM-ELM, the extra damping is properly identified by the optimized equivalent damping term. It is also found that the proposed bivariate GM-ELM approach outperforms TELM as shown in Figure 3.6, though they in general provide a similar level of accuracy. However, it is noted that TELM requires repeated executions of FORM analysis for selected threshold values while GM-ELM can reuse the established equivalent linear system throughout the threshold range.

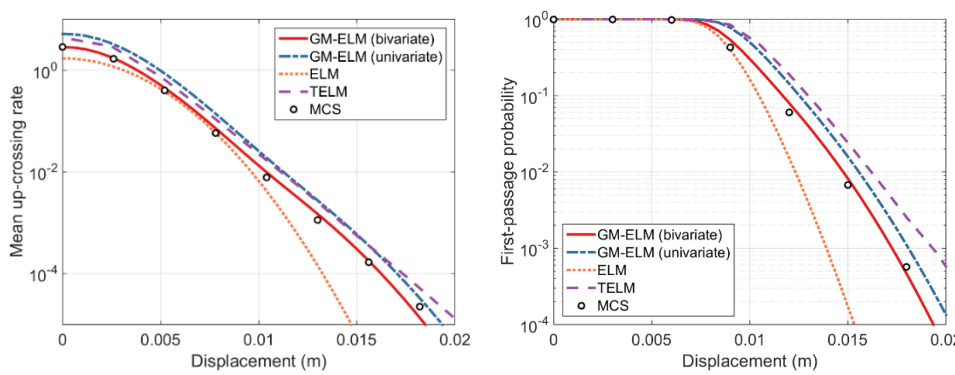

Figure 3.6 Mean up-crossing rates and the first-passage probabilities obtained from various methods

Finally, the mean peak absolute responses estimated from ELM, the univariate GM-ELM (using the response spectrum formula Eq. (2.23) and Eq. (3.14)), the proposed bivariate GM-ELM (using Eq. (2.23) and Eq. (3.14)) and MCS are provided in Table 3.3. To illuminate the proposed method, the elastic linear spectrum ordinates of equivalent linear SDOF oscillators of bivariate GM-ELM are provided in Figure 3.7. GM-ELMs can provide accurate estimates on the mean peak nonlinear responses using linear elastic spectra. It is noted that, as discussed above, TELM cannot be used in conjunction with response spectrum method.

Table 3.3 Mean peak absolute drift of SDOF structure estimated from various methods (unit: meter)

ELM	Univariate GM-ELM		Bivariate GM-ELM		MCS
	Eq. (3.14)	Eq. (2.22)	Eq. (3.14)	Eq. (2.22)	
0.0096 (3.4%)	0.0101 (2.3%)	0.0089 (10.7%)	**0.0097 (2.2%)**	0.0088 (11.4%)	0.0099

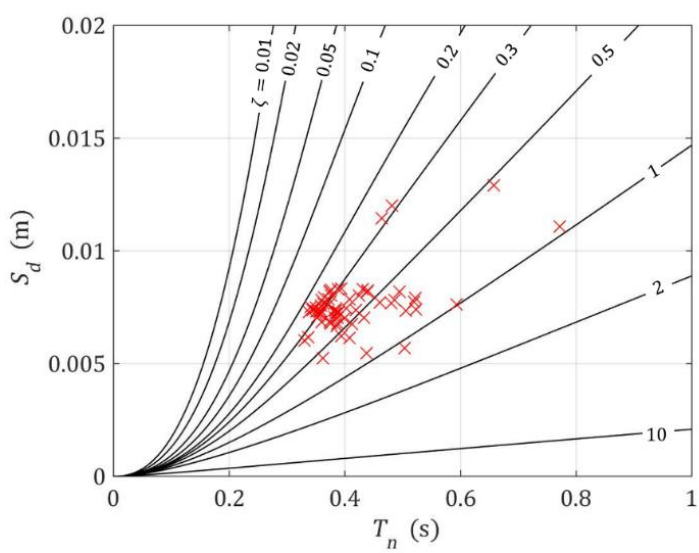

Figure 3.7 Elastic response spectra and spectral displacements used in bivariate GM-ELM

It is seen that for all response statistics considered in this example, the proposed bivariate GM-ELM shows superior accuracy compared to ELM and the univariate GM-ELM. The bivariate GM-ELM provides accuracy comparable to TELM, but is more efficient, free from convergence issues and applicable to response spectrum-based analysis.

3.5.2 MDOF nonlinear system

Consider a 6-DOF shear-building model shown in Figure 3.8. The force-deformation behavior of each column is described by a Bouc-Wen hysteresis model. The yield deformation of each story is set to 0.01m. The structure has an initial fundamental period of 0.332 seconds and the second mode period of 0.138 seconds. 5% Rayleigh damping is assumed for modes 1 and 2. The building is subjected to a stochastic ground motion with the auto-PSD described by the modified Kanai-Tajimi model used in the previous example except $S_0 = 0.125\ \mathrm{m}^2/\mathrm{s}^3$. The duration of the (strong stationary) ground motion is assumed to be 30 seconds.

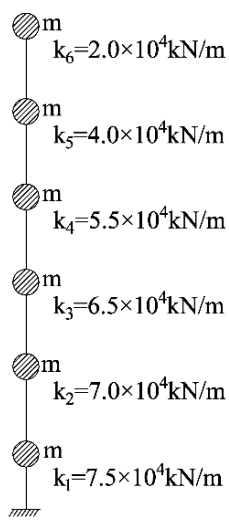

Figure 3.8 6-DOF shear-building model (m=1×10^{4}kg)

The results of GM-ELM with 64 uni- and bivariate Gaussian densities are obtained using response samples obtained from 150 runs of dynamic analysis. Typical hysteretic loops for the 1st and 6th columns subjected to the stochastic ground motion are illustrated in Figure 3.9.

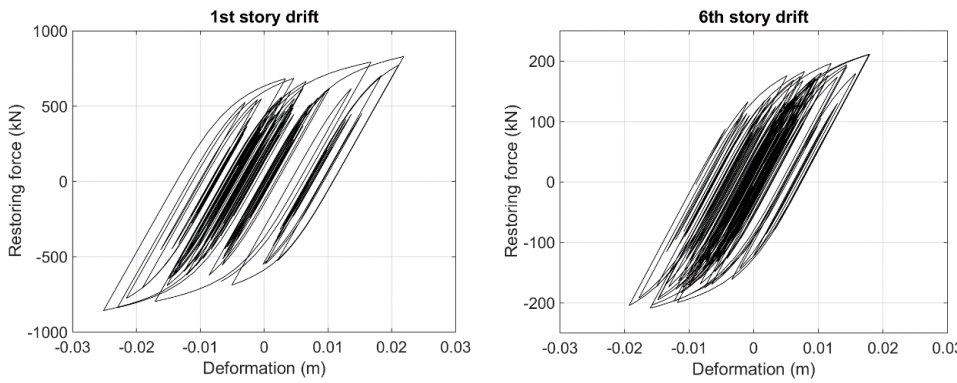

Figure 3.9 Typical hysteretic loops for 1st and 6th column

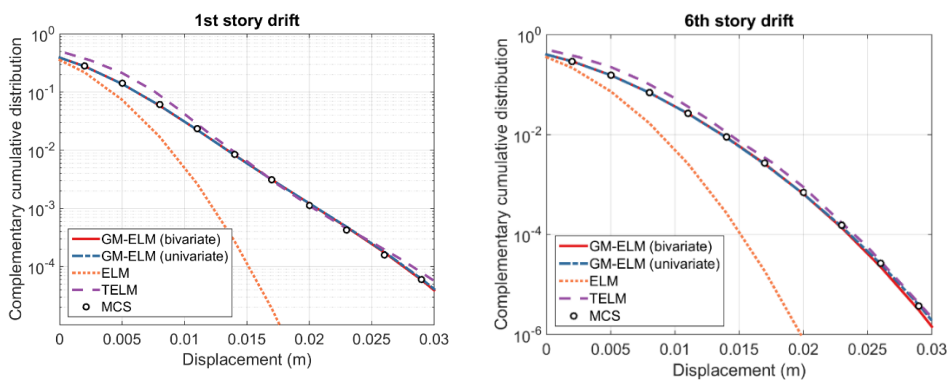

Figure 3.10 Complementary CDF estimations of the MDOF system by various methods

The instantaneous complementary CDFs obtained by GM-ELM methods, the conventional ELM, TELM, and MCS are illustrated in Figure 3.10. Note that the m_{eq}, c_{eq} and s_{eq} in original univariate GM-ELM are computed using the first modal vector for the 1st story drift, and the second modal vector for the 6th story

drift. In these results, both versions of GM-ELM and TELM provide accurate results except that TELM tends to overestimate the probabilities for lower threshold values. As shown in the SDOF example, the conventional ELM should not be used to estimate the complementary CDF or instantaneous failure probability.

Figure 3.11 and Figure 3.12 respectively show the mean up-crossing rates and first-passage probabilities for the 1st and 6th story drifts obtained from GM-ELM methods, ELM, TELM and MCS using 3.0×10^4 samples. As with the previous example, it is seen that for crossing rate and first-passage probability estimations, bivariate GM-ELM is far more accurate than ELM, and significantly better than univariate GM-ELM. The discrepancy in ELM arises from non-Gaussianity of nonlinear structural responses. It is also noted that GM-ELM is at least as accurate as TELM. It is also observed that effect of using bivariate GM-ELM instead of univariate is significant especially in lower threshold of mean up-crossing rates. It should be noted that while TELM analysis should be repeated to get response of each floor as well as each threshold, GM-ELM utilizes only one set of simulations, i.e. 150 response time histories, and all the results are obtained by the post-processing.

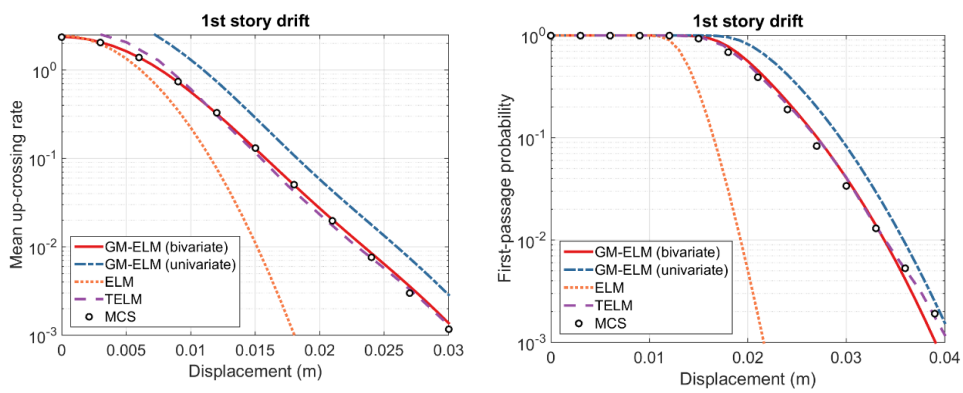

Figure 3.11 Mean up-crossing rates and first-passage probabilities for the 1st story drift

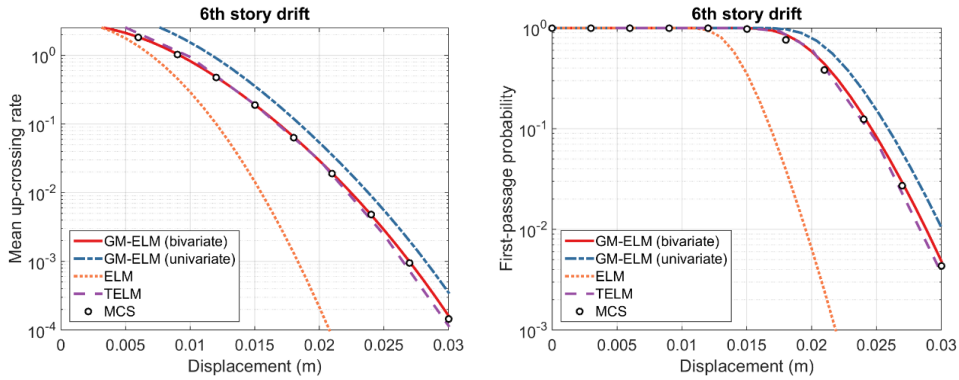

Figure 3.12 Mean up-crossing rates and first-passage probabilities for the 6th story drift

Finally, the mean peak absolute drifts estimated from ELM, GM-ELMs and MCS are listed in Table 3.4. Figure 3.13 shows actual ordinates in elastic response spectra used for response spectrum analysis of bivariate GM-ELM. It can be seen from Table 3.4 that the performance of the proposed bivariate GM-ELM is generally better than ELM and univariate GM-ELM, and the one using the combination rule in Eq. (3.14) seems to be most stable.

Table 3.4 Mean peak absolute drifts of MDOF structure estimated from various methods (unit: meter)

Story	ELM	Univariate GM-ELM		Bivariate GM-ELM		MCS
		Eq. (3.14)	Eq. (2.23)	Eq. (3.14)	Eq. (2.23)	
1	0.0153 (29.1%)	0.0221 (2.4%)	0.0214 (0.6%)	0.0209 (3.0%)	0.0198 (8.1%)	0.0215
2	0.0147 (23.7%)	0.0206 (6.4%)	0.0201 (4.2%)	0.0195 (1.0%)	0.0188 (2.6%)	0.0193
3	0.0134 (11.3%)	0.0168 (11.6%)	0.0175 (15.7%)	0.0160 (5.9%)	0.0166 (10.6%)	0.0151
4	0.0128 (6.8%)	0.0158 (14.7%)	0.0167 (21.4%)	0.0145 (5.7%)	0.0190 (16.3%)	0.0138
5	0.0130 (9.7%)	0.0166 (15.7%)	0.0173 (20.6%)	0.0157 (9.1%)	0.0195 (14.8%)	0.0143
6	0.0156 (26.4%)	0.0228 (7.5%)	0.0224 (5.7%)	0.0217 (2.2%)	0.0215 (1.2%)	0.0212

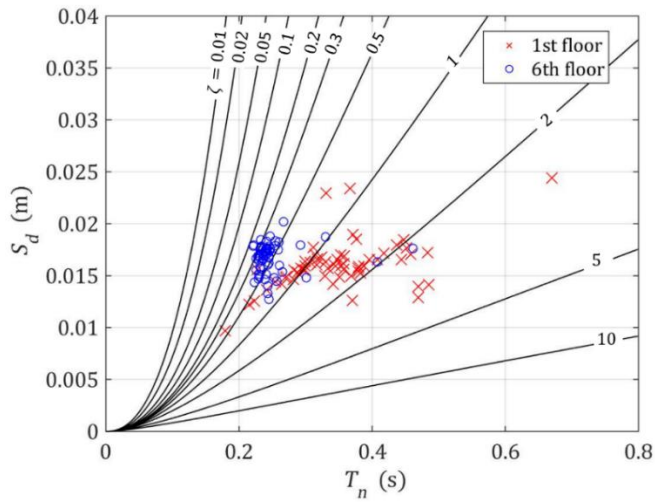

Figure 3.13 Elastic response spectra and spectral displacements used in bivariate GM-ELM (1st and 6th drift)

3.6 Approximation of equivalent damping values

In some applications, for example, when a large number of mixture components are required due to severe nonlinearity of the structure, the procedure of GM fitting in 2-dimension may be cumbersome. Theoretically, the EM algorithm introduced in Section 3.3.1 can be applied regardless of the number of components and the dimensions, however, on the other hand, the computational cost could increase up to the impractical range. In such cases, it may be desirable to maintain the univariate concept although the numerical examples in this section indicate that the univariate GM-ELM could lead to incorrect estimations. Hence, heuristic yet reasonable alternative strategies are provided here to better optimize the structural parameters when univariate GM-ELM analysis is adopted.

Let us consider GM-ELM with only one Gaussian component. The equivalent structural parameters, i.e. stiffness and damping, of this single linear oscillator could be easily optimized by the bivariate response PDF and Eqs. (3.4a) and (3.4b). This

linear system will be referred to as *transitory ELS* and its parameters as $k_{eq,T}$ and $c_{eq,T}$, respectively throughout the dissertation. Though it is clear that this linear oscillator does not capture non-Guassianity, it can still be a useful indicator for effective damping as well as for spectral characteristics.

For example, one could set the equivalent damping value for all GM-ELM linear oscillators as

$$c_{eq,T} = c_{eq,k} \tag{3.18}$$

where $k = 1, \dots K$, instead of the initial damping. Although it may not be the optimum, this modified damping will reflect the energy dissipation to some extent and mitigate the overestimation problems discussed throughout this chapter. The assumption in this strategy is that each linear oscillator shares the same damping values.

On the other hand, instead of damping values, one could impose the common bandwidth parameters for each linear oscillator. In the theory of random vibrations, the spectral characteristic of a random process is often represented in terms of the bandwidth parameters (Lutes and Sarkani 2004). For example, one of the bandwidths parameter for the response of transitory ELS can be calculated by $\alpha_{1,T} = \sqrt{\lambda_{1,T}^2/\lambda_{0,T}\lambda_{2,T}}$, where $\lambda_{j,T}$ is the *j*-th order spectral moment. One could optimize the equivalent linear parameters $k_{eq,k}$ and $c_{eq,k}$ with the following relationships instead of Eq. (3.7b):

$$\alpha_{1,T} = \sqrt{\frac{\lambda_{1,k}^2}{\lambda_{0,k}\lambda_{2,k}}} \tag{3.19}$$

along with Eq. (3.7a). Alternatively, $\delta_T = \sqrt{1-\alpha_{1,T}}$ can be used for the same purpose (Lutes and Sarkani 2004). Finally, it is also a reasonable approximation to fix the variance of the derivative of the linear response as $\sigma^2_{\dot{Z},T}$, i.e using the following relationship instead of Eq. (3.7b):

$$\sigma^2_{\dot{Z},T} = \int_{-\infty}^{\infty} \omega^2 |H_k(\omega)|^2 S_g(\omega) d\omega, \qquad k = 1, \dots, K \tag{3.20}$$

It is noted that these approximation methods all show similar levels of accuracy suitable for the class of examples presented in this dissertation. Furthermore, the modified versions of GM-ELM will be introduced in Chapter 4, which usually involve a highly irregular response PDF or a response PDF with higher dimension. In such applications, it is often desired to simplify the structural optimization phase using these techniques to make the whole process more efficient.

3.7 Conclusions

GM-ELM is further developed to improve accuracy. By extending GM-ELM into two-dimensional space determined by the response and its time derivative, improved estimates of response statistics are acquired. The proposed approach is illustrated and tested by two numerical examples. In the first example of a hysteretic SDOF oscillator subjected to a stochastic ground motion described by a modified Kanai-Tajimi model, the analysis results indicate that the proposed bivariate GM-ELM is significantly more accurate than the univariate GM-ELM and the conventional ELM in estimating mean crossing rate, first-passage probability and mean peak response estimations. It is observed that the bivariate GM-ELM is at least as accurate as the tail-equivalent linearization method (TELM) while the bivariate GM-ELM is more

efficient. The second example is a 6-DOF shear-building model that has hysteretic force-deformation relation for the lateral load-carrying mechanism of each story. As with the first example, the second example also confirms the superior accuracy of the proposed bivariate GM-ELM compared to the original GM-ELM, ELM and TELM. Moreover, the results obtained in the two numerical examples confirm that the newly developed response spectrum combination rule can be as accurate as the original combination rule developed in the previous study of GM-ELM, and the overall performance of the newly developed formula seems more stable than the original one.

Chapter 4. GM-ELM for Seismic Fragility Analysis

4.1 Introduction

Analysis of structures subjected to earthquake events may encounter various sources of randomness. Therefore, it has been widely studied in earthquake engineering how to systematically and quantitatively account for randomness inherent in the seismic intensity, structural damage, and resulting losses (Cornell and Krawinkler 2000). As one of the procedures developed from such efforts, the *fragility analysis* evaluates the conditional probability of the structural failure given a range of the selected ground motion intensity measure, e.g. spectral acceleration. Among the fragility analysis methods developed for nonlinear systems, one of the most widely used approaches in the current practice is the incremental dynamic analysis (IDA), which performs several rounds of nonlinear time history analysis using a set of selected and scaled actual ground motion records. The analysis results of IDA, such as the peak responses, are fitted to a probability distribution model, for which the lognormal distribution is often adopted, to compute the failure probability for each of the presumed limit states (Vamvatsikos and Cornell 2002; Vamvatsikos and Cornell 2004). This approach is systematic, well-established and practically convenient, but still the selection and scaling of ground motions remain a source of debate (Der Kiureghian and Fujimura 2009).

An alternative fragility analysis strategy is to evaluate the seismic reliability of the system by nonlinear stochastic dynamic analysis employing a site-specific

stochastic ground motion model (Der Kiureghian and Fujimura 2009; Alibrandi and Mosalam 2018; Tubldi *et al*. 2014; Marano *et al.* 2011; Mai *et al.* 2017; Zentner 2017). For example, nonlinear random vibration analysis methods such as conventional ELM and TELM have been applied to the seismic fragility analysis of general MDOF structures (Der Kiureghian and Fujimura 2009). Especially, TELM is proven to have a desirable property of scale-invariance. Meanwhile, despite its merits discussed in previous sections, GM-ELM has yet been used for seismic fragility analysis, which mainly attributes to the two practical restrictions: (1) GM-ELM requires the assumption of stationary response, and (2) ELS identified by GM-ELM is highly dependent on the scaling of the input excitation. In this chapter, these challenges are overcome by two improved versions of GM-ELM, which are either jointly or individually applicable. Throughout the dissertation, each improvement will be referred to as *temporal-average* and *intensity-augmented* GM-ELM, respectively (Yi *et al*. 2019).

4.2 Challenges in seismic fragility analysis using GM-ELM

The original version of GM-ELM has shown room for significant improvement to facilitate their applications to seismic fragility analysis. First, fragility analysis using GM-ELM can be inefficient due to the dependency of the ELS on the ground motion intensity. This is because the identification of ELS hinges on the response PDF of the system. In order to construct the fragility curve of a nonlinear structures, the failure probabilities need to be computed for a sequence of discretized intensity levels. Therefore, the straightforward application of the GM-ELM would require a tedious repetition of the whole linearization process for each of the selected ground

motion intensities. Thus, it is desirable to have a universal ELS that is independent of the change of the ground motion intensity.

Second, the underlying assumption of stationarity may restrict applications of GM-ELM to nonstationary excitations (including ground motions) and responses. The GM-ELM approaches exploited the fact that the linear response of the stationary Gaussian excitation is also a stationary Gaussian process (after a certain time period required to achieve the stationarity). This presumption becomes a strict constraint when one needs to take into account non-stationarity of (ground motion) excitations and responses.

In order to facilitate practical applications of GM-ELM, especially in seismic fragility analysis, these challenges are overcome by the intensity-augmented GM-ELM and temporal-average GM-ELM, respectively.

4.3 Intensity-augmented GM-ELM

4.3.1 Intensity-augmented probability density function (PDF) and universal ELS

This section first establishes the concept of universal ELS to encapsulate the nonlinear behavior for a range of excitation scales. The goal is achieved by incorporating the effect of excitation intensity before fitting the GM model. To this end, the domain of the response space is extended by introducing an axillary random variable of intensity measure, denoted by IM. As a result, GM-ELM is performed for the "intensity-augmented" domain characterized by the joint PDF of the response $\boldsymbol{z}$ and IM, i.e.

$$f(\boldsymbol{z}, IM) = f(\boldsymbol{z}|IM)f(IM) \tag{4.1}$$

This joint PDF could be fitted by a higher dimension GM model, i.e.

$$f_{GM}(\boldsymbol{z}, IM; \boldsymbol{\nu}) = \sum_{k=1}^{K} \alpha_k f_{\mathcal{N}}(\boldsymbol{z}, IM; \widetilde{\boldsymbol{\mu}}_k, \widetilde{\boldsymbol{\Sigma}}_{\boldsymbol{k}}) \tag{4.2}$$

The distribution parameter set $\boldsymbol{\nu}$ includes the means $\widetilde{\boldsymbol{\mu}}_k$ and the covariances $\widetilde{\boldsymbol{\Sigma}}_{\boldsymbol{k}}$ which are obtained by augmenting response means and variances in Eq. (3.2) $\{\boldsymbol{\mu}_k, \boldsymbol{\Sigma}_k\}$ (or Eq. (2.10) for the case of univariate GM-ELM) with those of IM, respectively. By imposing statistical independence condition between IM and $\boldsymbol{z}$ in each Gaussian density in the mixture, Eq. (4.2) becomes

$$f_{GM}(\boldsymbol{z}, IM; \boldsymbol{\nu}) = \sum_{k=1}^{K} \alpha_k f_{\mathcal{N}}(IM; \mu_{IM,k}, \sigma_{IM,k}^2) f_{\mathcal{N}}(\boldsymbol{z}; \boldsymbol{\mu}_{\boldsymbol{z},k}, \boldsymbol{\Sigma}_{\boldsymbol{z},k}) \tag{4.3}$$

where $\mu_{IM,k}$ and $\sigma_{IM,k}^2$ are respectively the mean and variance of the k-th component in terms of IM. It is remarked that the statistical independence in each mixture component does not imply the statistical independence between $Z(t)$ and $\dot{Z}(t)$ to the given IM. The corresponding marginal distribution of IM is then derived as

$$f_{GM}(IM; \boldsymbol{\nu}) = \int_{-\infty}^{\infty} f_{GM}(\boldsymbol{z}, IM; \boldsymbol{\nu}) d\boldsymbol{z} = \sum_{k=1}^{K} \alpha_k f_{\mathcal{N}}(IM; \mu_{IM,k}, \sigma_{IM,k}^2) \tag{4.4}$$

From Eqs. (4.3) and (4.4), the conditional PDF of the response given the intensity is

$$f_{GM}(\boldsymbol{z}|IM) = \frac{f_{GM}(\boldsymbol{z}, IM; \boldsymbol{\nu})}{f_{GM}(IM; \boldsymbol{\nu})} = \sum_{k=1}^{K} \alpha_k^*(IM) f_{\mathcal{N}}\left(\boldsymbol{z}; \boldsymbol{\mu}_{\boldsymbol{z},k}, \boldsymbol{\Sigma}_{\boldsymbol{z},k}\right) \tag{4.5}$$

where

$$\alpha_k^*(IM) = \frac{\alpha_k f_{\mathcal{N}}(IM; \mu_{IM,k}, \sigma_{IM,k}^2)}{\sum_{m=1}^{K} \alpha_m f_{\mathcal{N}}(IM; \mu_{IM,m}, \sigma_{IM,m}^2)} \tag{4.6}$$

Note that the conditional PDF in Eq. (4.5) is another GM model whose dimension is reduced back to the dimension of $\boldsymbol{z}$. Moreover, the value of IM only affects the mixing coefficient term $\alpha_k^*(IM)$ while the other parameters of Gauss distributions, i.e. $\boldsymbol{\mu}_k, \boldsymbol{\Sigma}_k$ are independent of IM.

From the perspective of GM-ELM, $\alpha_k^*(IM)$ represents the relative contributions of the *k*-th linear oscillator to the nonlinear responses, while $\boldsymbol{\mu}_k$ and $\boldsymbol{\Sigma}_k$ determine its structural locations and properties. Therefore, as seen in Eq. (4.5), even if the ground motion scale IM is varied, e.g. for fragility analysis, the equivalent linear system identified by the intensity-augmented GM-ELM in Eq. (4.3) remains unchanged and thus named as *universal ELS*. In other words, if $\boldsymbol{z}$ and IM can be described by the model in Eq. (4.3), one can utilize the same universal ELS for a range of IM. The relative occurrence rate will change as shown in Eq. (4.6), but the calculation is trivial once the mixture parameters are identified. Finally, it is noted that the choice of $f(IM)$ in Eq. (4.1) does not affect the results of fragility analysis. Therefore, one may choose the shape of this distribution based on the relative importance of the IM values within the range of interest.

The procedure of fragility analysis by the intensity-augmented GM-ELM is presented in Table 4.1 and Figure 4.1. It is modified from those presented in Chapter 2 and Chapter 3.

Table 4.1 Procedure of intensity-augmented GM-ELM

Step	Procedure
1	Obtain the intensity-augmented response PDF, $f(\boldsymbol{z}, IM)$ as in Eq. (4.2)
2	Identify the Gaussian mixture PDF model $f_{GM}(\boldsymbol{z}, IM; \boldsymbol{v})$ that best fits the intensity-augmented PDF
3	Obtain the universal ELS associated with each Gaussian density in GM model using Eq. (3.7a) and one of Eqs. (3.7b), (3.19)-(3.20)
4	Random vibration analysis/fragility analysis using universal ELS

Step 1 will be further explored in the Sections 4.3.3 and 4.3.4. In Step 2, the number of the intensity-augmented GM components (and the universal ELS) should be determined through a trade-off between the computational cost and the fitting precision. One could use maximum likelihood criteria to select the optimal number of mixture components as proposed in Wang and Song (2017), while it is remarked that using about 200 mixture components provide the degree of accuracy presented in this dissertation. Once the universal ELS is identified in Step 3, the response combination formulations such as presented in Section 2.5.1 can still be applied. The only changes are to replace α_k in Eqs. (2.15), (2.17), (2.20), and (2.21) by $\alpha_k^*(IM)$ depending on the intensity level of interest.

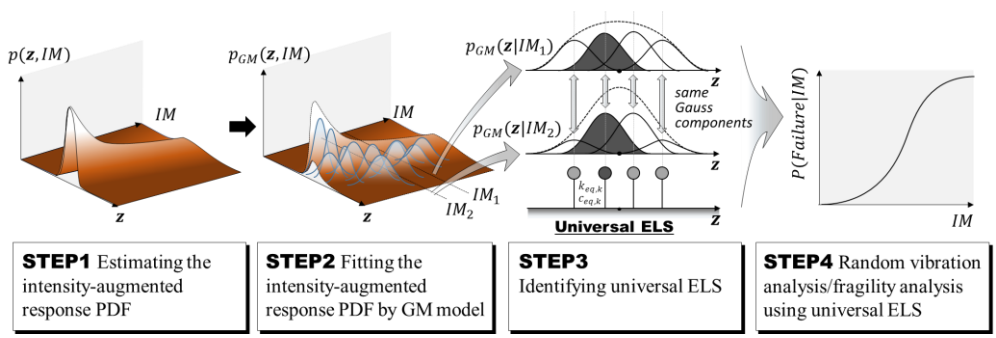

Figure 4.1 Procedure of fragility analysis using intensity-augmented GM-ELM and universal ELS

4.3.2 Modified universal ELS

The uncorrelated condition imposed for each Gaussian component will now be released. With the correlated Gaussian components, the Eq. (4.3) is modified as

$$f_{GM}(\boldsymbol{z}, IM; \boldsymbol{\nu}) = \sum_{k=1}^{K} \alpha_k f_{\mathcal{N}}(IM; \mu_{IM,k}, \sigma_{IM,k}^2) f_{\mathcal{N}}(\boldsymbol{z}|IM; \boldsymbol{\mu}_{\boldsymbol{z},k}, \boldsymbol{\Sigma}_{\boldsymbol{z},k}) \tag{4.7}$$

Since $\boldsymbol{z}$ and IM are jointly Gaussian, the conditional distribution of $\boldsymbol{z}$ given IM can be represented as another Gaussian distribution with modified mean $\boldsymbol{\mu}_{\boldsymbol{z},k}^*$ and covariance $\boldsymbol{\Sigma}_{\boldsymbol{z},k}^*$, i.e.

$$f_{\mathcal{N}}(\boldsymbol{z}|IM; \boldsymbol{\mu}_{\boldsymbol{z},k}, \boldsymbol{\Sigma}_{\boldsymbol{z},k}) = f_{\mathcal{N}}\left(\boldsymbol{z}; \boldsymbol{\mu}_{\boldsymbol{z},k}^*, \boldsymbol{\Sigma}_{\boldsymbol{z},k}^*\right) \tag{4.8}$$

where

$$\boldsymbol{\mu}_{\boldsymbol{z},k}^* = \boldsymbol{\mu}_{\boldsymbol{z},k} + \boldsymbol{\Sigma}_{\boldsymbol{z}IM,k} \boldsymbol{\Sigma}_{IM,k}^{-1} \left(IM - \mu_{IM,k}\right) \tag{4.9a}$$

$$\boldsymbol{\Sigma}_{\boldsymbol{z},k}^* = \boldsymbol{\Sigma}_{\boldsymbol{z}IM,k} \boldsymbol{\Sigma}_{IM,k}^{-1} \boldsymbol{\Sigma}_{IM\boldsymbol{z},k} \tag{4.9b}$$

It is noted that unlike the case with uncorrelated components in Section 4.3.1, the conditional means of the response $\boldsymbol{\mu}_{\boldsymbol{z},k}^*$ now depend on IM value. By substituting Eq. (4.8) into Eq. (4.7), the conditional PDF of the response given the intensity is rewritten as

$$f_{GM}(\boldsymbol{z}|IM) = \sum_{k=1}^{K} \alpha_k^*(IM) f_{\mathcal{N}}\left(\boldsymbol{z}; \boldsymbol{\mu}_{\boldsymbol{z},k}^*(IM), \boldsymbol{\Sigma}_{\boldsymbol{z},k}^*\right) \tag{4.10}$$

where $\alpha_k^*(IM)$ is the same as Eq. (4.6). It is noted that similarly to the contribution factor $\alpha_k^*(IM)$, the mean $\boldsymbol{\mu}_{\boldsymbol{z},k}^*(IM)$ can be easily re-evaluated as the value of IM changes, i.e. we now allow the base location of each linear oscillator to vary depending on the intensity measure values. Thus, both correlated (Eq. (4.7)) and uncorrelated (Eq. (4.3)) GM model can be used to fit intensity-augmented GM-ELM.

However, it is recommended to use the correlated model since it is generally more flexible.

4.3.3 Identification of intensity-augmented PDF

As a price for avoiding the repetition of the whole linearization process for each intensity level, the proposed approach requires extra information to obtain the intensity-augmented response PDF $f(\boldsymbol{z}, IM)$. In general applications, the PDF could be retrieved from the samples of nonlinear dynamic simulation results and corresponding ground intensities. From the conditional density expressions in Eq. (4.1) and selected distribution of $f(IM)$, a stepwise sampling method is introduced: A value of IM is first sampled, and a ground acceleration time history is generated accordingly. A set of samples of the conditional response PDF $f(\boldsymbol{z}|IM)$ can be obtained by a single run of dynamic analysis, under the stationary and ergodic assumptions. Repetition of this two-step procedure will generate samples for the intensity-augmented PDF $f(\boldsymbol{z}, IM)$. Although this procedure is computationally more demanding than that for the fixed-intensity response PDF, the proposed approach can still secure efficiency in the perspective of entire fragility analysis. Because of the interpolating effect between the different intensity levels, the required number of simulations corresponding to a specific intensity level becomes much smaller. Unlike existing GM-ELM, the additional knowledge of response PDF at specific intensity could be "borrowed" from the neighboring intensities.

4.3.4 Simple scaling approach

To provide an alternative to the direct sampling approach described in Section 4.3.3,

this section proposes an efficient approach termed simple scaling method, which enables us to obtain intensity-augmented response PDF from the knowledge of response at a specific intensity level. The method is based on the first-order approximation of the instantaneous failure probability, or the tail-probability. Figure 4.2 presents the difference between the crude sampling-based approach in Section 4.3.3 and the simple scaling approach.

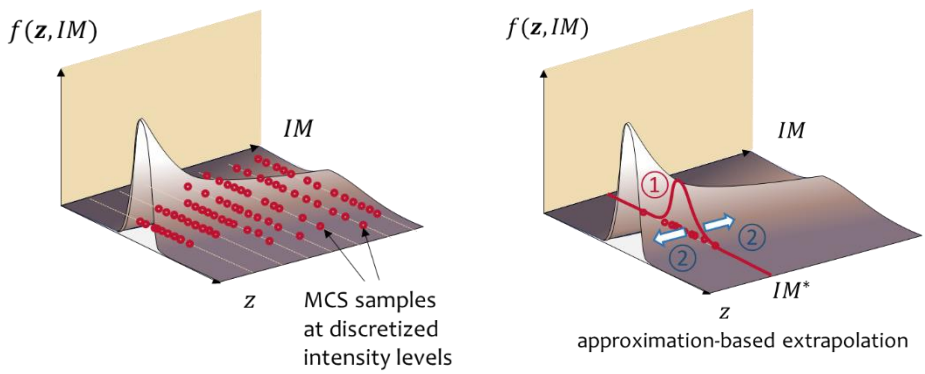

(a) Crude sampling approach (Section 4.3.3) (b) Simple scaling approach (Section 4.3.4)

Figure 4.2 Two methods to estimate intensity-augmented response PDF

Particularly, consider a linearly filtered Gaussian white process excitation $f_g(t)$. It is known that the random process can be approximately represented as a linear combination of a finite number of the standard normal random variables (Der Kiureghian and Fujimura 2009):

$$f_g(t) = \boldsymbol{s}(t)^{\mathrm{T}}\boldsymbol{u} \tag{4.11}$$

in which $\boldsymbol{s}(t)$ and $\boldsymbol{u}$ are column vectors of deterministic basis functions, e.g. delta Dirac functions, linear filters (Fujimura and Der Kiureghian 2007), and sinc function (Broccardo and Der Kiureghian 2017; Broccardo *et al*. 2017), or sine and cosine (Garrè and Der Kiureghian 2010, Broccardo 2017). Particularly, in time-domain

representation, $\boldsymbol{u}$ may represent the intensity of random pulses at the discretized time points while $\boldsymbol{s}(t)$ describe the linear filter(s) through which the pulses pass. Alternatively, the excitation can be described in the frequency-domain, in which the basis functions consist of sine and cosine functions. The uncertainties in the excitation – represented by the random variables $\boldsymbol{u}$ – propagate through structural analysis to the response of interest, $Z(t)$. Therefore, this approach enables us to describe the instantaneous failure event $Z(t) > z$ in the domain of random variables $\boldsymbol{u}$ as in Figure 4.3(a). Fujimura and Der Kiureghian (2007) showed that the first-order approximation of the limit-state surface $z - Z(t) = 0$ at the design point leads to the failure probability estimation

$$Pr(Z(t) > z|IM) \cong \Phi(-\beta_z) \tag{4.12}$$

where IM is the intensity measure corresponding to the random excitation $f_g(t)$, and β_z is the "reliability index" which is the Euclidian distance from the design point to the origin of the $\boldsymbol{u}$ space, denoted by $\boldsymbol{u}^*$ (Der Kiureghian 2005). This approximation is conceptually presented in Figure 4.3(b). Note that the left-hand side term of Eq. (4.12) corresponds to the notation of complementary CDF of responses.

Now suppose the excitation is scaled by an arbitrary constant c to obtain $f_{g,c}(t) = cf_g(t) = \boldsymbol{s}(t)^{\mathrm{T}}(c\boldsymbol{u})$. Appendix B of Fujimura and Der Kiureghain (2007) provided a proof that the design point $\boldsymbol{u}_c^*$ of the failure event $Z_c(t) > z$ can be obtained by scaling that of the unscaled excitation, i.e. $\boldsymbol{u}_c^* = \boldsymbol{u}^*/c$. Therefore, the reliability index is also scaled to $\beta_{z,c} = \beta_z/c$ as shown in Figure 4.3(c). Accordingly, the first order approximation of the complementary CDF of the scaled response $Z_c(t)$ is

$$Pr(Z_c(t) > z|IM_c) \cong \Phi\left(-\frac{\beta_z}{c}\right) \tag{4.13}$$

where IM_c is the intensity measure of the scaled excitation $f_{g,c}(t)$. This implies that if we choose a specific value of IM, denoted by IM^*, as a "representative" intensity measure and obtain the response PDF $f(z|IM^*)$, the result can be extended to obtain general distribution of $f(z|IM)$ for various IM levels, with only trivial calculations. By implementing it into Eq. (4.1), the intensity-augmented PDF can be obtained for general IM values. As for the choice of representative intensity IM^*, although generally the result is not too sensitive to the choice, it is recommended to select the intensity that produces the spectral displacements 1.5-2.0 times greater than the yield displacement in order to capture nonlinearity and prevent numerical issues.

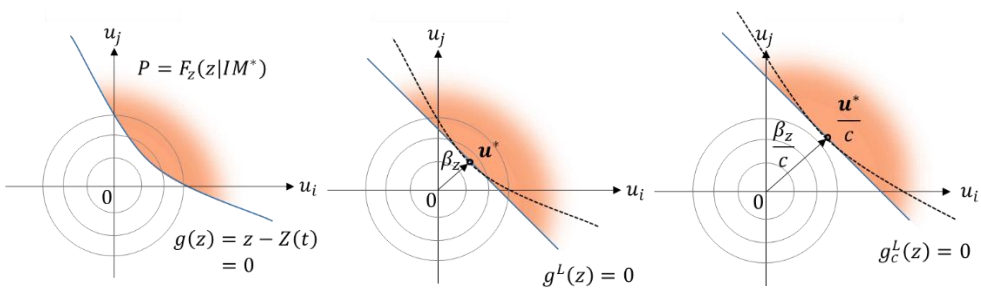

(a) Failure domain corresponding to the conditional CDF value

(b) First-order approximation of the limit state surface

(c) Approximated limit state surface for a scaled excitation

Figure 4.3 Failure domain and its linear approximations corresponding to the conditional CDF value in the standard normal space

It is noted that the proposed simple scaling approach could only be applied to the univariate GM-ELM, which may be relatively inaccurate compared to bivariate GM-ELM for certain structures as discussed in Chapter 3. Nevertheless, the accuracy of estimation could be significantly improved by applying the approximated

damping strategy introduced in Section 3.6. The additional assumption introduced here is that the shared value of equivalent damping $c_{eq,k}$, the bandwidth parameter $\delta_{eq,k}$, or the variance of response time-derivative $\sigma_{\dot{z},k}$ depending on the choice of the user, is consistent not only within the ELS but also throughout a range of intensity measures. As presented in Figure 4.4, the procedure of the proposed extrapolation involves only the elementary calculations that require the minimal computational effort.

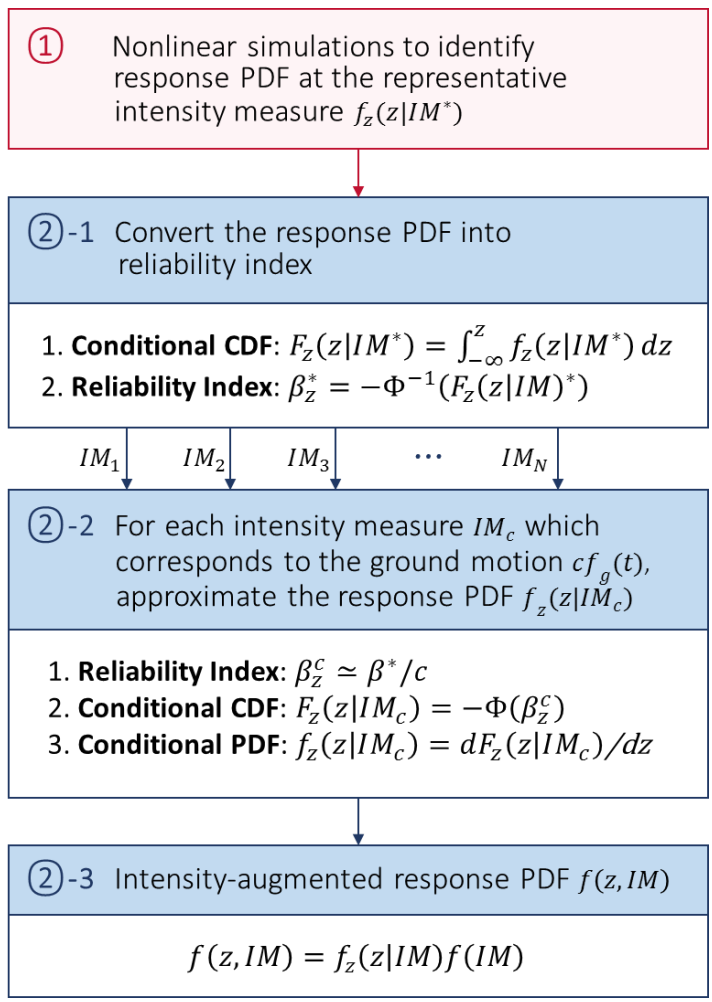

Figure 4.4 Procedure for simple scaling approach (see Figure 4.2(b) for ① and ②)

4.3.5 Numerical examples

To demonstrate the intensity-augmented GM-ELM and the simple scaling approach, let us consider a nonlinear SDOF oscillator whose equation of motion is

$$m\ddot{X}(t) + c\dot{X}(t) + k_0[\alpha X(t) + (1-\alpha)Y(t)] = -m\ddot{U}_g(t) \tag{4.14}$$

where $\ddot{X}(t)$, $\dot{X}(t)$, and $X(t)$ respectively denote the acceleration, velocity and displacement of the oscillator. The mass, damping and the initial stiffness are set respectively as $m = 3 \times 10^5$ kg, $c = 1.5 \times 10^5$ N·s/m, and $k_0 = 2.1 \times 10^7$ N/m. The corresponding initial natural period and damping ratio are calculated as 0.75s and 0.03, respectively. The parameter $\alpha = 0.1$ represents the ratio of post- to pre-yield stiffness. The hysteretic response term $Y(t)$ follows the Bouc-Wen hysteresis model (Wen 1980, Wen 1976), i.e.

$$\dot{Y}(t) = -\gamma\left|\dot{X}(t)\right||Y(t)|^{\bar{n}-1}Y(t) - \eta|Y(t)|^{\bar{n}}\dot{X}(t) + A\dot{X}(t) \tag{4.15}$$

in which the shape parameters are set as $\gamma = \eta = 1/(2u_y^{\bar{n}})$ where the yielding displacement is $u_y = 0.23$m. The values of the other parameters are $\bar{n} = 3$ and $A = 1$. The stationary ground acceleration $\ddot{U}_g(t)$ is characterized by the Kanai-Tajimi filter PSD model

$$S_f(\omega) = S_0 \frac{\omega_f^4 + 4\zeta_f^2\omega_f^2\omega^2}{\left(\omega_f^2 - \omega^2\right)^2 + 4\zeta_f^2\omega_f^2\omega^2} \tag{4.16}$$

where $\omega_f = 5\pi$ rad/s and $\zeta_f = 0.6$. Note that in this model, the parameter S_0, which represents the intensity of the underlying white-noise is varied to obtain the fragility for each intensity scale. The stationary "strong motion" duration is assumed to be 10 seconds. The filtered ground motions are generated by discretization in the frequency domain. The failure threshold of the response is provided in terms of

yielding displacement, i.e. $1.0u_y$, $1.5u_y$, and $2.0u_y$.

For GM-ELM analysis, seismic intensity scale that makes the pseudo spectral displacement ($S_d = S_a/\omega^2$) for the initial stiffness match $1.7\,u_y$ was first found and used it as the reference intensity of the scaling process. The value 1.7 is selected from our experience such that the response samples could reflect both nonlinearity and non-Gaussianity. Figure 4.5 shows typical hysteresis loops for the reference intensity. A total of 200 artificial ground acceleration time histories are generated from the PSD model to conduct nonlinear dynamic analyses. The intensity-augmented PDF $f(z, IM)$ is obtained at discretized grids of z and IM using the simple scaling approach, and the modified EM-algorithm is used to fit GM model having $K = 100$ components. Note that in this example, adoption of the simple scaling approach in Section 4.3.4 has saved about a third of the total computational cost in terms of the required number of dynamic simulations, compared to the direct sampling approximation stated in Section 4.3.3.

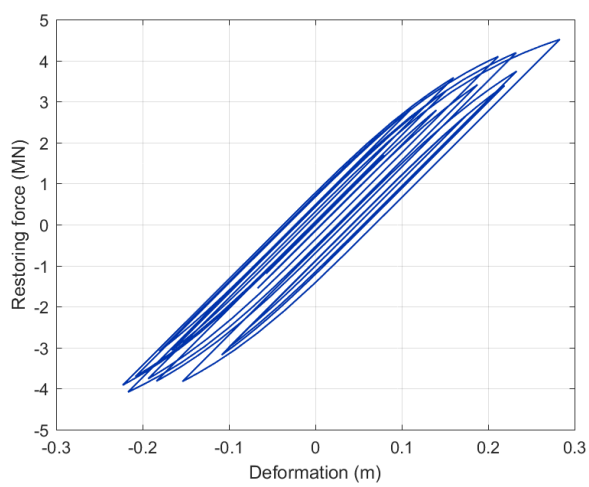

Figure 4.5 Typical hysteretic loops for the SDOF oscillator

The results of the proposed GM-ELM-fragility analysis are compared with those by Monte Carlo simulation (MCS) with 3×10^4 dynamic nonlinear simulations for each of 10 intensity levels of S_a (Total number of simulations: 3×10^5). In this analysis, S_a represents the mean spectral acceleration at the initial natural frequency and damping ratio of the oscillator. The fragility curves for three threshold levels ($1.0u_y, 1.5u_y$ and $2.0u_y$) are provided in Figure 4.6 in which the probability of failure is represented in the log-scale to inspect accuracy of rare-event probabilities. TELM analysis results are also represented in the same figure for comparison. It is noted that GM-ELM fragility results well match the MCS results.

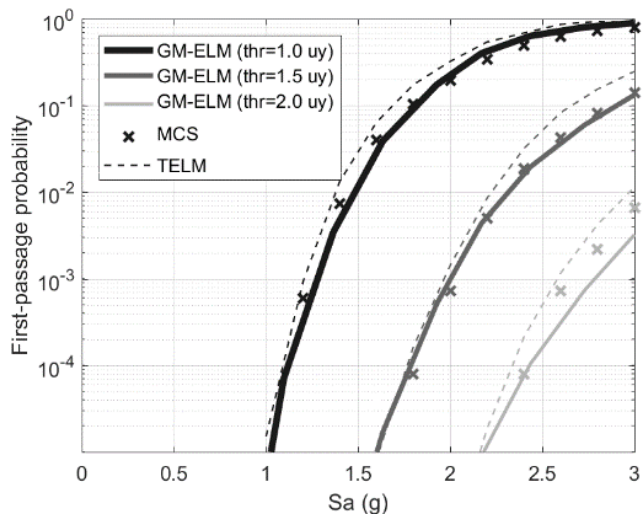

Figure 4.6 Fragility curves for hysteretic oscillator obtained by intensity-augmented GM-ELM

Figure 4.7 shows the relative contributions of the Gaussian components to the nonlinear response at three intensity levels. It is noteworthy that when the excitation intensity is low, only few Gaussian components contribute to the response, as shown in Figure 4.7(a). This is because the structure behaves almost linearly, and therefore, the response is near-Gaussian. On the other hand, as the ground intensity increases,

more components are involved to approximate the non-Gaussian responses. In this example, most of the component means tend to have near-zero values because of the symmetry of the excitation and responses.

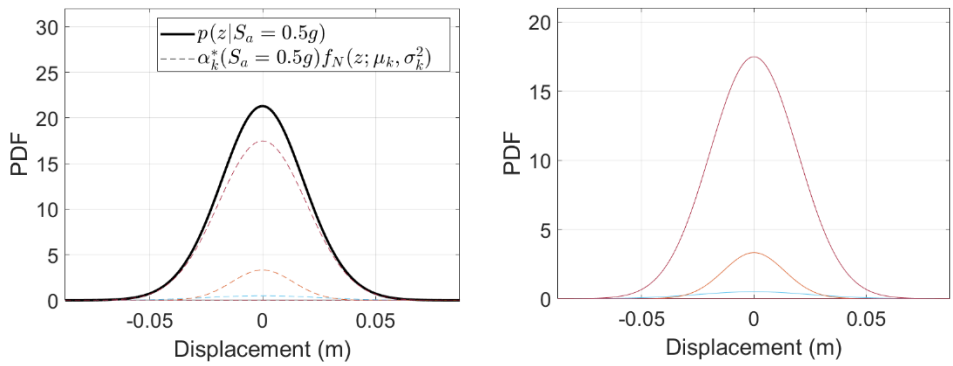

(a) S_a=0.5 g

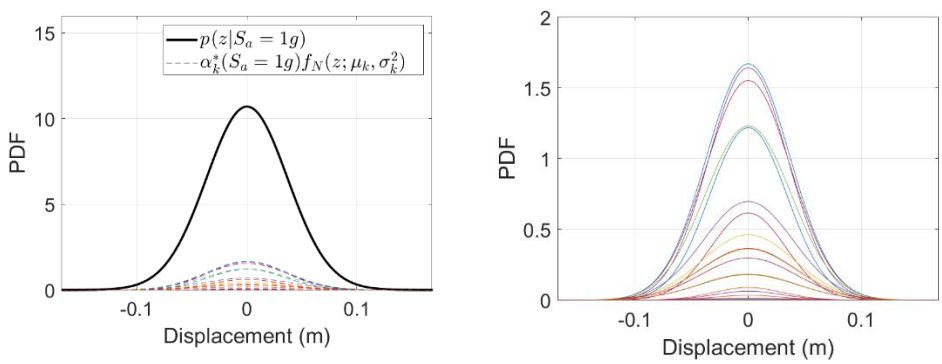

(b) S_a=1.0 g

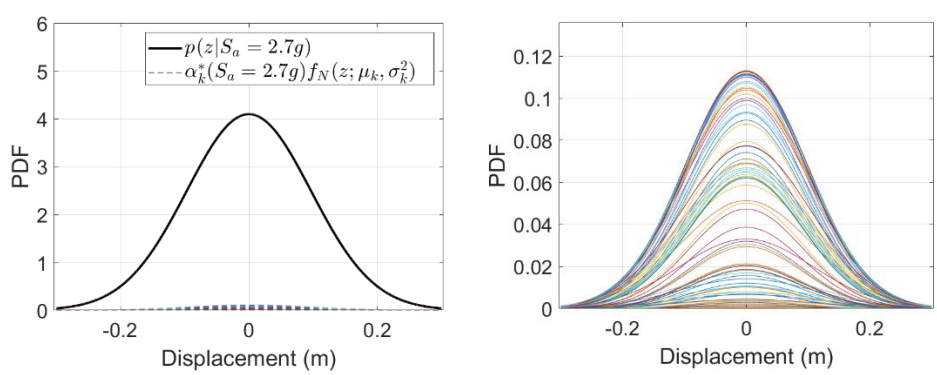

(c) S_a=2.7 g

Figure 4.7 GM fitting results (left) and relative contributions of Gauss components (right)

4.4 Temporal-average GM-ELM for nonstationary responses

4.4.1 Temporal-average PDF

As the first step to deal with nonstationary responses, it is proposed to integrate the time-dependent instantaneous PDF of the response over the time duration, i.e. temporal average to obtain a time-independent PDF representing the whole excitation duration. To this aim, the concept of temporal average PDF is introduced. For the convenience in illustration, the discussion in this section will start from the existing GM-ELM without using the intensity variables, but the extension to the intensity-augmented GM-ELM is fairly straightforward. Let us consider the temporal average of a transient nonstationary response PDF $f(\boldsymbol{z};t)$ given as

$$\hat{f}(\boldsymbol{z}) = \frac{1}{T_d}\int_{T_i}^{T_e} f(\boldsymbol{z};t)\,dt \tag{4.17}$$

where $T_d = T_e - T_i$ represents the time duration susceptible to the failure, and the parameters T_i and T_e respectively denote the starting and ending points of the duration (T_i, T_e), which will be further described in the next subsection. Throughout this dissertation, the hat (^) notation represents the temporal average values. By using $\hat{f}(\boldsymbol{z})$ in Eq. (4.17) to fit the GM model in Eq. (3.2) (or Eq. (2.10) for univariate case), one could extend the framework to nonstationary GM-ELM (See Figure 4.8).

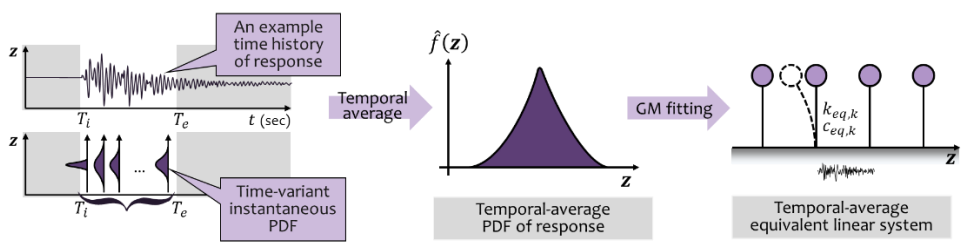

Figure 4.8 Concept of temporal-average GM-ELM

Although the actual implementation is relatively simple, the proposed concept represents fundamental developments in the philosophy from previous GM-ELM analysis. Recall that existing GM-ELM assumes the nonlinear responses are stationary (or at least almost stationary) to approximate them by a set of stationary linear responses. In the proposed temporal-average GM-ELM, nonlinear responses caused by stationary or "nonstationary" excitation are approximated by a set of "stationary" linear responses (as the mixture of the Gaussian distributions).

4.4.2 Failure-susceptible duration of nonstationary excitation

In this study, the failure-susceptible duration of the response in Eq. (4.17) is defined as the strong motion excitation duration (Zembaty 1988), which can be identified by use of an energy-based intensity measure. This study uses the Arias intensity, i.e.

$$I_A(t) = \frac{\pi}{2g}\int_0^t f_g(t)^2\,dt \tag{4.18}$$

where $f_g(t)$ is the excitation time history. To relate the Arias intensity in Eq. (4.18) with a stochastic model of ground motions, let us consider an evolutionary PSD $S_g(\omega, t)$:

$$S_g(\omega, t) = \left|A_g(\omega, t)\right|^2 S_o \tag{4.19}$$

where S_o is the intensity of underlying white noise process and $A_g(\omega, t)$ is the frequency-time modulating function of the evolutionary process. Note that $S_g(\omega, t)$ is a nonstationary counterpart of the stationary auto-PSD $S_g(\omega)$ in Eq. (3.7). The relationship between the mean of the Arias intensity and the evolutionary PSD is described as (Zembaty 1988)

$$E[I_A(t)] = \frac{\pi}{2g} E\left[\int_0^t f(\tau)^2 \, d\tau\right] = \frac{\pi}{g}\int_0^t \int_0^\infty S_g(\omega,\tau) d\omega \, d\tau \tag{4.20}$$

which can be normalized by the mean for overall duration T to obtain the ratio

$$r_s(t) = \frac{E[I_A(t)]}{E[I_A(T)]} \tag{4.21}$$

The starting and ending time points of strong motion duration in Eq. (4.17) can be identified as the values of t, where the ratio in Eq. (4.21) reaches the pre-specified lower and upper threshold values. This energy-based threshold of the input excitation is adopted because the global peak of the structural response is expected to occur only while the external energy is being supplied. The thresholds of 5% and 99% of Arias intensity ratio are recommended to safely cover the time-interval in which the first-passage event of the response is likely to occur. If one takes overly long time interval, the duration may include trivial but long-lasting small vibrations whose corresponding response is negligible. The temporal average PDF including this kind of responses could be overly sharp, and fitting it into the mixture distribution may be challenging.

Next, in order to identify the parameters of the ELS by using Eq. (3.7a) and one of Eqs. (3.7b), (3.19)-(3.20), one should define time-independent auto-PSD that will replace $S_g(\omega)$ in the existing GM-ELM for stationary responses. In this research, the following temporal average of $S_g(\omega, t)$ is proposed as the equivalent stationary excitation:

$$\hat{S}_g(\omega) = \frac{1}{T_d}\int_{T_i}^{T_e} S_g(\omega, t) \, dt \tag{4.22}$$

4.4.3 Random vibration analysis by temporal-average GM-ELM

The first-passage probability of a structure subjected to a nonstationary excitation can be estimated by assuming that the arrivals follow a nonhomogeneous Poisson process, i.e.

$$Pr[\max Z(t) > a]_{t\in T_d} = 1 - A\exp\left[-\int_{T_i}^{T_e} \nu^+(a;t)\,dt\right] \tag{4.23}$$

where the term $\nu^+(a;t)$ represents time-dependent mean occurrence rate of the failure. Although temporal-average GM-ELM cannot estimate $\nu^+(a;t)$, the time integral of $\nu^+(a;t)$ in Eq. (4.23) can be derived directly from the equivalent linear system responses. Recall Eq. (3.9), which was used to derive combination rules of the crossing rates in the existing GM-ELM. By replacing stationary $\nu^+(a)$ and $p(z,\dot{z})$ by nonstationary $\nu^+(a;t)$ and $p(z,\dot{z};t)$, respectively, and taking temporal-average for both sides we obtain

$$\frac{1}{T_d}\left(\int_{T_i}^{T_e} \nu^+(a;t)dt\right) = \lim_{\Delta t\to 0}\frac{1}{\Delta t}\int_0^{\infty}\int_{a-\dot{z}\Delta t}^{a}\left(\frac{1}{T_d}\int_{T_i}^{T_e} f(z,\dot{z};t)dt\right)dzd\dot{z} \tag{4.24}$$

or in a simple form:

$$\hat{\nu}^+(a) = \lim_{\Delta t\to 0}\frac{1}{\Delta t}\int_0^{\infty}\int_{a-\dot{z}\Delta t}^{a}\hat{f}(x,\dot{x})\,dxd\dot{x} \tag{4.25}$$

where

$$\hat{\nu}^+(a) = \frac{1}{T_d}\int_{T_i}^{T_e}\nu^+(a;t)dt \tag{4.26a}$$

$$\hat{f}(x,\dot{x}) = \frac{1}{T_d}\int_{T_i}^{T_e} f(x,\dot{x};t)dt \tag{4.26b}$$

Adopting the derivation used for the stationary case, a combination rule analogous to Eq. (3.12) (or Eq. (2.17) for univariate case) is derived as

$$\hat{\nu}^{+}(a) = \sum_{k=1}^{K} \alpha_k \hat{\nu}_k^{+}(a) \tag{4.27}$$

$$\hat{\nu}_k^{+}(a) = \frac{1}{2\pi}\sqrt{\frac{\hat{\lambda}_{2,k}}{\hat{\lambda}_{0,k}}}\exp\left[-\frac{\left(a-\hat{\mu}_{z,k}\right)^2}{2\hat{\lambda}_{0,k}}\right] \tag{4.28}$$

where $\hat{\mu}_{z,k}$, $\hat{\lambda}_{0,k}$ and $\hat{\lambda}_{2,k}$ are mean, first- and second-order spectral moments of *k*-th linear oscillator in the ELS obtained using the PDF of Eq. (4.17). In other words, only by using the temporal-average response PDF instead of the stationary instantaneous PDF in identifying ELS, one can acquire the temporal-average value of the mean up-crossing rate. It is noted that this approach can take into account the effects of non-stationarity without major modifications. Following this approach, the first passage probability is obtained by combining Eqs. (4.23), (4.26a), and (4.27), i.e.

$$Pr[\max Z(t) > a]_{t\in T_d} = 1 - A\exp\left[-\sum_{k=1}^{K}\alpha_k \hat{\nu}_k^{+}(a)\, T_d\right] \tag{4.29}$$

which has the exact same form as that of the stationary GM-ELM. In the same manner, double-sided first passage probability is estimated by Eq. (2.21) in which $\nu_k^{+}(a)$ is replaced by $\hat{\nu}_k^{+}(a)$. The parameter A, i.e. the probability of starting from the safe zone, corresponds to 1 in seismic fragility analysis.

4.4.4 Numerical examples

To demonstrate the proposed temporal-average GM-ELM, the hysteretic system in Section 4.3.5 is investigated again. For the structural parameters, the initial natural period of 0.2 s, damping of 0.1, and yield displacement of 0.024 m are used while

the others follow the previous settings. The ground motion time history is modeled by a nonstationary process whose evolutionary PSD shown in Eq. (4.19) (Broccardo 2014; Priestley 2965; Broccardo and Der Kiureghian 2014; Broccardo and Dabaghi 2017) is defined by use of the following modulating function:

$$A_g(\omega, t) = q(t)\Phi_g(\omega|t) \tag{4.30}$$

in which $q(t)$ is the time-modulating function and $\Phi_g(\omega|t)$ is the frequency-modulating function that depends on time. This is termed as a non-separable evolutionary PSD. To describe strong ground motions, the widely recognized Kanai-Tajimi filter model is introduced with the time-varying parameters for the frequency-modulating function:

$$\Phi_g(\omega|t)^2 = \frac{\omega_f(t)^4 + 4\zeta_f(t)^2\omega_f(t)^2\omega^2}{\left(\omega_f(t)^2 - \omega^2\right)^2 + 4\zeta_f(t)^2\omega_f(t)^2\omega^2} \tag{4.31}$$

in which the parameters are chosen as $\omega_f(t) = 22.37 - 0.44(t - 22.59)$ in the unit of rad/s and $\zeta_f(t) = 0.22$. For the sake of simplicity, these values are taken from the strike-slip faulting earthquake model developed by Rezaeian *et al.* (2008). However, it should be remarked that these parameters are originally derived for the second-order filter which is similar but not equal to Kanai-Tajimi filter. For $q(t)$ in Eq. (4.30), the gamma modulating function is used, i.e.

$$q(t; \boldsymbol{\alpha}) = \alpha_1 t^{\alpha_2 - 1} \exp(-\alpha_3 t) \tag{4.32}$$

with the parameters of $\boldsymbol{\alpha} = \{\alpha_1, \alpha_2, \alpha_3\} = \{1.2 \times 10^{-10}, 11.6,\ 0.47\}$. These three parameters depend on the pre-assumed characteristics of earthquake: the effective duration of the motion (16.36 sec), Arias intensity (0.05 sec$\cdot g^2$), and the time at the middle of the strong shaking phase (22.59 sec). Derivation of the relations are

beyond the scope of our discussion and the details are available in Rezaeian *et al.* (2008) and Rezaeian and Der Kiureghian (2010)

The artificial ground motions are generated by sampling in the discretized frequency domain in terms of a finite number of random variables, i.e.

$$\ddot{U}_g(t) = \sum_{j=1}^{n/2} \sigma_j(t)\left[u_j \cos\left(\omega_j t\right) + \hat{u_j} \sin\left(\omega_j t\right)\right] \tag{4.33a}$$

$$\text{with } \sigma_j(t) = \sqrt{2S_g\left(\omega_j, t\right)\Delta\omega} \tag{4.33b}$$

where the discretized frequency point is given by $\omega_j = j\Delta\omega$, and the terms u_j and $\hat{u_j}$ are independent standard normal random variables. A total of $n/2 = 400$ frequency points and the cutoff frequency of $\omega_{cut} = 20\pi$ rad/s are used throughout the examples of this dissertation.

The temporal-average GM-ELM approach is applied to the nonlinear SDOF oscillator in Section 4.3.5 with the nonstationary ground motion model described above. The failure-susceptible duration of the nonstationary response is first identified as $T_i = 15.6\,\text{s}$ and $T_e = 35.6\,\text{s}$ using Eqs. (4.20) and (4.21), which respectively correspond to the time points giving 5 and 99% of arias intensity ratio. The first and second time history graphs of Figure 4.9 are respectively an artificial ground motion $\ddot{U}_g(t)$ generated from Eq. (4.33), and the corresponding displacement. The hysteresis behavior of the nonlinear system during the significant duration is also presented in Figure 4.10.

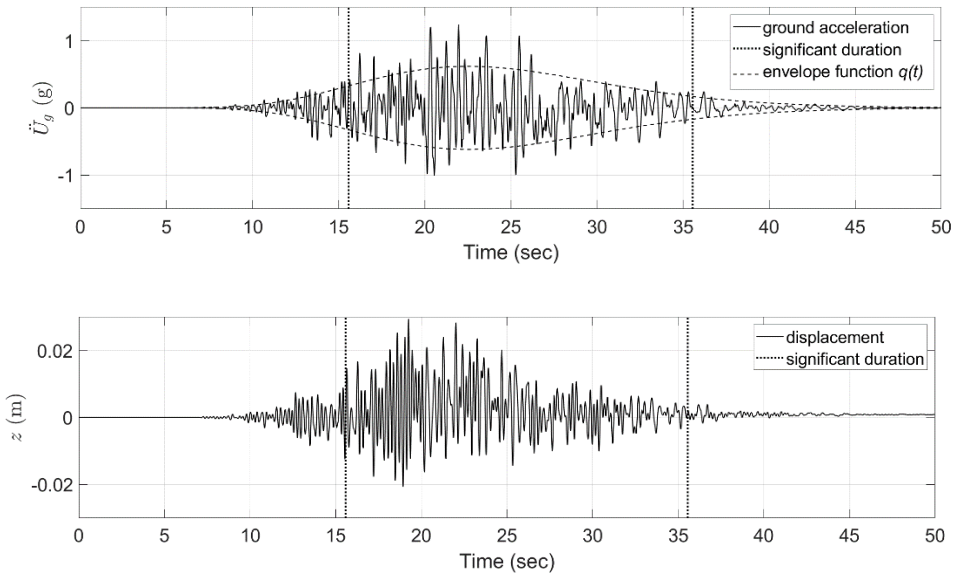

Figure 4.9 A sample of artificial ground motion and resulting nonlinear response

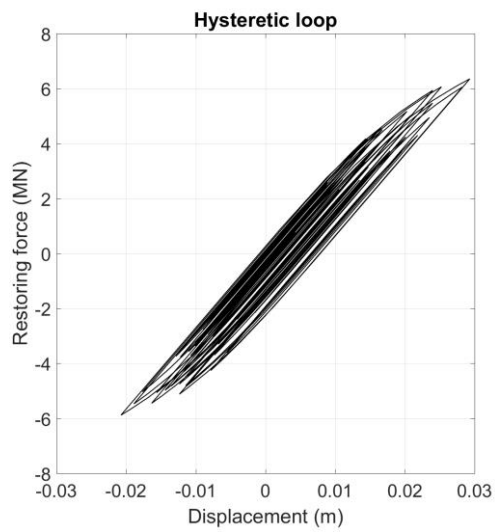

Figure 4.10 Hysteretic behavior of system

Figure 4.11 shows the mean up-crossing rates and first-passage probabilities obtained by the temporal-average bivariate GM-ELM analysis. For each intensity level, 300 runs of dynamic analysis are performed to identify ELS using 169 GM components. To get reference MCS results, 5×10^4 runs of dynamic analysis are

performed for each intensity level. The proposed temporal-average GM-ELM provides the results that are close to those by the MCS estimations. For the comparison purpose, the results of original GM-ELM analysis using equivalent stationary excitation are also presented. The stationary strong motion duration is defined as the time segment in which intensity of the excitation peaks exceed a half of the maximum peak intensity, and the corresponding equivalent stationary PSD is the temporal average of PSD throughout the duration (Duan and Chen 1999). From the results, one can confirm that equivalent stationary response could highly underestimate the failure probability of the nonlinear system, therefore it is necessary to assess nonstationary responses by using methods proposed in this study.

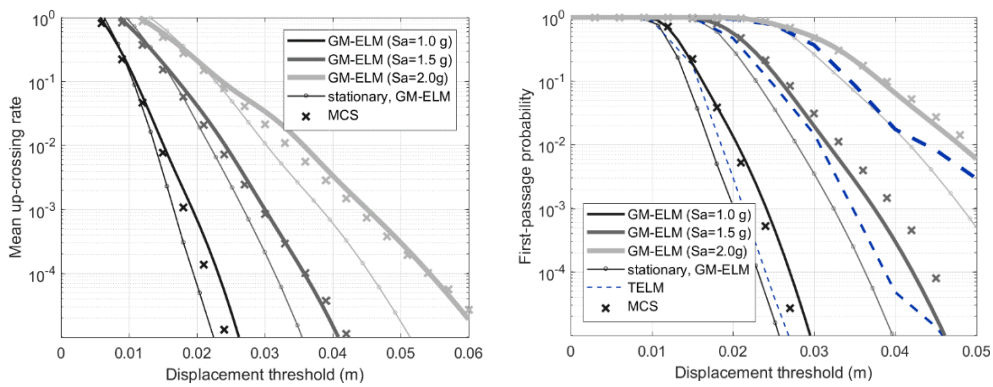

Figure 4.11 Mean up-crossing rates (left) and first-passage probabilities (right) obtained by temporal-average GM-ELM, equivalent stationary GM-ELM, TELM, and MCS

4.5 Combining intensity-augmented and temporal-average GM-ELM

4.5.1 Simple scaling approach for nonstationary responses

Combination of the intensity-augmented GM-ELM and the temporal average approach is rather straightforward because one can replace $f(\boldsymbol{z}|IM)$ in Eq. (4.1) by

the temporal average PDF, i.e. $\hat{f}(\boldsymbol{z}|IM)$. The same sampling approach in Section 4.3.3 can be used to acquire the samples of the temporal-average intensity-augmented PDF. Among the responses from nonlinear dynamic analysis, only those inside the significant excitation duration are collected.

Alternatively, the simple scaling approach proposed in Section 4.3.4 could also be applied for temporal-average GM-ELM. Similar to the stationary excitation case, the nonstationary excitation can be modeled as a linear combination of a finite number of standard normal random variables, i.e. $f_g(t) = \boldsymbol{s}(t)^{\mathrm{T}}\boldsymbol{u}$. For the nonstationary responses, a new variable $\hat{z}$ that represents the random response at a random time point $t \in [T_i, T_e]$ is considered. Notice that in this way, the random variable $\hat{z}$ will follow the temporal-average PDF at given intensity measure, $\hat{f}(z|IM)$. By introducing first-order approximation to the limit-state surface $z - \hat{z} = 0$, the Eq. (4.12) is modified as

$$Pr(\hat{z} > z|IM) \cong \Phi(-\beta_z) \tag{4.34}$$

At the same time by scaling excitation by factor c, i.e., $f_{g,c}(t) = cf_g(t) = \boldsymbol{s}(t)^{\mathrm{T}}(c\boldsymbol{u})$, the first-order approximation of the complementary CDF of the scaled response $\hat{z}_{\mathrm{c}}$ is derived as

$$Pr(\hat{z}_c > z|IM_c) \cong \Phi\left(-\frac{\beta_z}{c}\right) \tag{4.35}$$

Thus, the approximation strategy is basically the same as the stationary case. The procedure in Figure 4.4 could be directly applied to nonstationary responses by only changing all the conditional response PDF $f(z|IM)$ into temporal-average response PDF $\hat{f}(z|IM)$. Again, since the proposed simple scaling approach is only applicable to univariate GM-ELM, it is encouraged to adopt heuristic strategies

proposed in Section 3.6 to tune or optimize the equivalent linear damping values.

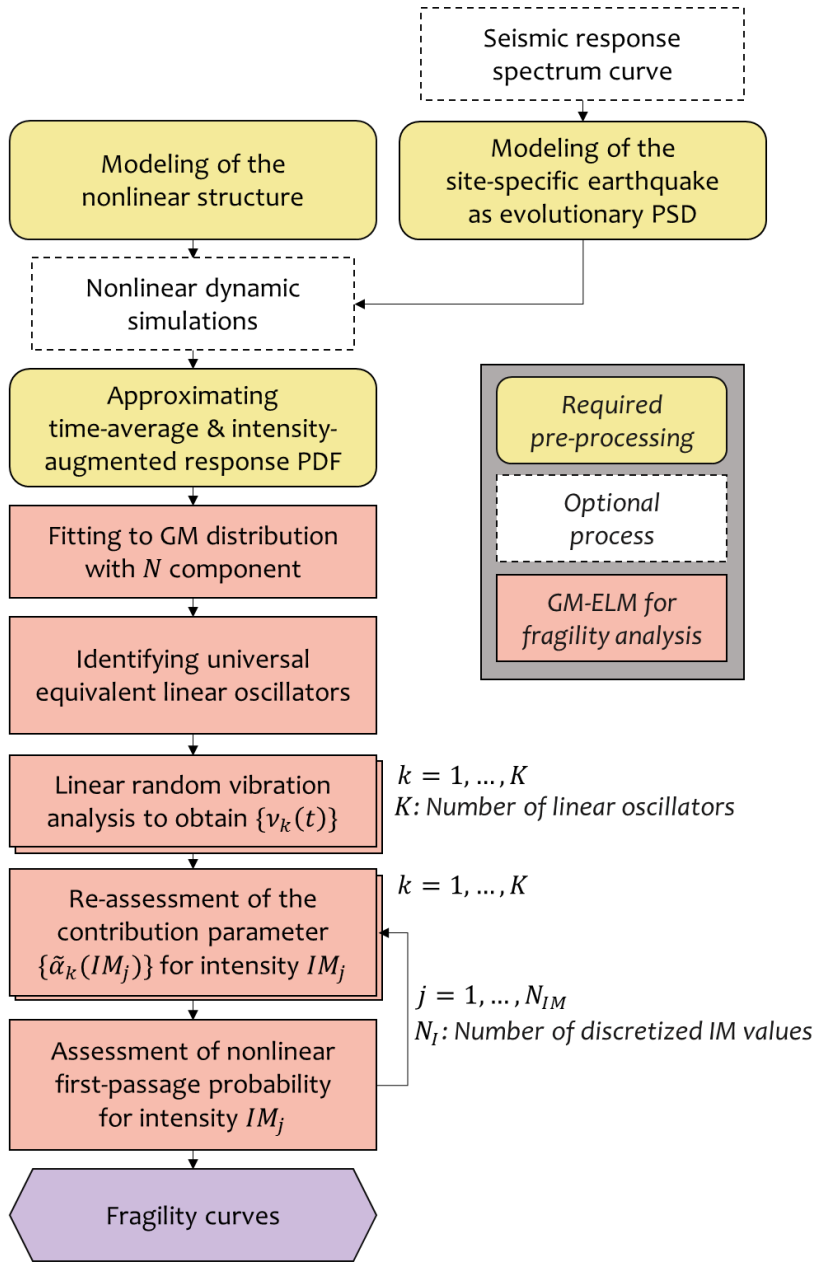

Figure 4.12 Procedure of GM-ELM fragility analysis

4.5.2 Numerical example 1

This section demonstrates the combination of the intensity-augmented and temporal-average GM-ELM to efficiently obtain fragility curves of the nonlinear system subjected to nonstationary excitation. The procedure is summarized in Figure 4.12. The first example extends the nonstationary example in Section 4.3.5 to the intensity-augmented GM-ELM to improve efficiency of the fragility analysis. The same structure and excitation models are used. The response PDF is estimated by direct sampling through nonlinear dynamic analysis. A total of 600 different IM values are sampled from uniform distribution $IM \sim U(0, 3.3)$, and the corresponding ground accelerogram is generated to obtain the samples of $\{Z, \dot{Z}, IM\}$. To increase numerical stability of EM algorithm in fitting GM model, the overlapped sample values of IM are split by introducing uniform kernel smoothing technique. The total length of symmetric uniform kernel is set as the intensity interval length of interest, i.e. $\max(IM) - \min(IM)$, divided by the number of the samples. A total of 196 Gaussian components are used to fit the 3-dimensional intensity-augmented PDF.

Figure 4.13 shows the results of the fragility analysis using nonstationary ground excitations and corresponding MCS results. It is confirmed that the combined application of temporal-average and intensity-augmented GM-ELM accurately evaluates the fragilities for nonstationary excitations. On the other hand, the identified universal ELS also allows us to readily estimate the mean up-crossing rates and first-passage probabilities for various threshold values. Figure 4.14 shows the first-passage probability identified by the intensity-augmented GM-ELM. The results show a level of accuracy similar to that in Figure 4.11 (right). However, it should be noted that a single set of universal ELS is needed for all results in Figure

4.14 while each curve in Figure 4.11 requires independent identification of ELS. It is also noted that since the results rely on random samples of dynamic simulation, each attempt may show a certain degree of variations. The analysis results which are typically expected are presented here.

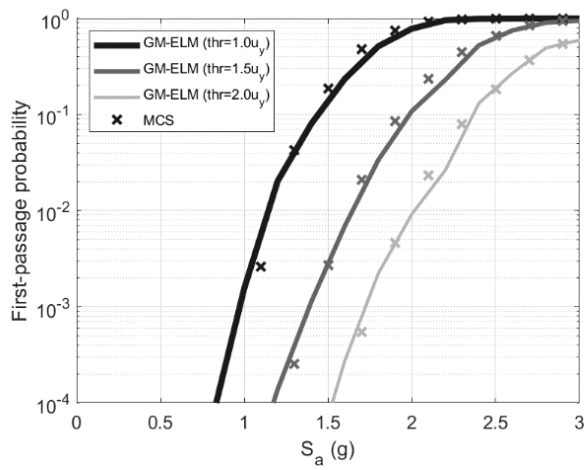

Figure 4.13 Fragility curves obtained by combining intensity-augmented and temporal-average GM-ELM, TELM, and MCS

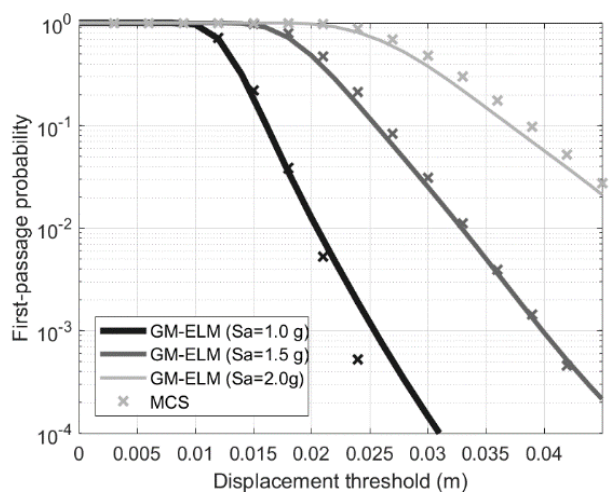

Figure 4.14 First-passage probabilities for different thresholds identified by combining intensity-augmented and temporal-average GM-ELM, and MCS

4.5.3 Numerical example 2

As a practical application of the proposed approach, a MDOF nonlinear system subjected to design code-conforming seismic excitations is next considered. In particular, let us consider a structure located in Massena, Italy (Alibrandi and Mosalam 2018), which is represented by a 6-DOF shear building model in Figure 4.15 (left). The mass and initial stiffness of the structure are given in the figure along with typical force-deformation behaviors of 1st and 6th story drifts represented by Bouc-Wen hysteresis model. The height of each floor is assumed to be 2.5m and the yield displacement corresponds to the inter-story drift of 1%. Using the initial stiffness, the first and second natural periods of the structure are identified as 0.58s and 0.24s respectively. For the initial damping, 5% of Rayleigh damping is assumed for the first and second modes.

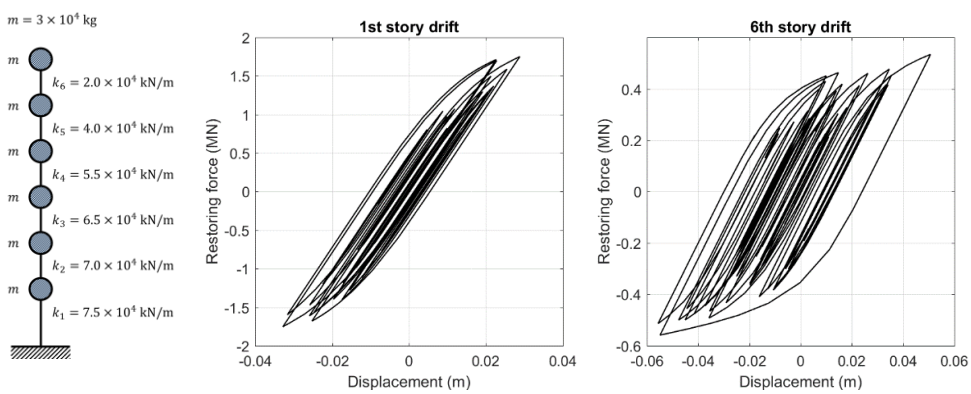

Figure 4.15 MDOF shear building model (left) and typical hysteresis curves (right)

As the site-specific response spectrum, Eurocode EC8 and Italian Annex are adopted in this example. The detailed setting of this ground motion modeling part is

from the example in Alibrandi (2018). In summary, the soil type is assumed as "B" and the return period of interest is 475 year. Figure 4.16(a) illustrates the response spectrum curve used in this example. This response spectrum is then used to develop a uniformly modulated PSD whose frequency component does not depend on time, i.e. $S_g(\omega,t) = |q(t)|^2 S_o(\omega)$. To convert the response spectrum into PSD representation of $S_o(\omega)$, the simple iterative formulation proposed by Cacciola *et al.* (2004) is employed. The iterative formulation can be written as,

$$S_o(\omega_i) = \begin{cases} 0 & 0 \le \omega_i \le \omega_o \\ \dfrac{4\zeta_o}{\pi\omega_i - \zeta_o\omega_{i-1}}\left[\dfrac{S_a^2(\omega_i,\zeta_o)}{\eta_x^2(\omega_i,\zeta_o)} - \Delta\omega\sum_{k=1}^{i-1} S_o(\omega_k)\right] & \omega_o < \omega_i \end{cases} \tag{4.36}$$

where ω_i is *i*-th discretized value of circular frequency domain, and $S_a(\omega_i,\zeta_o)$ is the coordinate of given response spectrum where the damping ratio $\zeta_o = 0.05$ is used in this example. The parameter ω_o is provided as 0.36 rad/s and $\eta_x(\omega_i,\zeta_o)$ is the "peak facter" which can be evaluated using the closed-form formulas by Der Kiureghian (1980) as,

$$\eta_x(\omega_i,\zeta_o) = \sqrt{2\log\left\{2N_x\left[1-\exp\left(-\delta_x^{1.2}\sqrt{\pi\log(2N_x)}\right)\right]\right\}} \tag{4.37}$$

with

$$N_x = \frac{t_s}{2\pi}\omega_i(-\log(0.5))^{-1} \tag{4.38}$$

$$\delta_x = \sqrt{1-\frac{1}{\zeta_o^2}\left(1-\frac{2}{\pi}\arctan\frac{\zeta_o}{\sqrt{1-\zeta_o^2}}\right)^2} \tag{4.39}$$

The parameter related to the stationary duration of the accelerogram is set to be $t_s =$ 35s. The identified shape of the PSD function $S_o(\omega)$ is shown in Figure 4.16(b).

Furthermore, the time modulating function proposed by Hsu and Bernard (1978) is adopted:

$$q(t) = \varepsilon_{HB} t \exp(-\mu_{HB} t) \tag{4.40}$$

where $\varepsilon_{HB} = 1/t_{max}$ and $\mu_{HB} = e/t_{max}$ with $t_{max} = 5$ sec. The shape of the time-modulating function is presented in Figure 4.16(c) along with a sample of artificially generated ground motion.

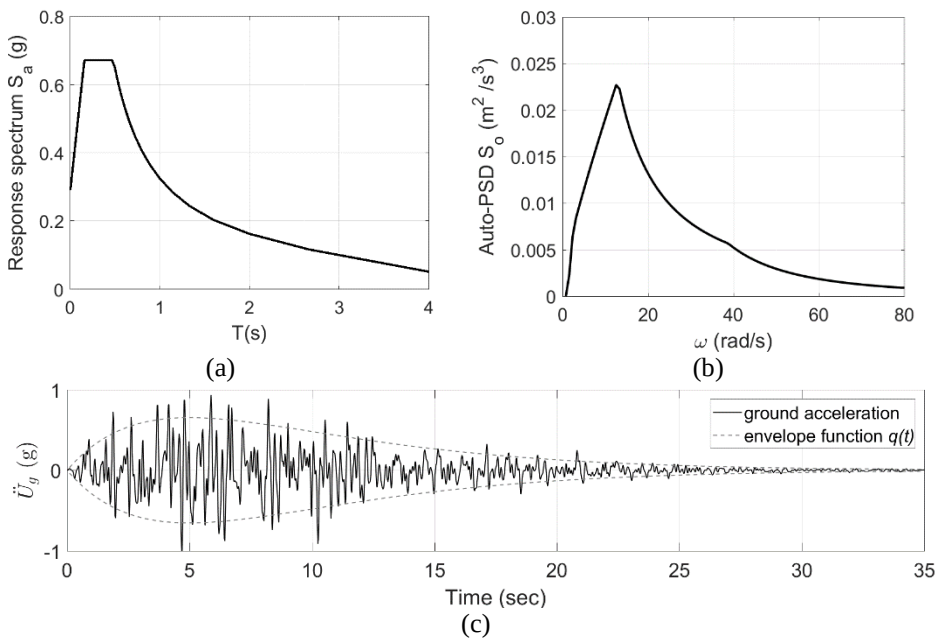

Figure 4.16 (a) Response spectrum, (b) corresponding PSD, and (c) a sample of artificial ground motion used in the example

For GM-ELM analysis of the MDOF structure, 600 runs of dynamic analysis are performed to identify the intensity-augmented PDF. One advantage of the proposed GM-ELM-based approach is that the required number of dynamic simulations is independent of the DOF of structure since each simulation provides the whole set of response samples for all DOFs. For each DOF, a total of 196 GM

components are used to identify universal ELS. Figure 4.17 shows the fragility curves of the 1st and 6th floors of the structure with respect to three thresholds on the inter-story drift ratios, 1%, 1.5%, and 2%. By comparing the results by the proposed method with those by MCS simulations (5.4×10^4 runs of dynamic analysis for each of the six intensity levels), it is confirmed that the proposed method enables efficient fragility analysis of MDOF structures under code-conforming excitations.

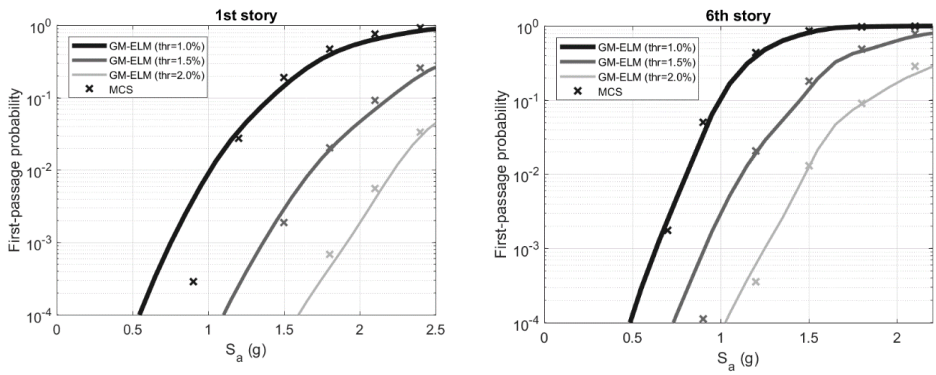

Figure 4.17 Fragility curves for the 1st (left) and 6th story (right) drift

Finally, to demonstrate the validity and efficiency of simple scaling approach for nonstationary excitations, the same 6 story structure located at the different region is considered. The response spectrum for Gyeongju is evaluated from the Building Design Code of Korea (KBC 2016). The response spectrum is first converted to the base stationary PSD function and time modulating function is imposed. Figure 4.18 shows the hysteretic behavior of the system and corresponding time history deformation.

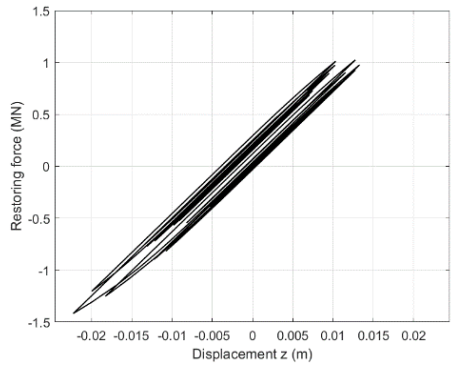

(a) Hysteretic loops for 1st column

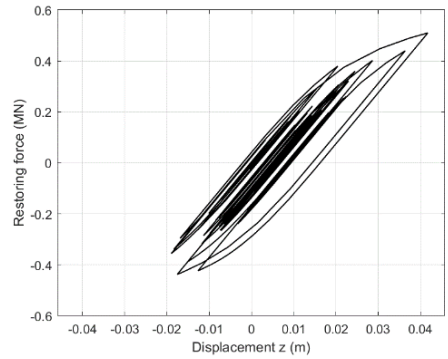

(b) Hysteretic loops for 6th column

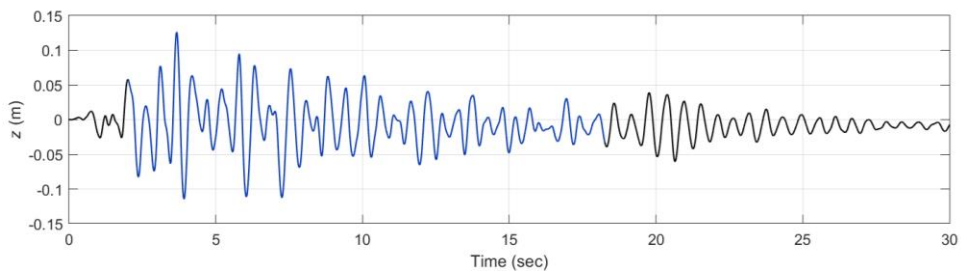

(c) Time history of 6th inter-story diaplacement response

Figure 4.18 Typical response of the structure on representative intensity measure

GM-ELM analysis is first performed using the simple scaling approach (denoted as GM-ELM(A) in Figure 4.19) with total of 400 rounds of nonlinear dynamic analysis. For the simple scaling, the reference intensity value was first found as a seismic intensity level that makes the pseudo-spectral displacement ($S_d = S_a/\omega^2$) for the initial stiffness match $6.0\,u_y$. It is noticed that the selected value 6.0 is higher than the stationary case, to ensure that the nonlinear behavior is sufficiently captured by the representative response PDF. Total of 100 components are used for GM-fitting. MCS results are obtained by 5×10^4 rounds of nonlinear dynamic analysis for each intensity level. For a comparison, crude sampling-based GM-ELM using 700 rounds of nonlinear dynamic analysis (GM-ELM(B)) is also introduced. It is shown that in this example, the proposed simple scaling approach shows

superior accuracy over crude sampling-based approach while it also required a smaller number of dynamic simulations. The discrepancy in the sampling-based approach attributes to (1) the lack of samples to fill the increased dimension of $\{z, \dot{z}, IM\}$ space, and (2) the perturbation associated with uniform kernel smoothing, which was discussed in Section 4.5.2. On the other hand, the approximation error due to the simple scaling method and approximated damping is hardly perceptible.

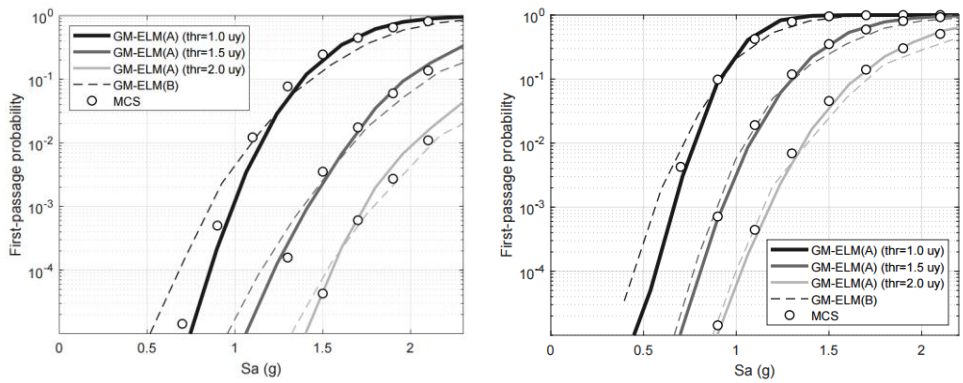

(a) 1st story drift (b) 6th story drift

Figure 4.19 Fragility curves obtained by temporal-average intensity-augmented GM-ELM (A:simple scaling approach; B:crude sampling approach) and MCS

4.6 Conclusions

GM-ELM is further developed in this study to facilitate seismic fragility analysis method based on stochastic dynamic analysis. Technical developments in this chapter are summarized as (1) identification of universally equivalent linear system, (2) embracement of the nonstationary excitations and (3) proposal of efficient extrapolation methods called a simple scaling approach. These further developments respectively allow us to re-use the identified ELS to obtain nonlinear response subjected to a range of excitation intensities, employ realistic, i.e. nonstationary

stochastic ground motion models, and further elevate the efficiency and stability of the proposed GM-ELM framework.

Numerical examples of nonstationary excitations are carefully developed and investigated to test the performance of the methods in practical applications. The examples feature both experimentally derived parametric strong ground excitation model, and design code-confirming ground motion model. Especially, the latter type of ground motion is applied to MDOF systems to demonstrate the performance of the proposed method in realistic problems. It was shown that the combination of the proposed three developments provides significant advantages for GM-ELM-based seismic fragility analysis.

Chapter 5. Estimation of first-passage probability by Poisson branching process model (PBP)

5.1 Introduction

The probability of the first-passage failure, i.e. the event that a random process response exceeds a certain threshold at least once during a finite time period, is often an important indicator of the structural performance level. In the previous chapters, to estimate the first-passage probability of the nonlinear system, GM-ELM has adopted the widely used Poisson approximation. The crossing events of the response are modeled as a Poisson point process, and therefore, the occurrence interval between each crossing event are assumed to be mutually independent.

However, the accuracy of Poisson approximation may depend on the bandwidth of the random process as well as the threshold level of interest. When the response is a relatively broadband process or the failure threshold level is high, Poisson assumption-based estimation is known to be generally admissible (Lutes and Sarkani 2004). However, when the process has very narrow bandwidth or a lower threshold level is involved, it may substantially overestimate the first-passage probabilities (Lutes and Sarkani 2004; Song and Der Kiureghian 2006). The error attributes to the high correlations between the nearby peaks which inflict a cluster of crossings. Therefore, when dealing with the narrowband processes, it is desired to adopt an improved first-passage probability equation which could account for this cohesive behavior of the crossing events.

Precise estimation of the first-passage probability has been recognized as one of the major topics in random vibration analysis. While the general exact solution for this probability is not available even for the stationary Gaussian processes, a number of approximation equations have been developed by Ditlevsen (1986), Vanmarcke (1975), Naess *et al*. (2010), Lutes (2012), and others. Those methods rely on the bandwidth parameters of the PSD and/or the extreme value regressions. Although each approach has significantly improved the first-passage probability estimations compared to the Poisson approximation, it is found that the accuracy of each method often depends on the bandwidth of the process as well as the specific shape of the underlying PSD. Following this line of research, and in order to gain consistent estimation accuracies throughout different spectral characteristics and threshold levels, the first part of this chapter presents a new first-passage probability equation. By describing the crossing events with a *Poisson branching process model* (PBP), alternative formulations and a bandwidth parameter for the first-passage probability are derived.

On the other hand, the first-passage probability estimation for the nonlinear system responses possesses further difficulties. This is because (1) the nonlinear response process is non-Gaussian while the most practical approximation equations are derived under the assumption of Gaussian process, and (2) the PSD of the nonlinear response process is generally not available. In light of the development of GM-ELM, the former issue is considerably improved by the GM-based linear decompositions. However, the latter remained as an unexplored topic. These aspects of GM-ELM are discussed in the second part of this chapter, and the new techniques to obtain improved first-passage probability are proposed. This is achieved by

introducing the bandwidth parameters obtained from a single component ELS, called *transitory ELS*, and by accounting for non-regular distribution of the *envelope process*. It is shown by numerical examples that by implementing the modified PBP-based first-passage probability equations into GM-ELM analysis, the estimation accuracy could be significantly improved especially when the narrowband spectral effect is dominant in the system response.

5.2 PBP for first-passage probability estimation

5.2.1 Review on first-passage probability approximation equations

Consider a stationary zero-mean Gaussian stochastic process $X(t)$ with the spectral density of $S_{XX}(\omega)$. The probability of the first-passage failure of this process during a time interval $[0, \tau]$ and given threshold a is defined as

$$p(a;\tau) = P\left(\max_{0\le t\le \tau} |X(t)| \ge a\right) \tag{5.1}$$

This definition corresponds to the double-barrier problem since the thresholds of both a and $-a$ are imposed. When only one side of the thresholds is considered, $|X(t)|$ in Eq. (5.1) should be substituted with $X(t)$ and it is called the single-barrier problem. It is noted that in this chapter, our primary interest is on the double-barrier problem, while the modification to the single-barrier case is straightforward. Eq. (5.1) is often presented in terms of the exponential function of time (Lutes and Sarkani 2004), i.e.

$$p(a;\tau) = 1 - A \exp \int_0^{\tau} \alpha(a;t)\, dt \tag{5.2}$$

where the second term in the right-hand side represents the probability of system

survival. The variable A denotes the probability that the process starts from the safe-domain, i.e. $A = P(|X(0)| \leq a)$. The parameter $\alpha(a;t)$ represents the *conditional crossing rate* for the threshold of a given the initial condition and the condition that no prior crossings occurred before t. However, the identification of $\alpha(a;t)$ is known to be challenging since its rigorous expressions require the conditional joint PDF of the process and its time derivative given no prior failures, which is usually unavailable. Other general solution for $\alpha(a;t)$ called inclusion-exclusion formulation consists of the infinite series with the entries again hardly acquirable (Lutes and Sarkani 2004).

As an alternative, the widely acknowledged approximation for the first-passage probability is to substitute the conditional crossing rate $\alpha(a;t)$ with the *unconditional* crossing rate of $\nu(a;t)$, i.e.

$$p(a;\tau) = 1 - A \exp \int_0^\tau \nu(a;t)\, dt \tag{5.3}$$

This expression is called the Poisson approximation. Unlike the conditional crossing rate, the unconditional crossing rate is easily acquirable from the closed-form relationship

$$\nu(a;t) = \frac{1}{\pi}\sqrt{\frac{\lambda_2}{\lambda_0}} \exp\left(-\frac{a^2}{2\lambda_0}\right) \tag{5.4}$$

It is known that for the Gaussian process, this Poisson approximation is asymptotically correct as the threshold level or the bandwidth of the process increases (Lutes and Sarkani 2004). However, when the smaller threshold level is involved and for the narrowband random process, the error could be significant.

On the other hand, a further modification is made by Ditlevsen (1986) and also

by Lutes and Sarkani (2004), with different reasoning, to substitute $\nu(a;t)$ by

$$\eta_P(a;t) = \frac{\nu(a;t)}{P(|X(t)| < a)} \tag{5.5}$$

This modification aims to account for the initial conditions of the first-passage problem by defining the first-passage time as an effective duration within the crossing interval. While the previous $\nu(a;t)$ considered the whole duration between the two up-crossing events as the first-passage time, $\eta_P(a;\mathrm{t})$ only considers the duration which the process stays under the thresholds, i.e. from a down-crossing to the subsequent up-crossing. It is noted that the proportion of the durations in which the process stays under the threshold and over the threshold could be respectively estimated as $P(|X(t)| < a)$ and $P(|X(t)| > a)$. It is more reasonable to choose $\eta_P(a;\mathrm{t})$ rather than $\nu(a;t)$ considering the fact that initial conditions are already accounted for by the factor A in Eq. (5.3).

Another widely acknowledged approximation proposed by Vanmarcke (1974) additionally accounts for the correlations between the crossing intervals by introducing the concept of the *cluster* of the crossings (See Figure 5.1). Vanmarcke's formulation replaces $\alpha(a;t)$ by

$$\eta_V(a;t) = \nu(a;t)\frac{1 - \exp\left[-\sqrt{\frac{\pi}{2}}\delta^{1.2}\frac{a}{\sqrt{\lambda_0}}\right]}{P(A(t) < a)} \tag{5.6}$$

$$P(A(t) < a) = 1 - \exp\left(-\frac{a^2}{2\lambda_0}\right) \tag{5.7}$$

where the bandwidth parameter $\delta = \sqrt{1 - \lambda_1^2/\lambda_0\lambda_2}$ adjusts the crossing rate expression to account for the spectral characteristics. The *j*-th order spectral moment of the process, λ_j was introduced and defined in Eq. (2.7). The random process

$A(t)$ denotes the envelope process of $X(t)$ and Eq. (5.7) is its instantaneous CDF. Eq. (5.6) is derived based on the introduction of slowly varying envelope process, combined with delicate assumptions on clumping behavior of the crossings (Vanmarcke 1975). On the other hand, the term $P(A(t) < a)$ in Eq. (5.7) is introduced for the same reason as $P(|X(t)| < a)$ in Eq. (5.5), where $|X(t)|$ is replaced by $A(t)$ to consider the effect of the clumping behavior on the first-passage time.

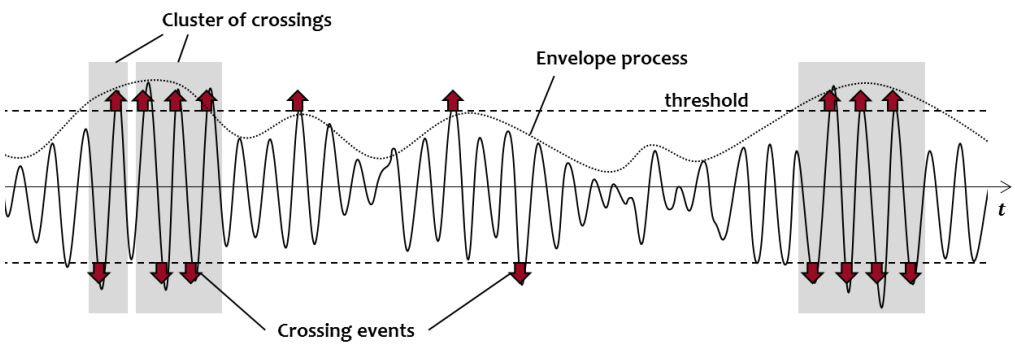

Figure 5.1 Typical behavior of narrowband process ($\alpha = 0.96,\ \delta = 0.2$)

Finally, Lutes (2012) recently proposed an approximation based on the correlation-amplitude technique. While the occurrence of the cluster is modeled as the event whose envelope process exceeds the threshold, $\{A(t) > a\}$, the Markov point process model is adopted to describe the envelope crossing event, i.e. the probability that crossing occurs at a certain time point depend only on the envelope value before one cycle of the process. The conditional crossing rate is estimated as

$$\eta_L(a;t) = -\frac{\ln q(a)}{\tau_c} \tag{5.8}$$

$$q(a) = \frac{P(A(t) < a, A(t+\tau_c) > a)}{P(A(t) < a)} \tag{5.9}$$

where the numerator and the denominator of Eq. (5.9) can be acquired by numerical integration of the joint PDF

$$P_{A(t-\tau_c)A(t)}(a_1, a_2) = \frac{a_1 a_2}{(1-\rho)\sigma_x^4} \exp\left(\frac{-(a_1^2 + a_2^2)}{2(1-\rho)\lambda_0^2}\right) I_0\left(\frac{\rho^{1/2} a_1 a_2}{(1-\rho)\lambda_0}\right) \tag{5.10}$$

in which $I_k(\cdot)$ is modified Bessel function of order *k*, and $\rho = \rho(\tau_c)$ is correlation coefficient of $A^2(t)$ and $A^2(t+\tau_c)$, which is derived as

$$\rho(\tau_c) = \frac{4}{\lambda_0^2} \int_0^\infty \int_0^\infty S_{XX}(\omega_1) S_{XX}(\omega_2) \left[\cos(\omega_1 \tau) \cos(\omega_2 \tau) + \sin(\omega_1 \tau) \sin(\omega_2 \tau)\right] d\omega_1 d\omega_2 \tag{5.11}$$

Lutes (2012) further proposed to modify the correlation coefficient by the formulations below in order to account for the effect of the multi-modal frequency.

$$\rho = \max\left[\rho(\tau_c), \exp\left(-\frac{\tau_c}{H}\right)\right] \tag{5.12a}$$

$$H = \int_0^\infty \rho(\tau) d\tau \tag{5.12b}$$

The second choice of the coefficients in Eq. (5.12a) is introduced to average out the oscillatory behavior of the multimodal correlation function $\rho(\tau_c)$ using the exponential base function.

5.2.2 Poisson branching process model of crossing events

This section presents a new first-passage probability formulation that is based on the stochastic point process model called *Poisson branching process*. Let us first consider a zero-mean stationary Gaussian process. As shown in Figure 5.1, crossing events of the narrowband process naturally tend to form the clusters. In each cluster,

the crossing events can be categorized into either the initiating crossing or the following crossings as marked by red and gray arrows, respectively in Figure 5.2(a). In the proposed model, the initiating crossings are considered to follow Poisson point process while the occurrences of the following crossings are governed by the Markov branching process. Here, the Markov branching process means that given a precedent crossing, either the initiating or the following crossing, the subsequent crossing may occur with a fixed probability. The cluster is closed once the following crossing does not occur. Figure 5.2(b) is the conceptual illustration of the proposed crossing model.

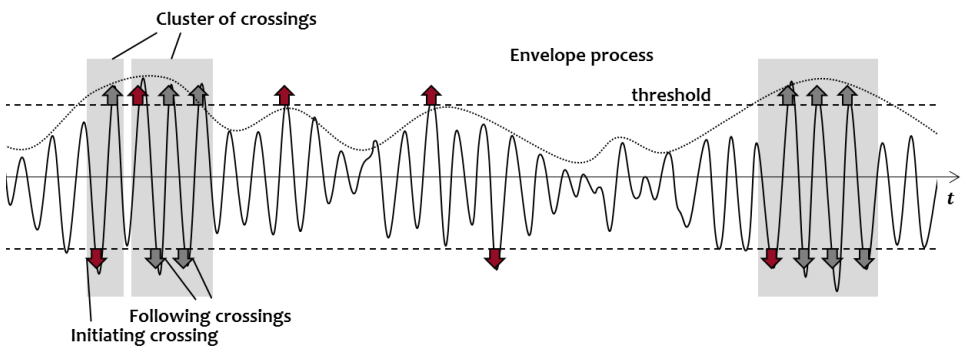

(a) Crossing events and clusters

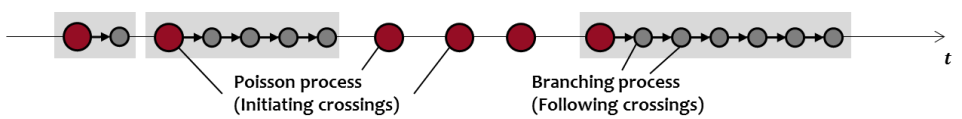

(b) Poisson branching process model

Figure 5.2 Poisson branching process model for crossing events

Assume that given the threshold of a, the initiating crossings have the mean occurrence rate of $\nu_{PB}(a)$, while each following crossing occurs with the probability of $p_o(a)$. The main idea of PBP-based first-passage probability equation

is to approximate the conditional crossing rate $\alpha(a;t)$ in Eq. (5.2) by the unconditional crossing rate of the initiating crossings, $\nu_{PB}(a)$. From the definition of the mean occurrence rate, the mean of the number of initiating crossings during $t \in [0, T_d]$ is $\nu_{PB}(a)T_d$. The average of the total number of crossings, $N_t(a)$ can be expressed as

$$E[N_t(a)] = \nu_{PB}(a)T_d E[N_c(a)] \tag{5.13}$$

where $N_c(a)$ denotes the number of crossings inside each cluster whose expectation is derived as the following series form:

$$\begin{aligned} E[N_c(a)] &= (1 - p_o(a)) + 2p_o(a)\big(1 - p_o(a)\big) + 3p_o^2(a)(1 - p_o(a)) + \cdots \\ &= \frac{1}{1 - p_o(a)} \end{aligned} \tag{5.14}$$

from the definition of the branching process.

On the other hand, it is noted that the total number of crossings, including the initiating and the following ones, during $t \in [0, T_d]$ can also be written in terms of the unconditional mean crossing rate $\nu(a)$ as

$$E[N_t(a)] = \nu(a)T_d \tag{5.15}$$

By substituting Eq. (5.14) into Eq. (5.13), and by finding its equivalency with Eq. (5.15), the relationship between $\nu(a)$ and $\nu_{PB}(a)$ is retrieved as

$$\nu_{PB}(a) = \big(1 - p_o(a)\big)\nu(a) \tag{5.16}$$

Finally, to account for the effect of initial condition as done in Eq. (5.5) and also in Eq. (5.6), the crossing rate is divided by the factor of $P(A < a)$ which considers the cluster of crossings as a lump of the failure domain. Thus, the final form of the proposed unconditional crossing rate is obtained as

$$\eta_{PB}(a) = \frac{\nu_{PB}(a)}{P(A < a)} = \nu(a)\frac{1 - p_o(a)}{P(A < a)} \tag{5.17}$$

The probability of consecutive crossing $p_o(a)$ will be derived in the next section.

5.2.3 Probability of consecutive crossing

Under the Markov assumption, the successive probability $p_o(a)$ can be defined as the conditional probability that a peak value p exceeds a threshold given the previous valley v exceeds the negative threshold, i.e.

$$p_d(a) = P(p > a | v < -a) = \frac{P(p > a, v < -a)}{P(v < -a)} \tag{5.18}$$

or vice versa. The probabilities in the numerator and the denominator could be integrated from the joint PDF of $f_{p,v}(p, v)$. To obtain this joint PDF, two different approaches are introduced.

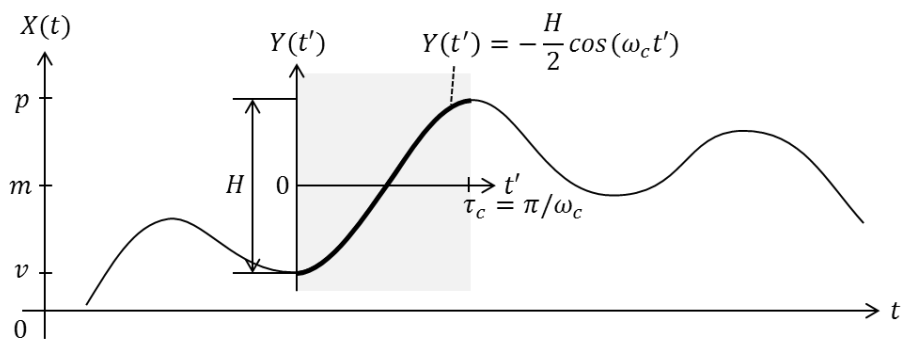

Figure 5.3 Piece-wise sinusoidal approximation of random process (Perng 1989; Ortiz 1985)

Firstly, the derivation in Perng (1989) which was originally developed in the purpose of the fatigue damage assessment is recast. In this derivation, it is assumed that a piece-wise trajectory of the random process, from a valley to the subsequent

peak, follows a sinusoidal function having the frequency of $\omega_c/2\pi$ in which $\omega_c = \sqrt{\lambda_4/\lambda_2}$ as shown in Figure 5.3. The frequency is determined by the occurrence rates of the peak of the process. Figure 5.3 also presents the related parameters, i.e. peak p, valley v, mean amplitude m and the height of rise H. In Figure 5.3, $Y(t')$ denote the sinusoidal function on the parallel translated coordinate system. Using this sinusoidal model, the acceleration process can be approximated, i.e.

$$Y(t') = -\frac{H}{2}\cos(\omega_c t') \tag{5.19a}$$

$$\ddot{Y}(t') = \frac{H}{2}\omega_c^2 \cos(\omega_c t') \tag{5.19b}$$

From Eq. (5.19b), the peak of acceleration in terms of H is written as

$$\ddot{x}_p = -\frac{H}{2}\omega_c^2 \tag{5.20}$$

while the peak of the displacement process can be represented in terms of m and H as

$$x_p = m + \frac{H}{2} \tag{5.21}$$

On the other hand, the joint distribution of x_p and $\ddot{x}_p$ is derived from the conditional joint distribution of the process $x = X(t)$ and its second derivative $\ddot{x} = \ddot{X}(t)$. Specifically, the condition on the occurrence of the peak is that the derivative of the process is zero $\{\dot{x} = 0\}$, while the second time derivative takes a negative value $\{\ddot{x} < 0\}$, i.e.

$$f(x, \ddot{x}|\dot{x} = 0) = \frac{f_{x,\dot{x},\ddot{x}}(x, \dot{x} = 0, \ddot{x})d\dot{x}}{\int_{-\infty}^{0} f_{\dot{x},\ddot{x}}(\dot{x} = 0, \ddot{x})d\dot{x}d\ddot{x}}, \quad \text{where } \begin{cases} -\infty < x < \infty \\ -\infty < \dot{x} < \infty \\ -\infty < \ddot{x} < 0 \end{cases} \tag{5.22}$$

where $f_{x,\dot{x},\ddot{x}}(\cdot,\cdot,\cdot)$ represents the joint distribution of x, $\dot{x}$, and $\ddot{x}$. By substituting

$d\dot{x} = \ddot{x}dt$, Eq. (5.22) can be reduced to

$$f_{x_p,\ddot{x}_p}(x_p, \ddot{x}_p) = -\frac{\sqrt{2\pi}}{\sigma_{\ddot{x}}} f_{x,\ddot{x}}(x_p, \ddot{x}_p)\, \ddot{x}_p, \quad \text{where } \begin{cases} -\infty < x_p < \infty \\ -\infty < \ddot{x}_p < 0 \end{cases} \tag{5.23}$$

where the joint distribution of x and $\ddot{x}$, $f_{x,\ddot{x}}(\cdot,\cdot)$ is known to be a bivariate Gaussian distribution with the correlation coefficient of $\rho_{x\ddot{x}} = -\alpha_2 = \sqrt{\lambda_2^2/\lambda_0\lambda_4}$ (Lutes and Sarkani 2004). From the relationship of Eq. (5.20) and Eq. (5.21), the joint PDF of Eq. (5.23) is converted into the joint PDF of m and H as

$$f_{m,H}(m, H) = f_N(m; 0, (1-\alpha_2^2)\lambda_0) f_R(H; 4\alpha_2^2\lambda_0) \tag{5.24}$$

Eq. (5.24) indicates that the variables m and H turn out to be independent on each other. Finally, from the relationships of $m = (p+v)/2$ and $H = p - v$, the joint distribution of a peak p and the subsequent valley v is derived as

$$f_{p,v}(p, v) = f_N\left(\frac{p+v}{2}; 0, (1-\alpha_2^2)\lambda_0\right) f_R(p-v; 2\alpha_2\,\lambda_0) \tag{5.25}$$

Thus, the successive probability $p_o(a)$ could be obtained by integrating Eq. (5.25) to get Eq. (5.18). No closed-from equation exists for these integrations, but they can be computed simply by numerical integration techniques.

However, it should be remarked that the presumption of the sinusoidal trajectory is often violated in the practical applications. For example, the peak of the displacement and the valley of the acceleration do not necessarily occur at the same time. Therefore, another derivation for $f_{p,v}(p, v)$ that removes this assumption is newly proposed, which can be regarded as a continuous extension of the prescribed approach. Consider a stationary Gaussian random process $X(t)$ with an auto-PSD of $S_{XX}(\omega)$. The random process can be decomposed into the "mean amplitude" process $m(t)$ and the "gap" process $\tilde{H}(t)$:

$$m(t) = \frac{X(t) + X(t + \tau_c)}{2} \tag{5.26a}$$

$$\widetilde{H}(t) = X(t) - X(t + \tau_c) \tag{5.26b}$$

where $\tau_c = \pi\sqrt{\lambda_0/\lambda_2}$ is used to approximate the half of the mean recurrence period of the peak. Since $X(t)$ and $X(t + \tau_c)$ are correlated Gaussian random variables, $m(t)$ and $\widetilde{H}(t)$ are both Gaussian distributions having the variances

$$\sigma_m^2 = \frac{\sigma_x^2}{2}(1 + \rho_{\tau_c}) \tag{5.27a}$$

$$\sigma_H^2 = 2\sigma_x^2(1 - \rho_{\tau_c}) \tag{5.27b}$$

respectively, where ρ_{τ_c} denotes the correlation coefficient between $X(t)$ and $X(t + \tau_c)$ which can be derived from the auto-PSD of the process as

$$\rho_{\tau_c} = \frac{1}{\lambda_0}\int_{-\infty}^{\infty} \cos \omega\tau_c \, S_{\mathrm{XX}}(\omega) \, d\omega \tag{5.28}$$

By substituting Eq. (5.28) into Eqs. (5.27a) and (5.27b), the variances can be re-written as

$$\sigma_m^2 = \left(1 - \alpha_d^2\right)\lambda_{x,0} \tag{5.29a}$$

$$\sigma_{\widetilde{H}}^2 = 4\alpha_d^2\lambda_{x,0} \tag{5.29b}$$

where

$$\alpha_d^2 = \frac{1}{\lambda_{x,0}}\int_{-\infty}^{\infty} \sin^2\frac{\omega\tau_c}{2} S_{\mathrm{XX}}(\omega) d\omega \tag{5.30}$$

It is noted from the form of Eq. (5.30) that the parameter α_d^2 provides the bandwidth measure of the process. The subscript d indicates that this parameter is derived for the double-barrier problem. It is noted from the definitions in Eq. (5.26) that at a given time point, $m(t)$ and $\widetilde{H}(t)$ are uncorrelated. Finally, the "height" process

$H(t)$, that is the random process extension of H in Figure 5.3, can be regarded as the envelope process of the gap process $\tilde{H}(t)$. It is known that the envelope process of a Gaussian process follows the Rayleigh distribution in which the parameter for this case is $\sigma_{\tilde{H}}^2$ (Lutes and Sarkani 2004). Thus, the instantaneous joint PDF of $m(t)$ and $H(t)$ is written as

$$f_{m,H}(m,H) = f_N\left(m; 0, \left(1-\alpha_d^2\right)\lambda_0\right) f_R\left(H; 4\alpha_d^2\,\lambda_0\right) \tag{5.31}$$

It turns out that although sinusoidal assumption is removed, the final form of Eq. (5.31) has the same mathematical form with Eq. (5.24) except that the conventional bandwidth parameter α_2^2 is replaced by the new parameter α_d^2. The joint PDF of p and v is given as

$$f_{p,v}(p,v) = f_N\left(\frac{p+v}{2}; 0, \left(1-\alpha_d^2\right)\lambda_0\right) f_R\left(p-v; 4\alpha_d^2\,\lambda_0\right) \tag{5.32}$$

The derivation can be further extended to consider single-barrier problems, which in this case either the neighboring peaks or the neighboring valleys are considered, instead of neighboring pair of a peak and a valley. In order to derive the "mean" and "gap" processes from the two adjacent peaks (or valleys), an additional technique is introduced here. The decomposition involves the process reflected over *x*-axis, i.e. $-X(t)$. The single-barrier version of Eq. (5.26) is

$$m(t) = \frac{X(t) - X(t+2\tau_c)}{2} \tag{5.33a}$$

$$\tilde{H}(t) = X(t) + X(t+2\tau_c) \tag{5.33b}$$

where $2\tau_c$ approximates the full return period of the peaks (or the valleys). Similar to the double barrier problem, the joint PDF of the adjacent peaks are derived as

$$f_{p,p'}(p,p') = f_N\left(\frac{p-p'}{2}; 0, (1-\alpha_s^2)\lambda_0\right) f_R(p+p'; 4\alpha_s^2\,\lambda_0) \tag{5.34a}$$

$$\alpha_s^2 = \frac{1}{\lambda_{x,0}}\int_{-\infty}^{\infty} \cos^2 \omega\tau_c\, S_{\mathrm{XX}}(\omega)d\omega \tag{5.34b}$$

Thus, the successive crossing probability for a single-barrier problem could be obtained by integrating Eq. (5.34a).

On the other hand, it is noted that this Markov branching assumption may work relatively well in a highly narrowband process that has a dominant central frequency, however, the proposed method may underestimate the successive probability if the process has a medium or wide bandwidth. To account for this, the following heuristic choice of the successive probability is recommended for the double-barrier problem:

$$p_o(a) = \max(p_d(a), \sqrt{p_s(a)}) \tag{5.35}$$

where $p_d(a)$ and $p_s(a)$ respectively denote the successive probability obtained from Eq. (5.32) and (5.34a). It is noteworthy that $\sqrt{p_s(a)}$ is a good approximation of $p_o(a)$ for a wideband process, while it may be underestimating in highly narrowband process.

One final remark is that in order to remove the long-tail effect of auto-PSD, it is proposed to cut-off the PSD of the process, e.g. at 3% of the volume, and substitute $S_{\mathrm{XX}}(\omega)$ and $\lambda_{x,0}$ in Eq. (5.30) and Eq. (5.34b) by those of the truncated PSD. It is observed that the bandwidth parameters, i.e. α_s and α_d could be overly sensitive to the existence of very high frequency values, while the first-passage probabilities are not significantly affected by those values.

Table 5.1 Procedure of Poisson branching process based first-passage probability

Step	Procedure
1	Identification of α_s and α_d based on Eqs. (5.30) and (5.34b) respectively.
2	Calculation of $p_s(a)$ and $p_d(a)$ by numerically integrating Eq. (5.32) and (5.34a), respectively, for a given the threshold value a
3	Calculation of $\eta_{PB}(a)$ by Eq. (5.35) and Eq. (5.17)
4	Estimation of first-passage probability by substituting $\eta_{\mathrm{I}}^{*}(a)$ in place of $\alpha(a)$ in Eq. (5.2)

5.2.4 Numerical examples

The proposed approach is verified by numerical examples. The double-barrier problem is examined with stationary Gaussian random processes having following auto-PSDs:

$$S_1(\omega;\omega_o,\zeta_o)=\frac{e^{-\frac{(\omega-\omega_o)^2}{2\zeta_o^2\omega_o^2}}+e^{-\frac{(\omega+\omega_o)^2}{2\zeta_o^2\omega_o^2}}}{2^{3/2}\pi^{1/2}\zeta_o\omega_o} \tag{5.36}$$

$$S_2(\omega;\omega_o,\zeta_o)=\frac{\zeta_o\omega_o^3}{\pi[(\omega^2-\omega_o^2)^2+(\zeta_o\omega_o\omega)^2]} \tag{5.37}$$

which respectively represent the exponential shape PSD and the PSD of response of a linear oscillator subjected to a white noise excitation. The central frequency value is fixed as $\omega_o=5$ rad/s. For ζ_o, which determines the bandwidth, a series of values ranging from 0.02 to 0.20 are investigated to inspect narrow- to wideband behaviors of the random processes. Finally, the following PSD representing the response of a linear oscillator subjected to the modified Kanai-Tajimi ground motion model (Clough and Penzien 1975) is investigated.

$$S_3(\omega;\omega_o,\zeta_o) = |H(\omega;\omega_o,\zeta_o)|^2 S_f^{KT}(\omega) \tag{5.38a}$$

$$S_f^{KT}(\omega) = S_0 \frac{\omega_f^4 + 4\zeta_f^2\omega_f^2\omega^2}{\left(\omega_f^2 - \omega^2\right)^2 + 4\zeta_f^2\omega_f^2\omega^2} \cdot \frac{\omega^4}{(\omega_s^2 - \omega^2)^2 + 4\zeta_s^2\omega_s^2\omega^2} \tag{5.38b}$$

$$H(\omega;\omega_o,\zeta_o) = \frac{1}{\omega_o^2 - \omega^2 + 2i\zeta\omega_o\omega} \tag{5.38c}$$

where $S_f^{KT}(\omega)$ is the modified Kanai-Tajimi PSD with parameters of $\omega_f = 15$ rad/s, $\zeta_f = 0.6$, $\omega_s = 1.5$ rad/s and $\zeta_s = 0.6$. The function $H(\omega;\omega_o,\zeta_o)$ is the FRF of a linear oscillator with the natural frequency $\omega_o = 5$ rad/s and damping ratio ζ_o. The scaling factor S_0 is chosen to normalize the underneath area of $S_3(\omega;\omega_o,\zeta_o)$.

Figures 5.4 to 5.6 present the estimations of conditional mean crossing rates and corresponding first-passage probabilities where $T_d\omega_o = 565$. Various methods are presented along with the reference MCS estimations obtained by 10^4 realizations of the process. The example shows that the proposed PBP-based method is in a close agreement with the MCS results, while the accuracy of other approaches tends to fluctuate more depending on the spectral shapes and the bandwidths. Especially, it is shown that the Poisson approximation could considerably overestimate the probability of failure in the highly narrowband processes.

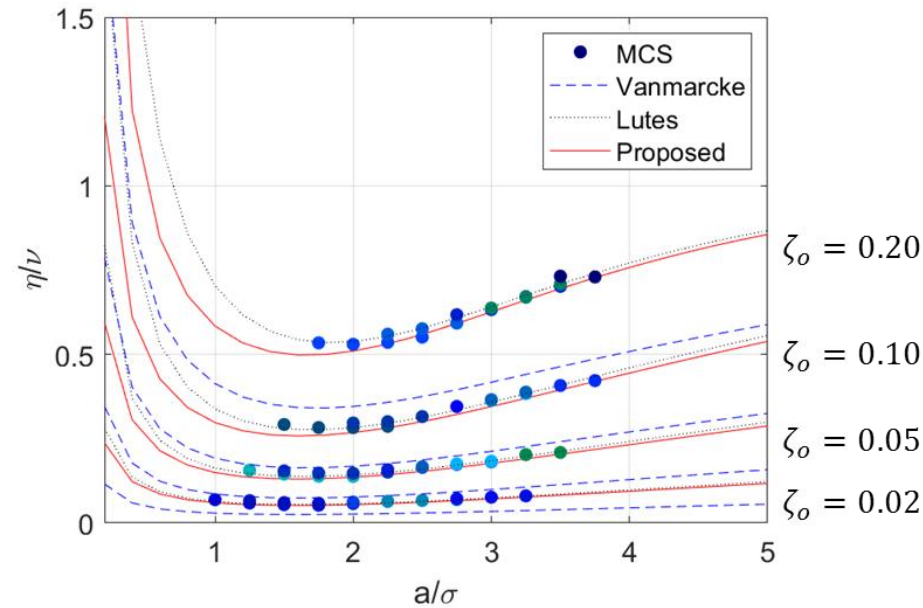

(a) Crossing rates

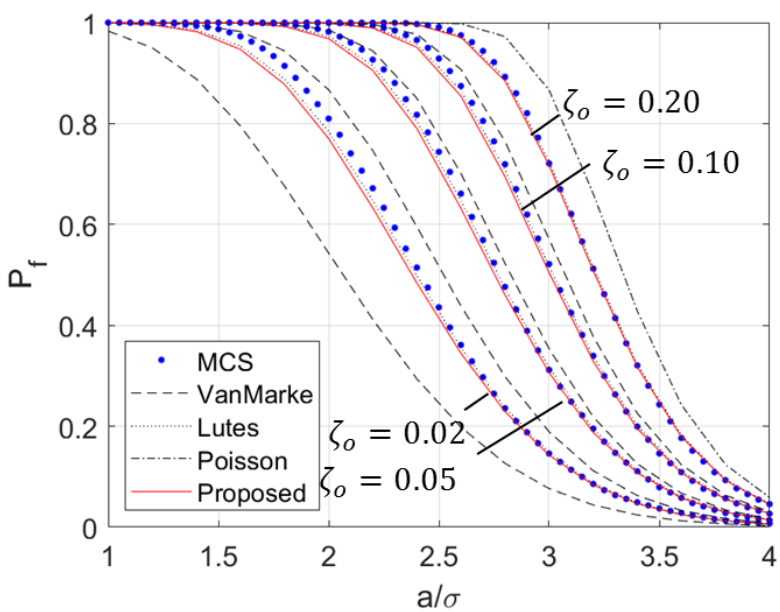

(b) Estimated first-passage probabilities

Figure 5.4 The crossing rates and first-passage probabilities ($S_1(\omega;\omega_o,\zeta_o)$)

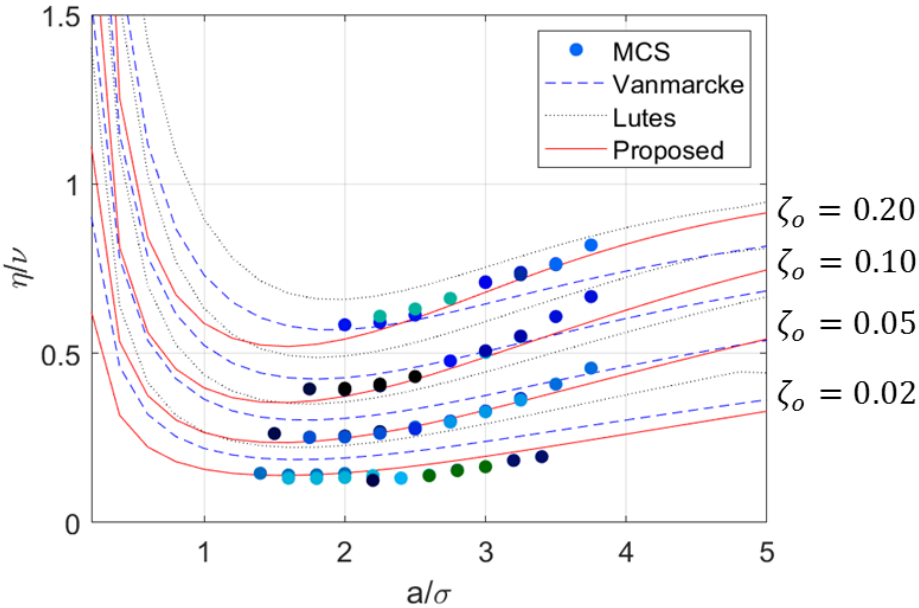

(a) Crossing rates

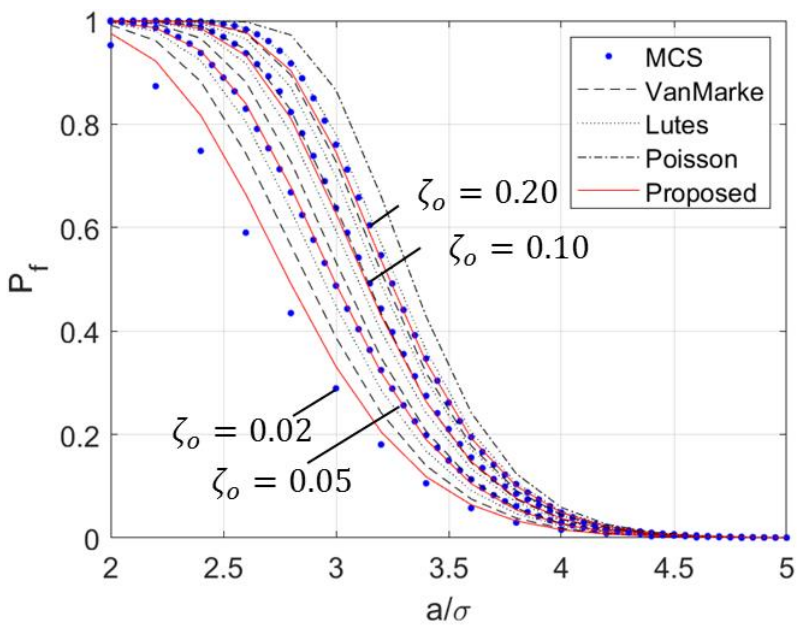

(b) Estimated first-passage probabilities

Figure 5.5 The crossing rates and first-passage probabilities ($S_2(\omega;\omega_o,\zeta_o)$)

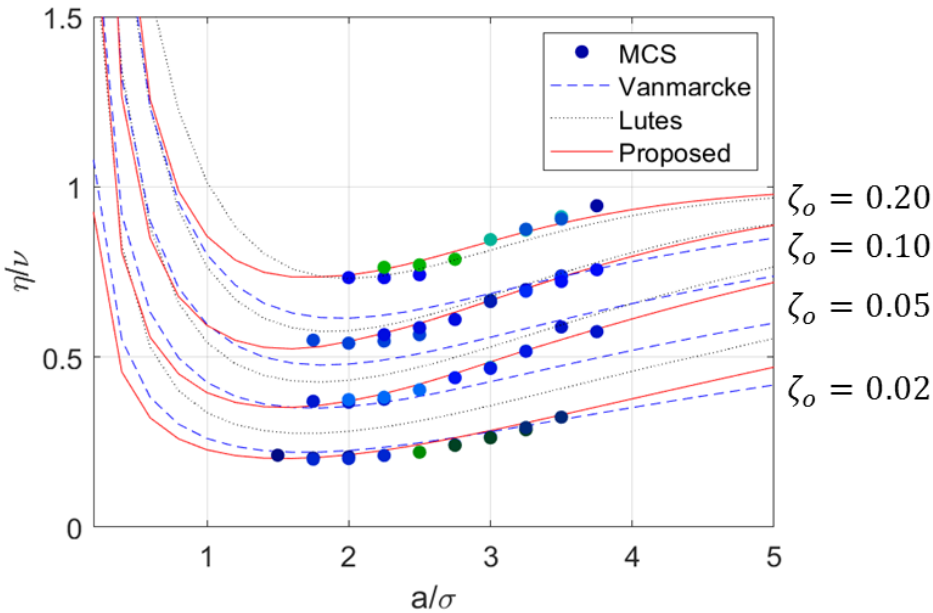

(a) Crossing rates

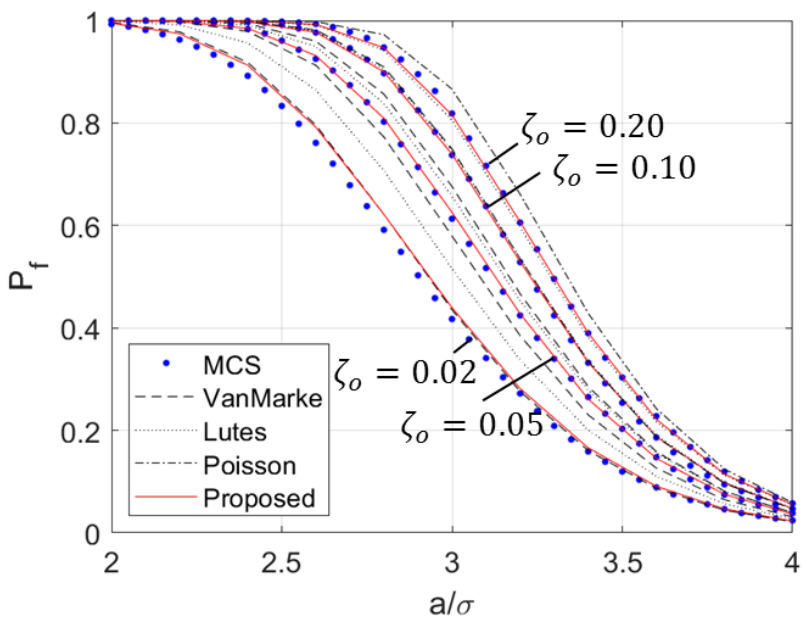

(b) Estimated first-passage probabilities

Figure 5.6 The crossing rates and first-passage probabilities ($S_3(\omega;\omega_o,\zeta_o)$)

5.3 PBP-based first-passage probability estimation using GM-ELM

5.3.1 Spectral effects in first-passage failure

This section proposes a new strategy to implement the PBP-based first-passage probability equation to the GM-ELM analysis. In order to approximate the unknown PSD of the nonlinear system response, it is recalled that the concept of transitory ELS which is a temporarily imported ELS with a single Gaussian component was introduced in Section 3.6. It was discussed that although transitory ELS does not capture the non-Gaussianity response, it could still provide useful approximations of spectral characteristics.

Let us first consider the stationary case. In the PBP-based first-passage probability formulation of Eq. (5.17), and also in Vanmarcke's formulation of Eq. (5.6), the unconditional crossing rate is represented in terms of unconditional crossing rate multiplied by a modification factor, i.e. in the form of

$$\alpha(a;\theta) \simeq \nu(a)k(a;\theta) \tag{5.39}$$

where θ represents the bandwidth parameters, e.g. δ, α_s, or α_d. Thus, in order to apply the above equation to the nonlinear system response, along with the mean crossing rate $\nu(a)$ which is available by GM-ELM analysis, the modification factor $k(a;\theta)$ needs to be provided. However, the bandwidth parameters of the nonlinear response are hardly acquirable. To overcome this difficulty, the approximated modification factor $k(a;\theta_T)$ which involves the bandwidth parameter θ_T of the transitory ELS is introduced.

Particularly, the modification factor for the PBP-based approach is denoted as

$$k(a;\alpha_{sT},\alpha_{dT}) = \frac{1 - p_o(a;\alpha_{sT},\alpha_{dT})}{P(A < a)} \tag{5.40}$$

where $p_o(a;\alpha_{sT},\alpha_{dT})$ is the consecutive crossing probability given the PSD of the transitory ELS. As an alternative, the following equation based on Vanmarcke's formulation is also investigated:

$$k(a;\delta_T) = \frac{1 - \exp\left[-\sqrt{\frac{\pi}{2}}\delta_T^{1.2}\frac{a}{\sqrt{\lambda_0}}\right]}{1 - \exp\left(-\frac{a^2}{2\lambda_0}\right)} \tag{5.41}$$

where δ_T is attained from the spectral moments of the response of transitory ELS.

5.3.2 Non-Gaussianity effects in first-passage failure

Considering the fact that the PBP-based first-passage probability equation as well as the Vanmarcke's formulation is derived under the assumption of Gaussian process response, it is required to modify each formulation to accommodate non-Gaussianity of the nonlinear responses. Therefore, the PBP-based approach is further modified for the nonlinear system response. It is proposed to replace $\eta_{PB}(a)$ in Eq. (5.17) by

$$\eta_{PB}^{nG}(a) = \nu(a)\frac{1 - \tilde{p}_o(a;\alpha_{sT},\alpha_{dT})}{P(A < a)} \tag{5.42a}$$

$$\tilde{p}_o(a;\alpha_{sT},\alpha_{dT}) = p_o(a;\alpha_{sT},\alpha_{dT})\min\left(\frac{P(A_{nG}(t) > a)}{P(A_G(t) > a)}, 1\right) \tag{5.42b}$$

where $A_G(t)$ is the envelope process of the (Gaussian) response of a transitory ELS, and $A_{nG}(t)$ is the envelope of the original (non-Gaussian) nonlinear response. It is noted that the ratio between the envelope densities is bounded to 1 to ensure the numerical stability along the extreme threshold levels. Although the reduction factor

introduced in Eq. (5.42b) is heuristic to some extent, it is noted that the use of the envelope distribution is closely related to the definition of $p_o(a;\alpha_{sT},\alpha_{dT})$. It is recalled that $p_o(a;\alpha_{sT},\alpha_{dT})$ is the conditional probability that peaks and valleys exceed a certain threshold, while these extreme values are *bounded* by the envelope process.

While it is widely accepted that $A_G(t)$ follows a Rayleigh distribution as it was used in Eq. (5.7), the PDF and CDF of $A_{nG}(t)$ could be approximated only as the combination of the responses of ELS obtained by GM-ELM analysis. To derive the distribution of $A_{nG}(t)$, it is recalled that a general envelope process consists of the extreme values of the original process and the values interpolating them as shown in Figure 5.1. Considering this, the PDF of the envelope process is approximated as

$$f_{A_{nG}}(a) = \frac{1}{M} a f_{x|\dot{x}}(a|\dot{x}=0), \quad \text{where } x > 0 \tag{5.43}$$

where $f_{x|\dot{x}}(x|\dot{x})$ represents the distribution of nonlinear response $x = X(t)$ given its time derivative value $\dot{x} = \dot{X}(t)$, and M is the normalization constant. The conditional PDF on the right-hand side is the distribution of extrema, and the contribution of each extreme value to the envelope distribution is assumed to be proportional to itself. Accordingly, the extreme distribution is multiplied by a as shown in Eq. (5.43). This weight factor a accounts for the envelope values within the time interval between the extrema.

By substituting the GM model to $f_{x|\dot{x}}(a|\dot{x}=0)$ in Eq. (5.43) and integrating $f_{A_{nG}}(a)$, the CDF of the nonlinear response envelope process could be derived as

$$P(A_{nG}(t) < a) = \frac{1}{M}\sum_{k=1}^{K} \alpha_k F_{A,k}(a) \tag{5.44}$$

where $F_{A,k}(a)$ stands for the relative contribution of the k-th linear oscillator to the envelope CDF that can be derived as

$$F_{A,k}(a) = F_r(r_k) - F_r(\delta_k) + \sqrt{2\pi}\delta_k\big(\Phi(r_k) - \Phi(-\delta_k)\big) \tag{5.45}$$

in which $r_k = (a - \mu_k)/\sigma_k,\ \delta_k = \mu_k/\sigma_k,\ \Phi(\cdot)$ is the standard normal CDF and

$$F_r(r) = 1 - \exp\left(-\frac{r^2}{2}\right) \tag{5.46}$$

It is noted that when the mean of the mixture component is zero, Eq. (5.45) reduces to a Rayleigh CDF that is equivalent to the form in Eq. (5.7). The normalization constant can be calculated by

$$M = \sum_{k=1}^{K} \alpha_k \left(1 - F_r(\delta_k) + \sqrt{2\pi}\delta_k\big(1 - \Phi(-\delta_k)\big)\right) \tag{5.47}$$

Figure 5.7 summarizes the procedure to estimate the first-passage probability of the nonlinear system by proposed PBP-based formulation and GM-ELM analysis.

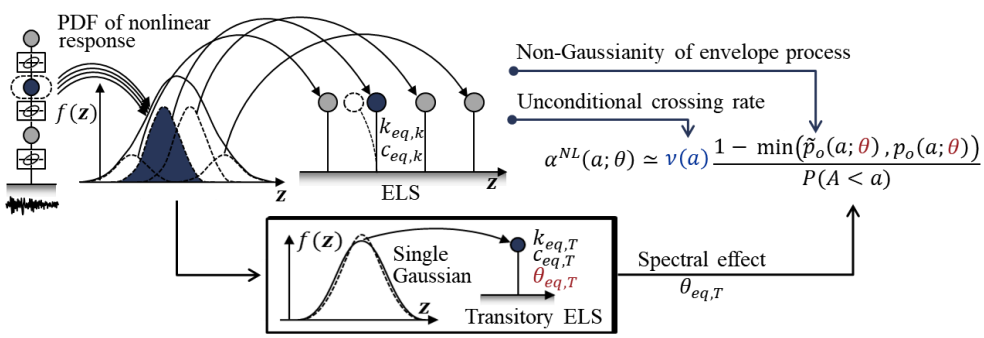

Figure 5.7 Estimation of nonlinear first-passage probability using GM-ELM

As an alternative, Lutes and Sarkani (2004) also introduced an equation for the unconditional crossing rate of the non-Gaussian response in terms of the CDF of the envelope distribution, i.e.

$$\eta_v^{nG}(a,t) = \frac{P(A_{nG}(t) > a)\nu(0)}{P(A_{nG}(t) < a)} \left(1 - \exp \frac{-\nu_A(a,t)}{P(A_{nG}(t) > u)\nu(0)}\right) \tag{5.48}$$

While the envelope CDF can be again estimated using Eq. (5.44), the mean crossing rate of the envelope process, $\nu_A(a,t)$ needs to be identified additionally. For this, it is assumed that the $A_{nG}(t)$ and its time-derivative $\dot{A}_{nG}(t)$ are independent while $\dot{A}_{nG}(t)$ is governed by Gaussian distribution having zero-mean and the variance of $\sigma_{\dot{A}}^2 = (1-\alpha_1^2)\lambda_{2,x} = \delta^2\lambda_{2,x}$, as often adopted for the stationary Gaussian base process. From the joint PDF of $A_{nG}(t)$ and $\dot{A}_{nG}(t)$, the mean crossing rate of $A_{nG}(t)$ can be obtained as (Lutes and Sarkani 2004)

$$\nu_A(a;t) = \frac{\delta}{\sqrt{2\pi}} f_{A_{nG}}(a) \sqrt{\frac{\lambda_{x,2}}{\lambda_{x,0}}} \tag{5.49}$$

It is noted that the PDF of the envelope process, $f_{A_{nG}}(\cdot)$ could be easily acquired by differentiating Eq. (5.44).

Finally, in order to handle the nonstationary excitations and responses, the ELS from temporal-average GM-ELM in Section 4.4 could be utilized. The proposed equations for PDF and CDF of the envelope process will then provide the temporal-average of PDF and CDF, respectively, and the resulting conditional mean crossing rates are approximately the temporally averaged values.

5.4 Numerical examples

The proposed approach is demonstrated by hysteretic systems subjected to stationary and nonstationary excitations. For the system, Bouc-Wen hysteresis model with the initial natural period of 0.5s and the damping ratio of 0.03 is first considered. The yielding displacement is $u_y = 0.07$ m and the post-yield stiffness ratio is $\alpha = 0.1$. For the other parameters, the same values as the previous examples are used. For the stationary excitation model, Kanai-Tajimi PSD in Eq. (3.1) is adopted with the same parameter values. Only the scale factor is changed to $S_0 = 20\text{m}^2/s^3$. The corresponding hysteretic behavior is illustrated in Figure 5.8(a). The stationary excitation duration is 15 seconds.

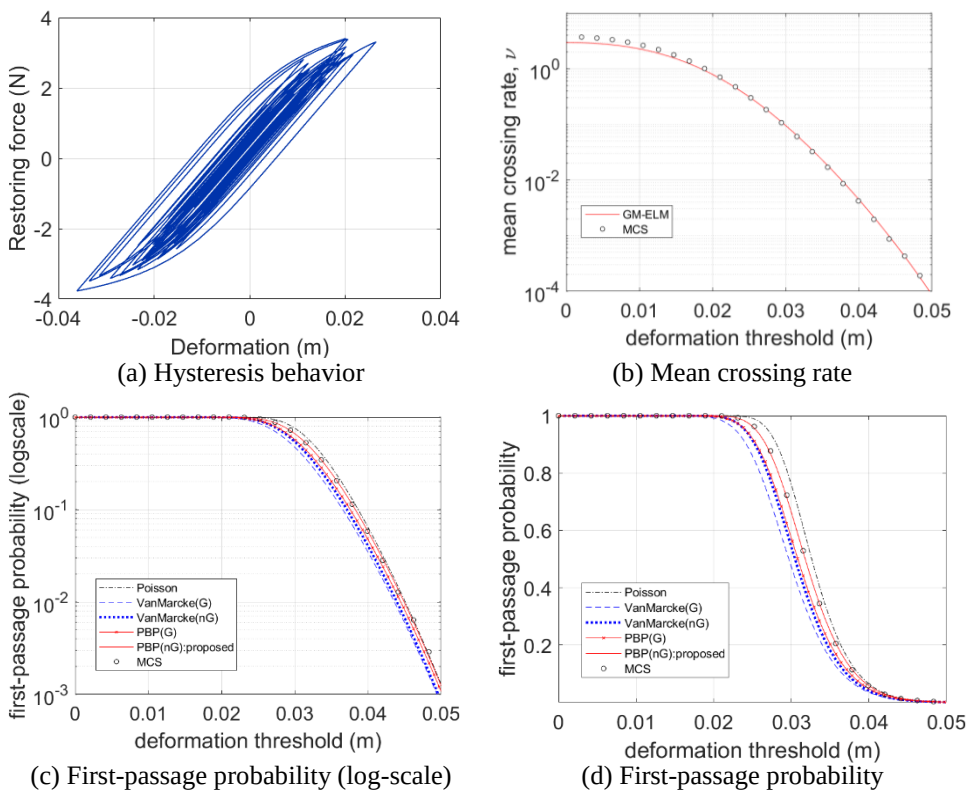

(a) Hysteresis behavior

(b) Mean crossing rate

(c) First-passage probability (log-scale)

(d) First-passage probability

Figure 5.8 First-passage probability estimation by GM-ELM with different modification factors (stationary)

GM-ELM analysis is performed by 400 rounds of nonlinear dynamic analysis, where 100 mixture components are used for GM fitting. Figure 5.8(b) presents the mean crossing rates acquired by GM-ELM analysis. The different modification factors addressed in this chapter are investigated, which are related to Eqs. (5.41), (5.48), (5.40) and (5.42). Those methods are respectively denoted as Vanmarcke (G), Vanmarcke (nG), PBP (G), and PBP (nG) in Figures 5.8(c) and (d). For the comparison, MCS results of first-passage probability estimations are obtained by 6×10^4 rounds of nonlinear dynamic analysis. It is shown that the proposed PBP-based approach with the additional non-Gaussianity factor shows the best performance in this example. It is also noted that the Poisson assumption is substantially overestimating the responses.

Next, the proposed approach is applied to the nonstationary design code-conforming ground motion introduced in the numerical example of Section 4.5.3. The response spectrum of Gyeongju is again considered, while the intensity is given as spectral acceleration of $S_a = 1.25g$, where g denotes the acceleration of gravity. In order to induce the narrowband response, the SDOF structure with the natural period of $T_n = 0.5$s, damping ratio of 0.03, and the post yield stiffness ratio of $\alpha = 0.05$ is considered. The yield displacement is $u_y = 0.07$m. One of the realizations of the hysteretic behavior of the system is illustrated in Figure 5.9(a).

Temporal-average GM-ELM analysis is performed with 800 rounds of dynamic simulations and 100 mixture components, in order to get the temporal-average of mean crossing rates $\hat{\nu}(a)$ as shown in Figure 5.9(b). The MCS results are estimated with 5×10^4 rounds of nonlinear dynamic analysis. It is shown from Figure 5.9 that, in this example, different approximation approaches in overall show a good

agreement with the MCS results. However, again, Poisson approximation gives significantly conservative estimations as shown in Figures 5.9(c) and (d).

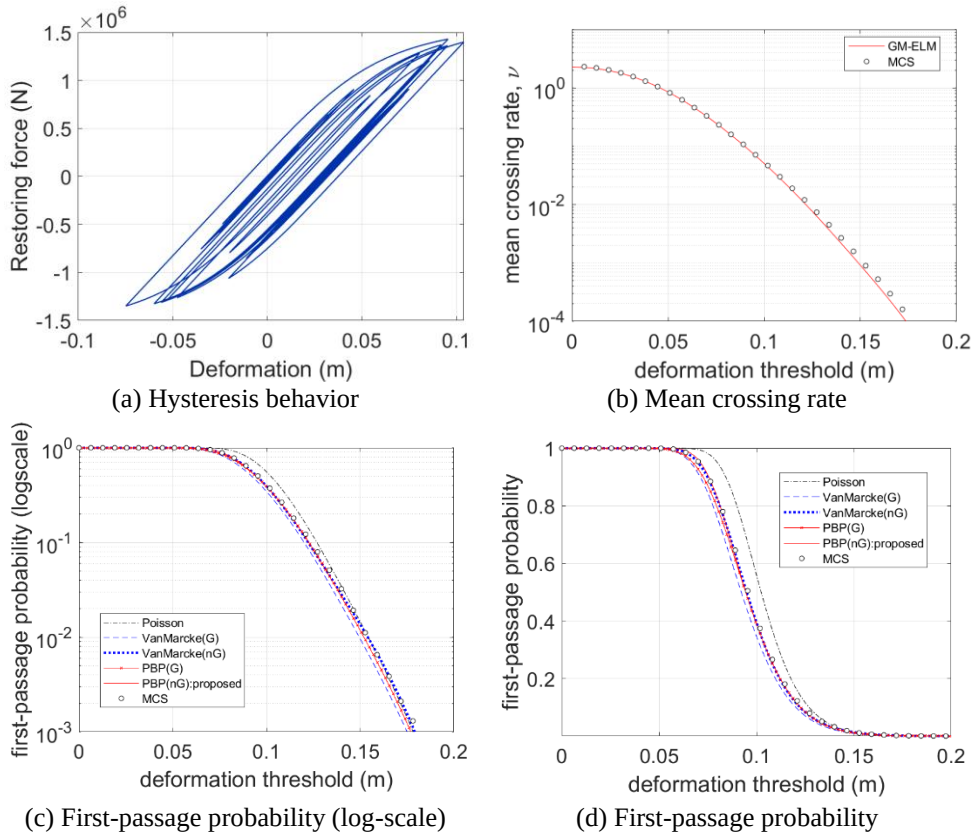

(a) Hysteresis behavior (b) Mean crossing rate

(c) First-passage probability (log-scale) (d) First-passage probability

Figure 5.9 First passage probability estimation by GM-ELM with different modification factors (nonstationary)

Additionally, the proposed approach is combined with the intensity-augmented GM-ELM to obtain fragility curves under the different scaling levels of excitations. The same set of samples is used to estimate only the shape of response PDF. Given the representative intensity of $S_a = 1.25g$, the simple scaling approach is applied to get intensity-augmented response PDF without any additional dynamic analysis. The number of 144 mixture components is employed to obtain universal ELS. MCS results are obtained by 4×10^4 rounds of nonlinear dynamic analysis for each

discretized intensity measure. Figure 5.10 presents the fragility curves. Only the results of the proposed PBP-based formulation of Eq. (5.42) are compared with conventional Poisson approximations. It is clear from the results that by accounting for the clustering behavior of the crossing events, the accuracy of fragility analysis is improved. It is observed that the overestimation due to the Poisson approximation is especially severe for higher excitation intensities.

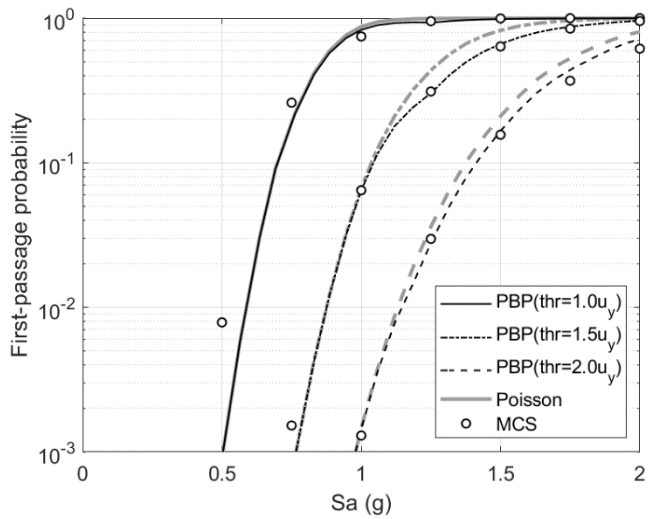

Figure 5.10 Fragility curves obtained by GM-ELM with PBP-based first-passage probability formulation

5.5 Conclusions

This chapter proposed a robust first-passage probability equation for GM-ELM analysis as well as general random vibration problems. To account for the clustering phenomena of the crossings in the narrowband processes, a Poisson branching process model is newly introduced. The occurrence time of the initial crossing in each cluster is assumed to follow a Poisson process, while the occurrence of the following crossings inside each cluster is governed by the Markov branching process.

The probability of the consecutive crossing in the branching model is derived by numerically integrating the joint PDF of the adjacent local extrema, i.e. peaks and valleys. For this, a new derivation to obtain the joint PDF of the adjacent local extrema is proposed. The proposed method is then further developed for its applications to GM-ELM-based nonlinear failure analysis. The proposed PBP-based first-passage probability equation is modified to account for both the spectral and non-Gaussianity effect. The required spectral characteristics of the response of nonlinear system are approximated by those of the transitory ELS, which is an ELS with the single Gaussian component. It is shown by the numerical examples that the PBP-based formulation combined with GM-ELM analysis gives satisfactory performances in capturing the narrowband effect in the first-passage failure.

It is noted that, at the current stage, the proposed first-passage probability formulation is applied only to the unimodal PSD in the examples. In multimodal problems, the Markov assumptions for the branching process may be violated. It is also noted that the modified first-passage probability for nonlinear system is derived based on the stationarity condition. Therefore, further involvement of the non-stationarity effect may improve the estimation accuracy further.

Chapter 6. Conclusions

6.1 Introduction

This chapter concludes the dissertation by summarizing the new developments and contributions introduced in each chapter. Additionally, current limitations and requirements that need further investigations are elaborated. The chapter ends with the potential applications of GM-ELM and recommendations on further research.

6.2 Summary and contributions of this dissertation

This dissertation proposes a collection of ideas to further improve GM-ELM analysis in terms of accuracy, efficiency and applicability. GM-ELM is a recently developed nonlinear stochastic analysis approach whose features are summarized as follows (Wang and Song 2017):

- GM-ELM identifies a group of linear oscillators as an equivalent linear system that collectively reproduces the instantaneous response PDF of the original nonlinear system. GM model fitting is introduced for the decomposition of nonlinear system response into the linear system responses. In its original version, GM-ELM assumes that nonlinear response is *stationary* so that its instantaneous PDF is consistent for the whole period of structural vibration.
- Physical parameters, i.e. equivalent stiffness, of each linear oscillator are optimized by matching its (Gaussian) response distribution to each Gaussian component in GM model. The instantaneous PDF of a stationary linear response

is always Gaussian distribution given a stationary Gaussian excitation.

- Once ELS is fully identified, the nonlinear response statistics such as mean crossing rate, first-passage probability, and the mean peak response can be estimated readily by only linear random vibration analysis of ELS and formalized response combination equations.
- The followings are the merits of GM-ELM for nonlinear stochastic dynamic analysis: (1) GM-ELM can capture the non-Gaussianity responses of the nonlinear system; (2) the identified ELS could be re-used for the different threshold levels of interest; (3) GM-ELM can be combined with the traditional linear response spectrum analysis technique; (4) the required number of nonlinear dynamic simulations is not proportional to the complexity of the nonlinear system; and (5) once the response PDF is identified, the complexity of GM-ELM analysis is independent of the degree of nonlinearity.

GM-ELM introduced a new interesting concept of GM-based probabilistic linearization, and provided the means for efficient and precise nonlinear stochastic dynamic analysis. Nevertheless, it had remained with significant chances for refinements and further developments. In this work, GM-ELM is further improved to overcome its drawbacks and to tackle the challenges in practical applications. Generalized modifications of GM-ELM are proposed, termed bivariate, temporal-average, and intensity-augmented GM-ELM, while retaining the fundamental principles and the procedures of GM-ELM. The methods respectively allow us to identify equivalent damping, embrace nonstationary excitations, and obtain universal ELS that does not depend on the scaling of excitations. Additionally, new

techniques, such as simple scaling approach that helps us to save computational effort in identifying universal ELS are introduced, and the Poisson branching process based first-passage probability equation is proposed as well as it is further extended for nonlinear dynamic analysis. New developments eventually allow us to increase the estimation accuracy, employ realistic, i.e. nonstationary, stochastic excitation models, and perform efficient fragility analysis. We believe this research can work as a springboard for further practical engineering applications of GM-ELM especially in the field of earthquake engineering. The followings summarize the major findings and contributions of this dissertation:

- *Bivariate GM-ELM* is developed to define the equivalent damping as well as the equivalent stiffness. By introducing the bivariate GM model when identifying ELS, independent two constraints are defined to optimize the both structural parameters. It was shown by numerical examples that the introduction of equivalent damping could substantially increase the estimation accuracy by capturing the effect of dissipated hysteretic energy.
- To embrace the nonstationary responses, *temporal-average GM-ELM* is introduced. By substituting the temporal-average of the instantaneous response PDF in the place of the stationary instantaneous response PDF, a generalized version of ELS which contains the nonstationarity information is identified within the same GM-ELM framework. As a result, the temporal-average of nonlinear response statistics, e.g. mean crossing rate, and the nonstationary first-passage probability could be estimated. Considering the fact that practical problems often deal with the nonstationary excitations and responses, e.g. earthquake shakes or strong wind loads, this generalization is expected to

broaden the applicability of GM-ELM to various engineering fields.

- In the original version of GM-ELM, ELS is dependent on the scaling of ground motions. This is because the identification of ELS hinges on the response PDF of the system. In this work, GM-ELM is further generalized by introducing the universal ELS which does not depend on the scaling of excitations. It is achieved by pre-incorporating the intensity dependency in ELS by means of intensity-augmented response PDF. For this reason, the approach is termed intensity-*augmented GM-ELM*. It is shown that the identification of this universal ELS is advantageous especially when one aims for efficient fragility analysis.
- A *simple scaling approach* is proposed for intensity-augmented and temporal-average GM-ELM analysis. The proposed approach aims to reduce the computational effort when identifying the intensity-augmented response PDF by employing the first-order approximation-based extrapolation. The intensity-augmented GM-ELM combined with this simple scaling approach could further increase the efficiency of GM-ELM-based fragility analysis.
- A new formulation for first-passage probability is proposed for a general stationary Gaussian process. The concept of *Poisson branching process model* is introduced to describe the clustering tendency of crossing events in the narrowband process. The temporal correlations are considered by the consecutive crossing probability. In order to obtain this, a new derivation for the joint distribution of the adjacent extrema is proposed. The numerical example confirms that the proposed approach well-estimates the first-passage probabilities of the narrowband process given different PSD shapes and

bandwidths.

- In order to get better estimates of the failure probability of nonlinear systems, the proposed first-passage probability formulation is combined with the GM-ELM framework. For this, the spectral property of nonlinear response is identified using the transitory ELS, and the first-passage probability equations are further developed to account for the non-Gaussianity effect. It is remarked that (1) this development solves the challenging problem of identifying the first-passage probability of the response of a nonlinear system subjected to nonstationary excitations, and (2) the proposed approach can be applied to general versions of GM-ELM to further improve its estimation accuracy especially under highly narrowband responses.

6.3 Limitations and needs for further investigations

There are unsolved questions that need to be further addressed in the proposed GM-ELM developments to enhance its usability. The topics range from parametric studies to a deeper level of philosophical interpretations on ELS.

- The number of Gaussian components in GM model needs to be strategically selected. When an insufficient number of components are introduced, the tail part of PDF may not be captured with the required degree of accuracy, while an excessive number of components may introduce unnecessarily high computational cost. The original paper of GM-ELM provides a technique to select the number of GM components based on maximum likelihood estimators (Wang and Song 2017), however it may require several trials of GM fitting. Especially since the higher-dimensional space of response PDF is involved in

the proposed GM-ELM approaches, it is desired to minimize the trials by providing an adequate starting point of the number of mixture components that can account for the expected degree of non-Gaussianity of the structures and required degree of accuracy.

- When identifying the response PDF, the proposed approaches, to some degree, rely on the samples of the responses acquired by the repetition of nonlinear dynamic simulations. Since the dynamic sampling is usually the most critical procedure which dominates the computational demand of this method, the user often needs to minimize the number of these expensive dynamic simulations. Thus, it is desired to pre-estimate the required number of simulations, considering the expected non-Gaussianity, required degree of accuracy and also spectral properties. It is noted that even when the same number of samples are employed, the effective sample size may depend on the correlation of the samples, i.e. broadband response gives well-mixed samples while narrowband process tends to be disproportionally sampled. For example, the effective sample size is often referred to as $N_{eff} = N/\tau$, in which N is the total number of samples, and τ is the effective correlation duration divided by the time step.
- In general GM-ELM applications, the continuous response of the system is discretized in order to obtain its instantaneous PDF (under the ergodic assumption) or temporal-average PDF. Therefore, the optimal step-size for the discretization needs to be inspected. It is noted that the optimal time step for GM-ELM analysis does not necessarily match that of nonlinear dynamic analysis.
- The simple scaling approach is used to approximate the intensity-augmented

response PDF. Current application results had shown good agreement with the exact results, however, the approximation may be violated if a highly nonlinear system is involved since the approach relies on the first-order approximation of the response limit state. It is required to investigate and quantify the bounds for the estimations.

- Since the current method identifies the response PDF based on the sampling approach, there are inherent variability in the estimations depending on the sample qualities. In order to suppress this variability, strategic sampling or inference schemes could be developed. For example, the introduction of Bayesian parameter estimation approaches, development of importance sampling technique or the introduction of meta-models such as response surface method could help obtain more consistent estimations on the response PDF.
- Finally, the identification of temporal correlations between the linear oscillators may be one of the most interesting and important unsolved topics. So far, the spectral characteristics of nonlinear responses were not fully addressed in GM-ELM. To accommodate this, an additional time series fitting scheme is required. For example, considering the alternating behaviors of equivalent linear oscillators which 'switches' from one to another, hidden Markov model is expected to have a potential to describe this unique transition of GM-ELM. For example, let us consider the bivariate GM-ELM. The vibratory response trajectory on the bivariate space of the response (x-axis) and its time derivative (y-axis) circles around in the clockwise direction. Accordingly, one could conceive a hidden Markov model with each discrete state representing each linear oscillator (or Gaussian component) that shows the highest transition

probability to the nearest one in the clockwise direction. This research is currently underway.

6.4 Further studies

Other than those discussed in the previous section, there are some more interesting yet uninvestigated topics:

- **GM-ELM under multi-component excitations**: At the current stage, only the single-dimensional excitations and responses are considered. However, it is often desired to introduce excitations having multidimensional components. For this, GM-ELM needs to be extended so that the ELS could jointly reconstruct the multiple response components of the nonlinear system.
- **GM-ELM to account for the uncertain structural parameters**: The structural properties are often uncertain, therefore, it is important to account for this randomness along with the excitation uncertainty. GM-ELM framework may be further extended to incorporate the various sources of randomness.
- **GM-ELM for multi-support excitations**: Assessment of the response of the multi-support system with each support being excited by different PSD models may be an important topic for a large-scale system.
- **GM-ELM analysis with a detailed finite-element (FE) model and analysis methods**: It should be noted that the application of GM-ELM is not limited to the lumped mass structural models. The presented GM-ELM approaches could be combined with the complicated FE analysis. GM-ELM rather possesses the advantages in those analyses since the MCS simulation phase (to approximate response PDF) and subsequent linearization phase are separated. It does not

necessarily require the repetitive switching from FE software to the programming environment and vice versa.

- **Application of GM-ELM to other vibrational loads and measured real-world data:** Other than the earthquake, wind is another important source of random vibration load to which infrastructures are subjected. However, several essential differences between the earthquake and wind load need to be addressed. For example, while GM-ELM assumes the Gaussian excitations, wind load is usually non-Gaussian. In order to apply GM-ELM to non-Gaussian excitations, it is required to adopt or develop a random process transformation technique to define the underlying Gaussian process of the excitations. The memoryless linear or nonlinear transformation (Soong and Grigoriou 1993) could be introduced for this purpose. Furthermore, since it is relatively easy to collect real-world time history data for the wind excitations compared to the earthquake shakes, one could try to extend the GM-ELM approaches to incorporate real-world observation data.

References

Alibrandi, U., & Der Kiureghian, A. (2010). A gradient-free method for determining the design point in nonlinear stochastic dynamic analysis. *Probabilistic Engineering Mechanics*, *11*, 2-10.

Alibrandi, U. (2014). A response surface method for stochastic dynamic analysis. *Reliability Engineering & System Safety, 126*, 44-53.

Alibrandi, U., & Mosalam. K. M. (2018). Response Spectrum Code-Conforming PEER PBEE using Stochastic Dynamic Analysis and Information Theory. *KSCE Journal of Civil Engineering, 22*(3), 1002-1015.

Atalik, T. S., & Utku, S. (1976). Stochastic linearization of multi-degree of freedom nonlinear systems. *Earthquake Engineering and Structural Dynamics*, *4*, 411–420.

Barbato, M., & Conte, J. P. (2006). Finite element structural response sensitivity and reliability analyses using smooth versus non-smooth material constitutive models. *International Journal of Reliability and Safety*, *1*, 3–39.

Bishop, C. M. (2006). *Pattern Recognition and Machine Learning*. New York, USA: Springer.

Broccardo, M., & Der Kiureghian, A. (2014). Simulation of near-fault ground motions using frequency-domain discretization. *In Proceedings of the 10th National Conference on Earthquake Engineering*. Anchorage, Alaska.

Broccardo, M. (2014). Further development of the tail-equivalent linearization method for nonlinear stochastic dynamics (Doctoral dissertation), UC Berkely.

Broccardo, M., & Dabaghi, M. (2017). A spectral-based stochastic ground motion model with a non-parametric time-modulating function. *In 12th International Conference on Structural Safety and Reliability*, Vienna, Austria.

Broccardo, M., & Der Kiureghian, A. (2017). Simulation of stochastic processes by sinc basis functions and application in TELM analysis. *Journal of Engineering Mechanics, 144(1)*, 04017154.

Broccardo, M., Alibrandi, U., Wang, Z., & Garre, L. (2017) The tail equivalent linearization method for nonlinear stochastic processes, genesis and developments. *In Risk and reliability analysis: Theory and applications*.

Springer, Cham.

Cacciola, P., Colajanni, P., & Muscolino, G. (2004) Combination of modal responses consistent with seismic input representation. *Journal of Structural Engineering, 130*(1), 47-55.

Cacciola, P., & Zentner, I. (2012). Generation of response-spectrum-compatible artificial earthquake accelerograms with random joint time–frequency distributions. *Probabilistic Engineering Mechanics, 28,* 52-58.

Caughey, T. K. (1963). Equivalent linearization techniques. *Journal of the Acoustical Society of America, 35*, 1706–1711.

Chakraborty, S., & Chowdhury, R. (2014). Polynomial correlated function expansion for nonlinear stochastic dynamic analysis. J*ournal of Engineering Mechanics*, *141*(3), 04014132.

Chen, L., Liu, J., & Sun, J. Q. (2017). Stationary response probability distribution of SDOF nonlinear stochastic systems. *Journal of Applied Mechanics, 84*(5), 051006.

Clough, R.W., & Penzien, J. (1975). *Dynamic of structures*, New York, USA: McGraw-Hill.

Crandall, S. H. (2001). Is stochastic equivalent linearization a subtly flawed procedure? *Probabilistic Engineering Mechanics*, *16*(2),169-176.

Der Kiureghian, A. (1980). Structural response to stationary excitation. *Journal of the Engineering Mechanics Division, 106*(6), 1195-1213.

Der Kiureghian, A. (1981). A response spectrum method for random vibration analysis of MDF systems. *Earthquake Engineering and Structural Dynamics, 9,* 419-435.

Der Kiureghian, A., & Li, C-C. (1996). Nonlinear random vibration analysis through optimization. In Reliability and Optimization of Structural Systems. In D. Frangopol, R. Corotis, & R. Rackwitz (Eds), *Proceedings of the Seventh IFIP WG 7.5 Working Conference on Reliability and Optimization of Structural Systems* (pp. 197-206). U.K.:Pergamon Press.

Der Kiureghia, A. (2000). The geometry of random vibrations and solutions by FORM and SORM. *Probabilistic Engineering Mechanics, 15,* 81–90.

Der Kiureghian, A. (2005). First- and second-order reliability methods. In: E. Nikolaidis, D.M. Ghiocel, & S. Singhal (Eds.), E*ngineering design reliability handbook*. Boca Raton , FL: CRC Press.

Der Kiureghian, A., & Fujimura, K. (2009). Nonlinear stochastic dynamic analysis for performance-based earthquake engineering. *Earthquake Engineering*

& Structural Dynamics, 38(5), 719-738.

Ditlevsen, O., & Madsen, H. O. (1999). *Structural reliability methods*. New York, USA:Wiley

Ditlevsen, O. (1986). Duration of visit to critical set by Gaussian process. P*robabilistic engineering mechanics, 1*(2) , 82-93.

Duan, L., & Chen, W. F. (1999). *Bridge engineering handbook, Second Edition: Seismic Design*. Boca Raton, FL: CRC press.

Faravelli, L. (1989). Response-surface approach for reliability analysis. *Journal of Engineering Mechanics,115*, 2763-2781.

Fan, F. G., & Ahmadi, G. (1990). Nonstationary Kanai-Tajimi models for El Centro 1940 and Mexico City 1985 earthquakes. *Probabilistic Engineering Mechanics, 5*(4), 171-181.

Franchin, P. (2004). Reliability of uncertain inelastic structures under earthquake excitation. *Journal of Engineering Mechanics (ASCE), 130*, 180–191.

Fujimura, K., & Der Kiureghian, A. (2007). Tail-equivalent linearization method for nonlinear random vibration. *Probabilistic Engineering Mechanics,* 22, 63–76.

Garrè, L,. & Der Kiureghian, A. (2010). Tail-equivalent linearization method in frequency domain and application to marine structures. *Marine Structures, 23*(3), 322-338.

Hagen, O., & Tvedt, L. (1991). Vector process out-crossing as parallel system sensitivity measure. *Journal of Engineering Mechanics, ASCE 117*(10), 2201–2220.

Hsu, T. I., & Bernard, M. C. (1978). A random process for earthquake simulation. *Earthquake Engineering & Structural Dynamics, 6*(4), 347-362.

Koo, H., Der Kiureghian, A., & Fujimura, K. (2005). Design point excitation for nonlinear random vibration. *Probabilistic Engineering Mechanics, 20*, 136–147.

Lutes, L. D., & Sarkani, S. (2004). *Random vibration: Analysis of Structural and Mechanical Systems.* Burlington, MA: Elsevier Butterworth Heinemann.

Lutes, L. D. (2012). Amplitude correlation in first-passage problems. *Journal of Engineering Mechanics, 138*(9), 1205-1213.

Li, C. C., & Der Kiureghian, A. (1995). Mean out-crossing rate of nonlinear response to stochastic input. In: M. Lemaire, J.L. Favre, & A. Mbarki (Eds). *Proceedings of 7th international conference on applications of statistics and probability in civil engineering reliability and risk analysis*. (pp.

295–302). Rotterdam, Netherlands: Balkema.

Mai, C., Konakli, K., & Sudret, B. (2017). Seismic fragility curves for structures using non-parametric representations. *Frontiers of Structural and Civil Engineering, 11*(2), 169-186.

Marano, G. C., Greco, R., & Morrone, E. (2011) Analytical evaluation of essential facilities fragility curves by using a stochastic approach. *Engineering Structures, 33*(1), 191-201.

McLachlan, G., & Peel, D. (2000). *Finite mixture models*. New York, NY: Wiley.

Naess, A., Gaidai, O., & Batsevych, O. (2010). Prediction of extreme response statistics of narrow-band random vibrations. *Journal of Engineering Mechanics, 136*(3), 290-298.

Newland, D. E. (2005). *An Introduction to Random Vibrations, Spectral & Wavelet Analysis*, 3rd Ed., Mineola, NY: Dover Publications.

Priestley, M. B. (1965). Evolutionary spectra and non-stationary processes. *Journal of the Royal Statistical Society. Series B (Methodological)*, 204-237.

Rahman, S., & Xu, H. (2004). A univariate dimension-reduction method for multi-dimensional integration in stochastic mechanics. *Probabilistic Engineering Mechanics, 19*: 393-408.

Kawabata, T. (2008). Multiple subunit fitting into a low-resolution density map of a macromolecular complex using a gaussian mixture model. *Biophysical journal, 95*(10), 4643-4658.

Rezaeian, S., Der Kiureghian, A., & Bozorgnia, Y. (2008). Stochastic Ground motion model with Time-Varying Intensity, Frequency and Bandwidth Characteristics. In *Fourteenth World Conference on Earthquake Engineering*.

Rezaeian, S., & Der Kiureghian, A. (2010). Simulation of synthetic ground motions for specified earthquake and site characteristics. *Earthquake Engineering & Structural Dynamics, 39*(10), 1155-1180.

Rice, S. O. (1944). Mathematical analysis of random noise. *Bell System Technical Journal, 23*(3), 282-332.

Schobi, R., Sudret, B., & Wiart, J. (2015). Polynomial-chaos-based Kriging. *International Journal for Uncertainty Quantification, 5*(2). 171–193.

Shinozuka, M., & Deodatis, G. (1991). Simulation of stochastic processes by spectral representation. *Applied Mechanics Reviews,* 25, 191–204.

Song, J., & Der Kiureghian, A. (2006). Joint first-passage probability and reliability of systems under stochastic excitation. *Journal of Engineering*

Mechanics, 132(1), 65-77.

Soong, T. T., & Grigoriu, M. (1993). *Random vibration of mechanical and structural systems*. NASA STI/Recon Technical Report A, 93.

Spencer, B. F., & Bergman, L. A. (1993). On the numerical solution of the Fokker-Planck equation for nonlinear stochastic systems. *Nonlinear Dynamics, 4*(4), 357-372.

Tubaldi, E., Barbato, M., & Dall'Asta, A. (2014). Performance-based seismic risk assessment for buildings equipped with linear and nonlinear viscous dampers. *Engineering Structures*, 78, 90-99.

Vamvatsikos, D., & Cornell, C. A. (2002). Incremental dynamic analysis. *Earthquake Engineering & Structural Dynamics, 31(3)*, 491-514.

Vamvatsikos, D., & Cornell, C. A. (2004). Applied incremental dynamic analysis. *Earthquake Spectra, 20*(2), 523-553.

Vanmarcke, E. H. (1975). On the Distribution of the First-Passage Time for Normal Stationary Random Processes. *ASME. Journal of Applied Mechanics, 42*(1), 215–220.

Wang, Z., Broccardo, M., & Der Kiureghian, A. (2016). An algorithm for finding a sequence of design points in reliability analysis. *Structural Safety, 58*, 52-59.

Wang, Z., & Song, J. (2017). Equivalent linearization method using Gaussian mixture (GM-ELM) for nonlinear random vibration analysis. *Structural Safety, 64*, 9-19.

Wen, Y. K. (1976). Method for random vibration of hysteretic systems. *Journal of the engineering mechanics division, 102*(2), 249-263.

Wen, Y. K. (1980). Equivalent linearization for hysteretic systems under random excitation. *Journal of Applied Mechanics*, 47(1), 150-154.

Yi, S. R., Wang, Z., & Song, J. (2018). Bivariate Gaussian mixture–based equivalent linearization method for stochastic seismic analysis of nonlinear structures. *Earthquake Engineering & Structural Dynamics, 47*(3), 678-696.

Yi, S. R., Wang, Z., & Song, J. (2019). Gaussian mixture–based equivalent linearization method (GM-ELM) for fragility analysis of structures under nonstationary excitations. *Earthquake Engineering & Structural Dynamics, 48*(10), 1195-1214.

Zentner, I. (2017). A general framework for the estimation of analytical fragility functions based on multivariate probability distributions. *Structural*

Safety, 64, 54-61.

Zembaty, Z. (1988). A note on non-stationary stochastic response and strong motion duration. *Earthquake engineering & structural dynamics*, *16*(8), 1189-1200.

Zhang, Y., & Der Kiureghian, A. (1997). *Finite element reliability methods for inelastic structures*. Report No. UCB/SEMM-97/05, Department of Civil and Environmental Engineering, University of California, Berkeley, CA.

초 록

이상리

건설환경공학부

서울대학교 대학원

지진, 강풍 등에 대비한 사회기반시설물의 동적 성능 평가는 설계와 유지보수의 중요한 기준이 된다. 많은 경우 외부에서 가해지는 진동하중은 불규칙적 시간이력을 보이므로 확률 모델에 기반한 해석 방법론이 필요하다. 특히 이를 위해 PSD(Power spectral density function) 모델과 불규칙진동 이론을 적용한 다양한 추계학적 신뢰도 평가 방법론이 정립되어있다. 그러나 비선형 구조물의 경우, 주파수 분해와 중첩원리에 의존하는 PSD 해석 방법론을 포함하여 다양한 불규칙 진동이론을 적용하기에 어려움이 있다. 이러한 한계를 극복하고 효율적이면서도 정확하게 비선형 구조물의 추계학적 성능을 평가하기 위해 가우스 혼합모델을 활용한 등가선형화 방법론(Gaussian Mixture-based Equivalent Linearization Method, GM-ELM)이 최근 새롭게 제안되었다.

구조물 응답의 평균 제곱근 오차를 최소화하는 하나의 등가선형 구조시스템을 도출하는 전통적 선형화 방법론과 달리 GM-ELM은 지진 응답 확률분포를 먼저 추정한 후 이를 정확히 모사하는 다수의 가상 선형 단자유도 시스템 조합을 동시에 정의한다. 정의된 등가선형시스템 집단의 응답으로부터 대상 비선형 구조물의 추계학적 응답을 역으로 근사하는 것이 GM-ELM 방법론의 핵심이다. 이때 응답확률분포의 분해는 가우스 혼합모델(Gaussian Mixture)을 도입하여 여러 개의 가우스 확률분포의 중첩으로 근사하는 과정으로서 이루어지며, 각 가우스 분포는 그와 같은 응답 분포를 가지는 독립적 가상 선형시스템으로 치환된다. 이 과정이 '선형화' 과정에 해당한다. 평균 횡단율(mean up-crossing rate), 최초통과확률(first-passage probability), 평균최대응답(mean

peak response) 등 비선형 응답을 근사하기 위한 조합식이 제안되어 있으며, 확률분포의 보존과 다수의 선형시스템 도입이라는 GM-ELM의 특성으로 인해 다양한 한계 상태에 대해서 우수한 예측 성능을 보여주었다.

그러나 기존 GM-ELM은 몇 가지 해결되지 않은 제약을 지니고 있다. (1) 각 등가시스템 당 한 개의 최적화 제약식만이 주어지므로 등가모델의 유연도가 부족하며, (2) 가진-응답이 정상과정(stationary process)으로 제한된다. 또한, (3) 등가선형시스템이 가진 세기에 따라 쉽게 변화하는 특성을 지니고 (4) 특정 조건에서 최초통과확률을 과대평가하는 경향을 보인다. 본 연구는 기존 개발된 GM-ELM을 보완함으로써 상기 네 가지 문제점을 해결하고 다양한 추계학적 공학 문제에 적용하도록 돕는 것을 목표로 한다.

첫 번째로, 기존 GM-ELM은 구조 응답의 시간이력을 1차원 응답 확률분포로 압축하여 표현하므로, 시간이력적 특성을 충분히 고려하기 어려운 한계가 있다. 또한 등가선형시스템을 정의하기 위해 '응답의 분산'에 대한 제약식만이 주어지므로 시스템의 강성/감쇠 특성 중 한 가지를 최적화하고, 다른 한 가지는 주관적 판단에 의존하였다. 이러한 가정에서 발생하는 오차를 제거하기 위해 본 연구에서는 이변량(bivariate) GM-ELM을 제안하여 확률변수 공간을 2차원으로 확장하고, 응답과 응답의 시간 변화율의 결합확률분포를 고려할 것을 제안하였다. 즉, 등가선형시스템 조합을 도출하기 위해 기존 일변량 가우스 혼합모델이 아닌 이변량 가우스 혼합모델을 도입하였다. '응답 시간변화율의 분산' 정보를 추가로 도입하여 강성/감쇠 모두 최적화된 선형시스템조합을 찾아내었으며, 이에 따라 추정 결과가 향상되는 것을 수치 예제를 통해 확인하였다.

다음으로 지진 취약도 해석에 GM-ELM을 적용하기 위한 기법을 개발하였다. 기존 GM-ELM에서는 시스템 응답을 정상과정으로 한정하여 응답의 순간확률분포가 전체 프로세스를 대표하도록 하였다. 그러나 응답이 비정상과정(nonstationary process)인 경우 순간확률

분포가 시간에 따라 변화하기 때문에 이를 전체 시간이력을 대표하는 확률분포로 사용하기에는 적합하지 않다. 본 연구에서는 이러한 문제를 해결하기 위해 시간에 따라 변화하는 응답의 확률분포를 시간 축 내에서 평균한 '시간평균 응답분포'를 활용할 것을 제안하였다. 기존 순간응답분포 대신 시간평균 응답분포를 재현하는 등가선형 시스템을 찾아냄으로써, 비정상과정 응답 특성 역시 정상과정의 경우와 유사한 방식으로 간편하게 근사 할 수 있음을 증명하였다. 지진동은 강한 비정상성(nonstationarity)을 지니므로, 본 개발을 통해 지진공학에 대한 GM-ELM의 적용성을 크게 향상하였다.

한편 기존 GM-ELM은 가진 세기에 따라 선형시스템 특성이 민감하게 변화하는 특성을 지닌다. 가진 세기가 변화하면 확률분포도 변형되므로 가우스 혼합 모델 근사 및 시스템 최적화 과정을 다시 반복해야 하기 때문이다. 그러나 지진 취약도 곡선을 얻기 위해서는 일련의 지진동 세기에 따른 구조물의 파괴확률을 산정하는 과정이 필요하며, 이때 각 세기마다 모든 선형화 과정을 반복하는 것은 비효율적이다. 즉, 효율적인 지진 취약도 해석을 위해서는 가진 강도에 따라 변하지 않는 '고정 선형시스템'의 개발이 요구되었다. 이를 위해 본 논문에서는 응답확률분포에 강도변수를 추가하여 한 차원을 높인 강도-응답 확률분포를 활용할 것을 제안하였다. 강도-응답 확률분포를 활용하여 기존과 같은 방법으로 등가선형시스템을 정의할 경우 그 시스템조합은 가진 강도에 따라 변하지 않으며, 다만 비선형 응답에 대한 각 시스템의 기여도만 가진 강도에 따라 재산정되는 것을 증명하였다. 이러한 기여도의 변화는 가우스 혼합 모델로부터 손쉽게 추론이 가능하므로 취약도 해석 효율성이 크게 개선되었다. 나아가 '고정 선형시스템'을 알아내는 데 필요한 강도-응답확률분포를 효율적으로 추정하기 위한 스케일링 근사 방법을 제안하였다.

마지막으로 최초통과확률 추정 공식을 새롭게 제안하고 GM-ELM에 적용할 수 있도록 추가 개발하였다. 최초통과확률은 시스템의 시간이력 응답이 특정 한계상태를 한 번 이상 초과할 확률을 의미하며, 지진

취약도 분석 등 다양한 공학 시스템의 신뢰도 평가에 활용되고 있다. 그러나 최초통과확률 해석의 경우 정상과정 및 선형 응답 가정하에서도 적용 가능한 정해가 존재하지 않는 난제로 알려져 있다. 따라서 이를 해결하기 위한 다양한 근사식이 제안되어 있고, 앞선 GM-ELM 해석 역시 대표적인 최초통과확률 추정 공식인 푸아송 근사법(Poisson approximation)에 의존하였다. 그러나 푸아송 근사의 경우 특정 주파수 대역폭(bandwidth) 응답에서 파괴확률을 지나치게 보수적으로 산정하는 한계가 있다. 이에 본 논문에서는 새로운 최초통과확률 공식을 제안하였다. 기존 방식과 다르게 각 '통과사건', 즉 진동하는 시간이력 응답이 한계상태를 넘어가는 사건의 발생 특성을 푸아송-가지치기 프로세스 모델(Poisson Branching Process model, PBP)로 모사하였으며, 모델 식으로부터 최초통과확률 파괴 공식을 유도하였다. 예제를 통해 제안 공식이 기존 공식들과 비교하여 안정되게 정확한 예측 성능을 보여주는 것을 확인하였다. 나아가 제안한 PBP 기반 최초통과확률 공식을 GM-ELM 해석결과와 결합하여 비선형 응답 해석에 적용하였다. 이를 위해 비선형 구조물 응답의 비정규성(non-Gaussianity)과 주파수대역 특성을 반영하도록 PBP 공식을 조정하였다. 수치 예제를 통해 제안 방법론이 비선형 비정상성 응답의 최초통과확률을 높은 수준의 정확도로 추정하는 것을 확인하였다.

제안된 GM-ELM 방법론은 모두 지진공학 예제를 사용하여 검증하였다. 다양한 비선형 다자유도 구조물과 비정상과정 가진에 적용된 수치 예제를 통해 성능과 적용성을 검증하였으며, 이를 바탕으로 GM-ELM을 활용한 추계학적 비선형해석이 추후 실질적인 공학 문제의 해결에 기여할 수 있을 것으로 기대된다.

주요어: GM-ELM, 가우스 혼합모델, 불규칙 진동론, 등가선형화 방법론, 취약도해석, 최초통과확률

학번: 2015-21302